Theory of protein thermophoresis

Thibaut Seuwin

université de BORDEAUX

THÈSE PRÉSENTÉE

POUR OBTENIR LE GRADE DE

DOCTEUR
DE L'UNIVERSITÉ DE BORDEAUX

ECOLE DOCTORALE SCIENCES PHYSIQUES ET DE L'INGÉNIEUR

LASER, MATIÈRE et NANOSCIENCES

Par **Thibaut SEUWIN**

THÉORIE DE LA THERMOPHORÈSE DES PROTÉINES

Theory of protein thermophoresis

Sous la direction de : **Aloïs WÜRGER**

Soutenue le 11 octobre 2024

Membres du jury :

M. Thomas BICKEL	Professeur des universités	Université de Bordeaux	Président du jury
M. Aloïs WÜRGER	Professeur des universités	Université de Bordeaux	Directeur de thèse
M. Frank CICHOS	Professsor	Université de Leipzig	Rapporteur
M. Guillaume BAFFOU	Chargé de Recherche	Institut Fresnel	Rapporteur
M. Nicolas COMBE	Professeur des universités	Cemes	Examinateur

Théorie de la thermophorèse des protéines

Résumé : La thermophorèse est l'emergence d'un gradient de concentration d'une espèce en solution sous l'effet d'un gradient de température. Selon le système, les molécules en solution s'accumulent côté chaud ou côté froid, selon plusieurs paramètres, tels que le solvent, la concentration, ou encore la température. Le cas de la thermophorèse des protéines dans l'eau en régime dilué est particulier : la direction du gradient de concentration dépend de la température elle même. A relativement basse température, typiquement en dessous de 20 Celsius degrees, les molécules s'accumulent côté chaud, et aux plus hautes températures côté froid. Ce comportement a été observé avec des systèmes divers, comme les polypeptides et l'ADN. Jusqu'ici, les théories développées autour de la thermophorèse ont été notamment capables d'expliquer avec succès la migration des aérosols et des colloïdes chargés vers le froid, mais n'ont pas pu rendre compte de l'accumulation vers le chaud à basse température, ni le changement de comportement observé aux alentours de 20 degrés Celsius. Les interactions entre le solvent et la surface des particles sont à l'origine du déplacement sous l'effet du gradient de température, mais dans le cas des protéines en milieu aqueux, les contributions des interactions électrostatiques, van der Waals et hydrophobes ont été montrées incapables de rendre compte de l'observation expérimentale. En se basant sur des indices montrant un lien entre hydrophilie et thermophorèse, nous soupçonnons les liaisons hydrogènes formées entre la surface de la particle et les molécules d'eau de jouer un rôle majeur dans l'accumulation vers les endroits chauds. Nous développons un modèle théorique, basé sur une approche mécanique où nous considérons les molécules d'eau comme des objects discrets, établissant des liaisons hydrogènes avec les sites hydrophiles à la surface de la particule, par des sauts. Les observations expérimentales indiquent une dépendance en température de ces sauts. Avec un gradient de température, cela pourrait résulter en un écoulement des molécules d'eau vers le bord froid, propulsant la particule vers le bord chaud. Notre modèle a donné des résultats encourageants, qualitativement et quantitativement, et semble valider l'hypothèse d'une contribution au mouvement, dirigée vers le chaud, ayant pour origine les sauts des molécules d'eau à la surface de la particule.
Mots-clés : Thermophorèse, liaisons hydrogènes, protéines, thermo-osmose

---

Theory of protein thermophoresis

Abstract: Thermophoresis is the emergence of a concentration gradient of a dissolved species generated by a temperature gradient. From one system to another, the molecules of the solute species accumulate on the hot side or the cold side, depending on several parameters, such as solvent, concentration, and temperature. The case of protein thermophoresis in water in dilute regime is particular, because the direction of accumulation depends on temperature: at relatively low temperatures, typically below 20 Celsius degrees, the molecules migrate to the hot side, but at higher temperatures to the cold side. This behavior has been reported for several systems, such as polypeptides or DNA. So far, the theoretical understandings of thermophoresis have notably been capable of explaining the migration of aerosols and charged colloids away from the hot spot, but have not been able to describe successfully the accumulation in hotter areas, nor the change of behavior reported at temperatures around 20 Celsius degrees. The interactions between the solvent and the particle's surface are responsible for the thermophoretic motion; however, in the case of protein thermophoresis in aqueous medium, the contributions of electrostatic, van der Waals and hydrophobic interactions cannot account for the experimental observation. Based on some clues that highlight a connection between hydrophilicity and thermophoresis, we suspect the hydrogen bonds formed between the particle surface and water to play a major role in the motion towards the hotter areas. We develop a theoretical model, based on a mechanical approach that treat water molecules as discrete objects, that establish hydrogen bonds with the hydrophilic spots at the surface of the particle, jumping tangentially. Experimental data support the idea that jumps feature a temperature dependence. Combined with a temperature gradient, this could result in a creep flow of water towards the colder areas, propelling the particle to hotter places. Our model has given encouraging results, both qualitatively and quantitatively, that those jumps could be responsible for a contribution directing the motion of particles towards the hot spot.
Keywords: Thermophoresis, hydrogen bond, proteins, thermo-osmosis

---

Laboratoire Ondes et Matière d'Aquitaine
UMR5798 , 351 Cr de la Libération, 33400 Talence, France

Remerciements

La première personne à qui je souhaite adresser des remerciements est mon directeur de thèse, Aloïs, qui aura su se montrer patient et bienveillant. Je le remercie pour la confiance qu'il m'a accordée, et l'opportunité d'accomplir cette tâche enrichissante mais éprouvante qu'est la thèse. Lors de notre première entretien, je lui avais demandé la principale qualité recherchée chez un thésard, il m'avait répondu « la résilience face à l'échec », je dois confirmer qu'effectivement c'était nécessaire, pour mener ce projet à terme. J'ai eu la chance de travailler sur un sujet qui m'a profondément plut, et d'avoir des discussions riches, qui m'ont permis de prendre du recul sur la Physique, et de développer mon goût pour l'exploration en milieu inconnu.

J'adresse naturellement mes remerciements à M. Guillaume Baffou et M. Frank Cichos, qui ont accepté d'être rapporteurs pour mon manuscrit, ainsi qu'à M. Nicolas Combe et M. Thomas Bickel qui intègrent également le jury. Je les remercie pour le temps qu'ils prennent pour se déplacer à Bordeaux afin de permettre le déroulement de la soutenance. Je remercie également mon laboratoire d'accueil, le LOMA, en particulier le directeur, Fabio, qui s'est toujours montré très disponible, ainsi que Benjamin, à l'accueil, toujours souriant et encourageant, qui aura su me fournir tout ce dont j'ai pu avoir besoin. Je remercie les services gestion et informatique, qui auront su répondre à mes besoins.

Passons aux remerciements plus affectifs, à commencer par ma famille. Mes parents, qui ont supporté mes difficultés, et ont tâché de me motiver comme ils le pouvaient, et d'être présents pour la soutenance. J'aurais aimé que mon grand-père puisse y assister également, j'aurais aimé qu'il puisse être fier de cet accomplissement.

Je veux particulièrement remercier Anna, qui aura su m'insuffler la détermination pour poursuivre inlassablement les efforts, et m'aura épaulé dans ses limites dans cette épreuve. Sa bienveillance, et la volonté de ne pas la décevoir m'auront permis de finaliser ce projet. Je lui dois tellement et j'ai peur de pas pouvoir lui dire assez merci pour le renouveau qu'elle a su m'apporter. J'ai voulu accomplir ce projet, pour qu'elle soit fière, qu'elle soit heureuse d'avoir été une grande source de de détermination.

Je souhaite adresser des remerciements à mes amis, qui m'ont prodigué beaucoup de conseils. Le premier d'entre eux est Henri, avec qui j'ai partagé tant de déjeuners et tant de problèmes de doctorants, qui aura accepté de lire mes premières versions de chapitres de manuscrit. Il aura vécu chaque jour mes difficultés. J'aimerais remercier Maxime, dont la rédaction de thèse n'a pas été simple, qui a su trouver les mots honnêtes et justes pour m'encourager dans la bonne direction. Egalement Antoine et Simon, pour compléter la fine équipe de tarot; être le dernier encore en études m'a donné la pression supplémentaire pour accélérer jusqu'à la ligne d'arrivée. J'étais heureux de vous compter présents le jour de la soutenance. Merci à Arthur, mon camarade de bureau, qui aura été également d'un grand soutien et avec qui j'ai beaucoup partagé, tant les tracas que les rires. Merci à Nico, qui m'aura passé son template et m'aura donné de bons conseils; merci à Benjamin, mon mentor de surf, à qui je dois tellement.

Ces remerciements ne sauraient être complets sans les adresser également à Thomas Salez, qui aura été la personne à me donner l'envie de faire une thèse, lors de ses cours en M1, et qui aura pu m'aiguiller vers Aloïs lorsque que je prospectais pour une thèse.

J'adresse également mes remerciements à l'ERC (European Research Council) qui a financé cette thèse.

Contents

Chapter 1

Thermophoresis: discovery and uses

1.1 Soret effect: presentation

The Soret effect, also known as Ludwig-Soret effect, is the establishment of a composition gradient in a mixture because of a temperature gradient. Usually, people know about matter transport due to concentration inhomogeneities, resulting in diffusion and Fick's Law; and about thermal energy transport due to temperature disparities, as described by Fourier's law. In this research, our attention is directed towards the consequences that arise when these two phenomena are intertwined, leading to the so-called *thermophoresis*, from the greek $\phi o \rho \eta \sigma \iota \varsigma$ (*phoresis*, transport). Solute particles are experiencing a motion induced by the temperature gradient. This directed displacement competes against the usual Fickian diffusion, and results, once the stationary state reached, in a concentration gradient. Particles accumulate on one side, hot or cold, depending on the system used, of the vessel, while the other side gets depleted.

This phenomenon has first been reported during the 19^{th} century. The oldest observation was made in liquids by Ludwig in 1856 and understood by Soret [1] in 1879. This phenomenon was also reported in gaseous media by Tyndall [2] in 1870. He notably observed the motion of dust and smoke particles, depleted away from heated surfaces. Reynolds [3] reported in 1879 a flow of gas through solid porous plates in a temperature gradient, and his observations were theoretically explained with success and completed by Maxwell [4] the same year. In the 20th century, Derjaguin [5] provided a comprehension of thermophoresis in liquids resorting to *thermo-osmosis*, a related phenomenon that will later be presented in details. This enabled to explain thermophoresis in liquids for several cases.

Nowadays, thermophoresis still receives attention. Its use as a sorting method to separate molecules is getting popular, and there are several modern experiments performed using biological macromolecules, such as DNA, proteins, sugars. [6–23].

1.2 Applications and recent developments

Here we display modern applications of thermophoresis, some of the latest developments resorting to it, and eventually some possible prospects.

1.2.1 Thermal Field-Flow Fractionation

Thermal Field-Flow Fractionation (TFFF) systems are used for separation of biological and synthetic materials, such as polymers, with different molecular weight. It is also used to quantify thermophoresis, having proved itself as particularly adapted for dissolved polymers and suspended particles, such as proteins [24–28].

A TFFF system is based on a micro-channel of length L and width w, with a Poiseuille flow, and a perpendicular temperature gradient, as illustrated with fig. 1.1. Separation of suspended particles are performed in a solvent such as methanol, THF, acetonitrile, or DMSO [29]. Water is not typically used as a carrier fluid for separation, unless an electrolyte is added.

On fig. 1.1, which illustrates a TFFF setup, thermodiffusion occurs vertically (concentration gradient represented by the shades of grey), and the solute is concentrated in the cold area. When a colloidal suspension is injected at the channel entrance and, after an equilibration time of some minutes, it reaches a steady state with a vertical concentration profile $c(z) = c_0 \mathrm{e}^{-\frac{z}{\ell}}$, where the retention length $\frac{1}{\ell} = \frac{S_T \Delta T}{w}$ [30] depends on the Soret coefficient and the temperature difference applied. At first the initial distribution of solute molecules is very narrow along the x axis, before getting stretched by the Poiseuille flow.

The larger the sensibility to thermophoresis of the solute, the more accumulated on one side the solute. The fluid has a laminar velocity profile, resulting from the applied Poiseuille parabolic profile. So, the solute that is more concentrated to an edge (regardless it is the cold or the hot) will have a lower average velocity, because of the velocity is smaller close to the edges. Samples that compact less will have on average a larger velocity. The difference in average velocity results in the spatial and temporal particle separation at the output of the TFFF channel. At the exit of the channel, the colloidal portion is determined by detection of the UV-absorption over time transverse to the velocity and the passage of suspended molecules. Because high-molecular-weight polymers are more concentrated to the cold edge than those of low molecular weight, the latter emerge first, followed by fractions of increasing molecular weight polymers.

TFFF experiments can be related to physical parameters such as molecular weight, polydispersity, or the thermal diffusion coefficient. Thus, TFFF can be used as an analysis tool for the previously mentioned physical parameters, as well as a separation device.

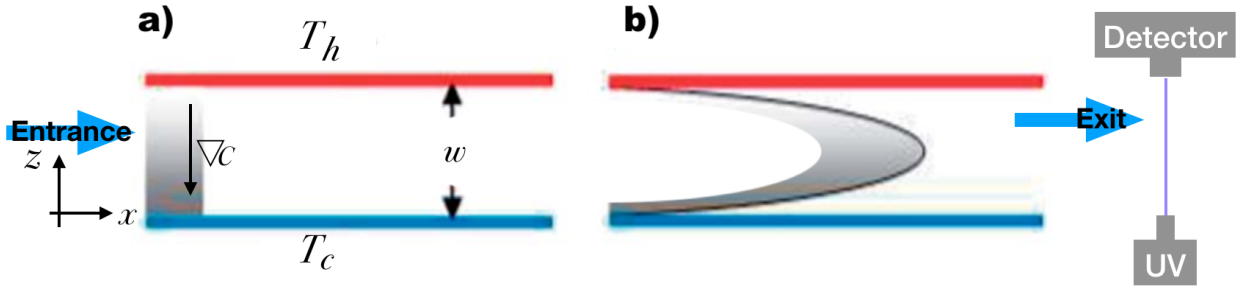

Figure 1.1: *Initially, a sample is prepared at the entrance of the channel. Under the vertical temperature difference, it experiences Soret effect. The vertical concentration profile is then given by* $c(z) = c_0 e^{-\frac{z}{\ell}}$ *. Applying a pressure gradient by pumping the suspension through the channel leads to a parabolic velocity profile. At the exit, the colloidal content is determined by detection of the UV absorption as a function of time. From ref. [30].*

Fig. 1.2 shows the UV-absorption profile as a function of time. Absorption is related to

concentration with Beer-Lambert's law. Since w is very small before L, the concentration's dependance varies tremendously with the advance of the solute in the channel, which results in a sharp gaussian.

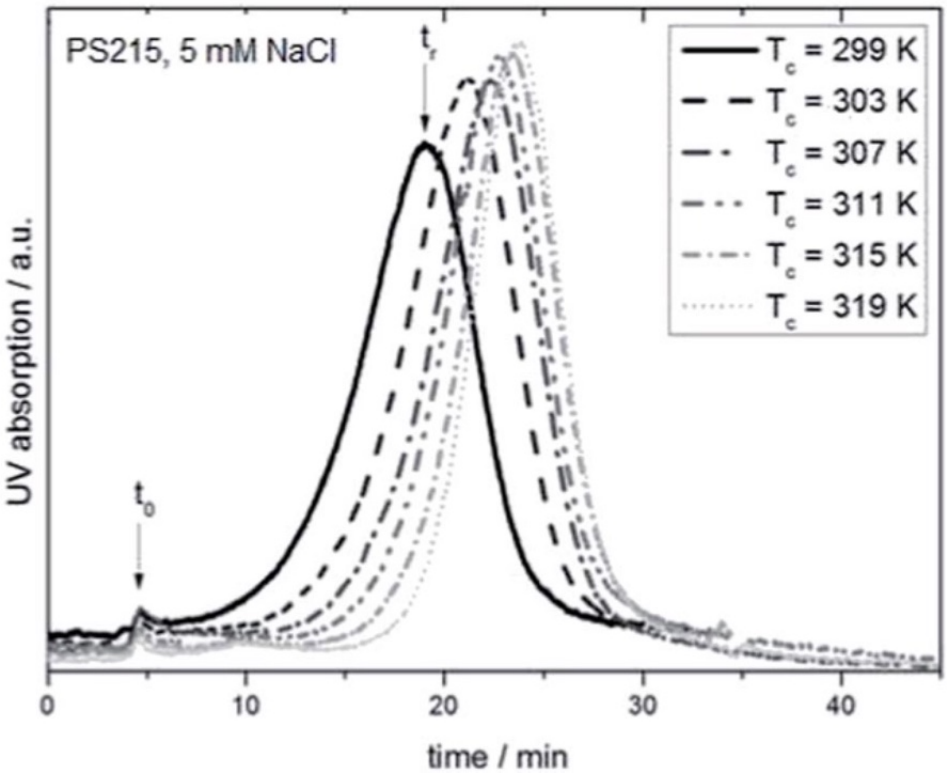

Figure 1.2: *Typical UV-absorption profiles over time at different temperatures for polystyrene sulfate beads. At higher temperature T, the position of the Gaussian is shifted to later times, implying a smaller retention length, and thus a higher Soret coefficient. The small peak indicates the arrival of the parabolic summit, and the main gaussian peak the one from the layer concentrated at the bottom of the channel. From ref. [30].*

1.2.2 Thermocolums

Thermogravitationnal cells (also referred as Clusius columns) are another method of species separation for colloidal particles [28]. Thermogravitational columns were one of the first applications of the effect, designed in 1938 by Clusius and Dickel. A schematic view is provided on fig. 1.3. This time, there is no external flux outside the Clausius column, contrary to TFFF setup where a Poiseuille flow is exerted. The temperature gradient is perpendicular to gravity, so water experiences convection. Close to the hot side, the fluid is less dense, so it moves upwards, while on the cold side water sinks to the bottom, as illustrated by the circular arrows on fig. 1.3. Meanwhile, thermophoresis occurs horizontally. Once again, the height L of the system is large compared to its width w.

To determine the horizontal concentration difference $\Delta_x c$ and the vertical concentration difference $\Delta_z c$, one finds: $\frac{\Delta_x c}{\Delta_z c} = \frac{w}{h} \ll 1$, thus c depends essentially on z. As a result, the combination of horizontal thermophoresis and vertical convection concentrates solute at the bottom of the column. In the steady state, there is a concentration gradient along the vertical axis in the column given by [31]:

$$\frac{d\ln(c)}{dz} = \kappa \frac{D_T}{D} \frac{\Delta T}{w}. \tag{1.1}$$

c is the concentration of suspended particles, essentially function of z. D is the diffusion coefficient, and D_T is the thermodiffusion coefficient. κ is given by: $\kappa = \frac{q/120}{1+q^2/10800}$, with the parameter $q = \frac{\alpha \Delta T g \rho_0 w^3}{6\eta D}$, α the thermal expansivity, ρ_0 the mass density at equilibrium. The Soret coefficient can even be calculated, and the thermocolumn can also be used as an instrument of measure. Since the device can provide a concentration difference between the top and the bottom by a factor h/w, larger than the horizontal concentration difference between the hot and cold plates, this results in a relatively large concentration at the bottom compared to the rest of the vessel.

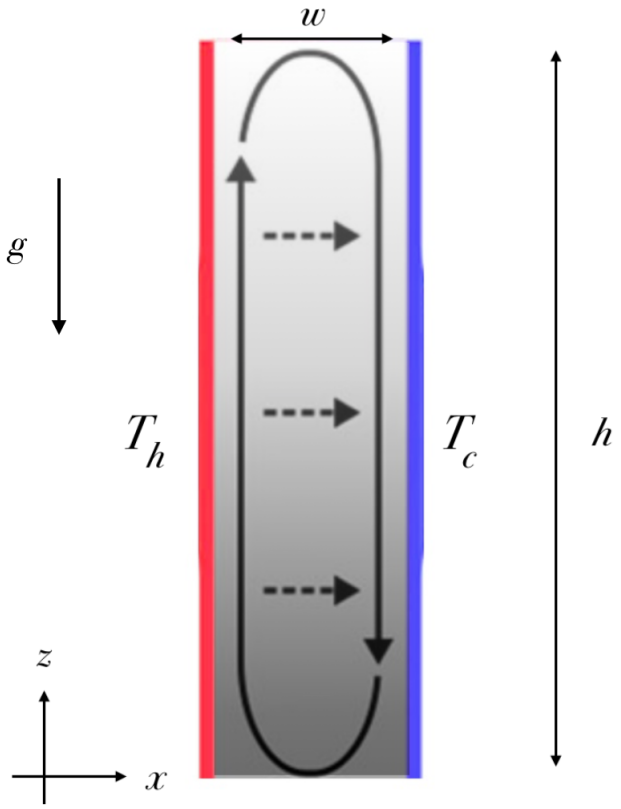

Figure 1.3: *Principle of a thermogravitationnal column. Circular arrows symbolize convection of water because of density differences. The temperature gradient acts perpendicular to the gravity, which results in an accumulation of the solute at the bottom cold side and a vertical concentration gradient, symbolized by shades of grey.*

Thermogravitational columns can also be used for isotopes sorting and were employed to enrich uranium during the Manhattan project [32]. Nowadays the strength of conventional thermogravitational columns lies in the study of ternary mixtures. This technique has advantages over optical methods, because "the extracted sample can be investigated using state of the art analytical methods and does not rely only on refractive index measurements" [33].

Besides its industrial and characterization applications, the concept of thermocolumns can hold a place in the fundamental field. Indeed, it could be a clue to understand the origin of life. Indeed, themocolumns could represent an explanation to an element lacking in the theory of evolution and the apparition of life. One step is missing to explain the emergence of living

organisms: thresholds concentrations reached for nucleotides, which are the monomers of the stands of DNA.

The submarine volcano-oceanic water interface is the place of a strong temperature gradient, and thermal hydropores act as thermocolumns [34, 35]. In porous rocks, nucleotides could experience thermophoresis and be gathered at threshold concentrations that could spark biological reactions [34]. Indeed, short genetic polymers replicate faster, and are more susceptible to create sequences than long chains. So one should expect short-chain polymers to appear. However, life is composed of long-sequence polymers, indicating that something seems to be missing. A selection on long chains could be however applied by thermophoresis [34]. So heated porous rocks could be the cradle for life.

1.2.3 Microscale thermophoresis

Thermophoresis is notably used for microscale applications: control of DNA concentration can be set up [21, 36–38], which could have applications in the field of bio-engineering, offering a good alternative where electrophoresis fails.

In their experiment, Duhr *et al.* [36] have shown that for a given temperature range, with a temperature gradient, DNA is depleted away from the heated spot. A temperature gradient is applied on an aqueous solution with a micrometer-sized focused infrared light. It has been shown that it was possible to replicate DNA strands by a polymerase chain reaction (PCR) in a thermophoretic cell with convection [19]. It is even possible to design thermal traps for nano objects such as DNA [23].

There are commercially available setups of microscale thermophoresis that can be used to determine physical and chemical parameters such as dissociation constants. Jerabek-Willemsen and co-workers [39] used microscale thermophoresis for characterization of protein binding. In small glass capillaries, an infrared laser is focused to produce the temperature gradient, and the trajectories of proteins are tracked by labelling them with fluorophores. The thermophoresis of a protein is significantly different from the thermophoresis of a protein–ligand complex, due to changes in size, charge and solvatation energy caused by the binding, which is illustrated with figure 1.4. The signal of fluorescence over time is modified with the binding or not of ligands. Exploiting this difference, it is possible to evaluate dissociation constants K_d. Those give access to the change in Gibbs free energy ΔG.

On fig. 1.4 the phenomenon of a different thermophoresis between a protein with and without a ligand is illustrated. Without a ligand the protein usually moves faster to the cold and farther from the hot side. Fig. 1.5 describes the principle to characterize protein thermophoresis and eventually the determination of the dissociation constants.

1.2.4 Other applications

Here we display some miscellaneous applications and impacts of thermophoresis.

Another application is the investigation and modeling of hydrocarbon reservoirs [40], where thermal gradients occur naturally. Those gradients are horizontal, and thermal diffusion lead to horizontal compositional variation, as depicted on fig. 1.6. Predicting those horizontal compositional variations allows to determine if two producing wells are draining the same reservoir or not, which is very helpful for the production engineer. Otherwise, the oil drained

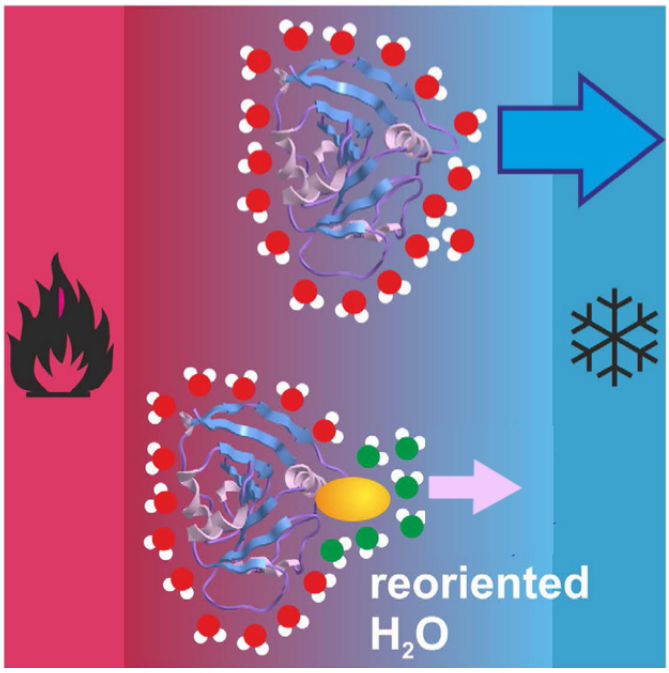

Figure 1.4: *Different situations: a lone protein and a protein which has bound with a ligand. The movement induced by thermodiffusion is different, notably because the solvation shell is different. Image from ref. [17].*

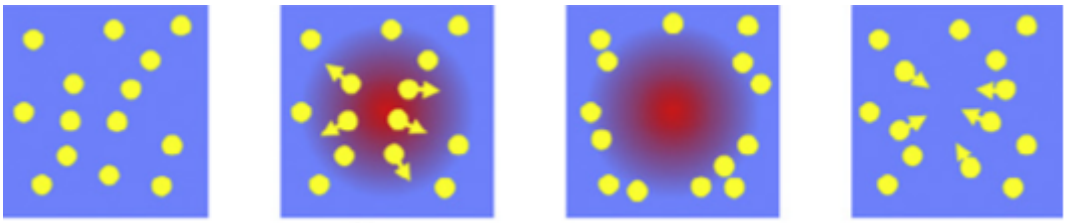

Figure 1.5: *Principle of the experiment. The IR laser creates the temperature gradient. The molecules are depleted away from the heated spot, and an excitation light excites the fluorophores. The emitted light is collected, and particle motion can be observed. Image from ref. [39].*

would be different from a composition point of view from a draining point to another, not taking this into account would lead to disparities in extraction facilities.

Rosner [41] showed that thermophoresis has to be considered in combustion processes. Technically, the gas composition has an impact on flames, so temperature gradients induce composition gradients for light gas such as H_2, but also heavy fuel vapor species like paraffin or other long-carbon-chain molecules. Thermophoresis of binary mixtures of gases can be used notably for the separation of the isotopes, such as $^{14}NH_3/^{15}NH_3$ [42]. More recently, in 2016, thermophoresis has also been observed in solids, in carbon nanotubes [43].

If we enter the field of prospects, an interesting potential application to be considered lies in the medical field. Indeed inflamed areas are temperature gradients, that could influence the transport across and through biological membranes in order to direct drug components into the targeted area. This could enable faster and more efficient drugs compared to the traditional Brownian molecules.

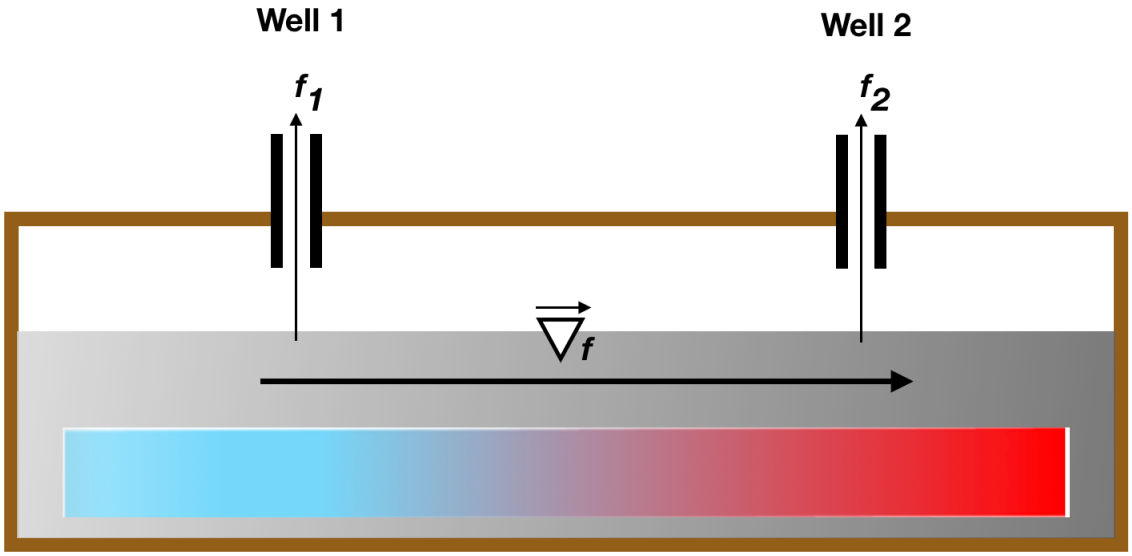

Figure 1.6: *Schematic view of the thermophoresis phenomenon consequences in the field of hydrocarbon reservoirs. The temperature gradient present naturally generates by thermophoresis a gradient of composition $\vec{\nabla} f$ in oil. Thus in two different wells 1 and 2 oil is extracted respectively at composition f_1 and f_2.*

1.3 Introduction to quantities describing thermophoresis

1.3.1 Emergence of a composition gradient under a temperature gradient in the stationary state

We introduce the physical quantities used to describe thermophoresis. As evoked previously, a temperature gradient leads to the establishment of a composition gradient. For the volume fraction f of a given species, its gradient is linked to the temperature gradient [44]:

$$\nabla f = -f(1-f)S_T \nabla T. \tag{1.2}$$

S_T is the Soret coefficient. This quantity contains all the information of the thermophoretic behavior of a given species: direction of motion and compactness of the concentration gradient. Note that eq. 1.2 is often adapted with other quantities such as mass fraction. S_T does not depend on the gradient of temperature itself, as we can see on fig. 1.7.

S_T characterizes thermophoresis on different aspects. The sign dictates the direction of the accumulation for the species. If $S_T > 0$, the species accumulates in cold areas. If S_T is negative, the compound migrates towards the hot spot. The case $S_T > 0$ is often called positive thermophoresis or *thermophobic* behavior, the species is depleted away from the hot spot. The opposite situation is negative thermophoresis, or *thermophilic* behavior, the species accumulates in the hot region.

We see that the volume fraction gradient ∇f in eq. 1.2 depends on the volume fraction f itself. So integrating to get the volume fraction profile is not trivial. On fig. 1.8 we can see that the dependence of the quantity $w(1-w)S_T$ with w is not monotonous, and can even feature sign changes. Moreover, the Soret coefficient also depends on the composition, as illustrated on fig. 1.9 and 1.10. We will first display the complex behavior the Soret coefficient can have with

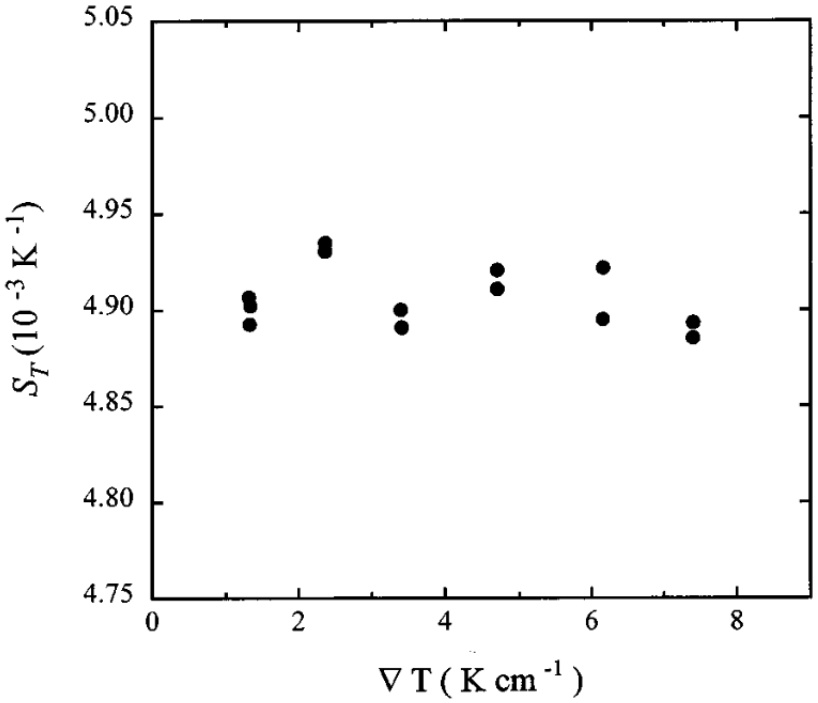

Figure 1.7: *Experimental data for S_T as a function of temperature gradient ∇T for an equimolar mixture of toluene and n-hexane at the average temperature $T = 25$ °C. We see that S_T is constant with the temperature gradient. From ref. [45].*

respect to the mixture's composition in the general case, then we explore the case the dilute regime in liquids, which is where our subject of interest takes place.

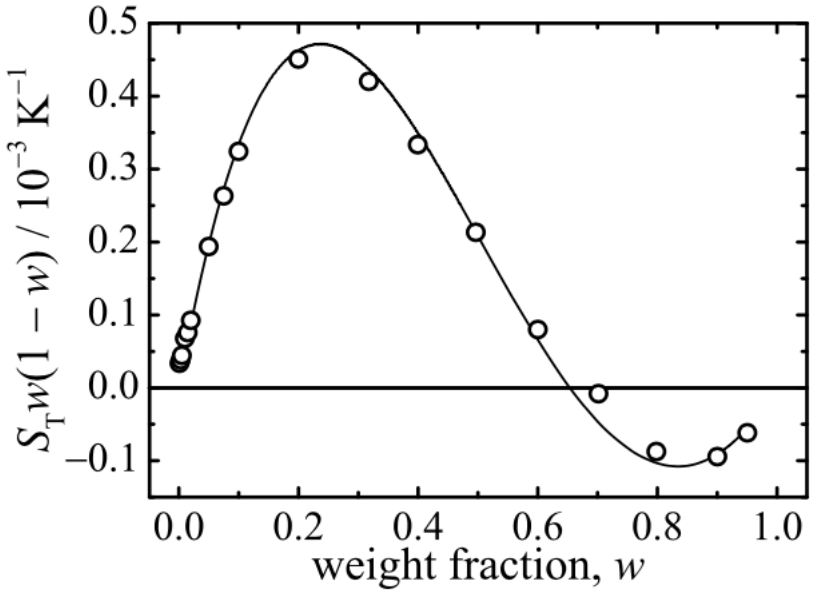

Figure 1.8: *$S_T w(1-w)$ as a function of weight fraction of ethylene glycol for aqueous solution of ethylene glycol, measured at 25 °C. From ref. [13].*

1.3.2 Molecular Mixtures: high molar fraction regime

On fig. 1.9 we see that the sign of S_T can change depending on the volume fraction.

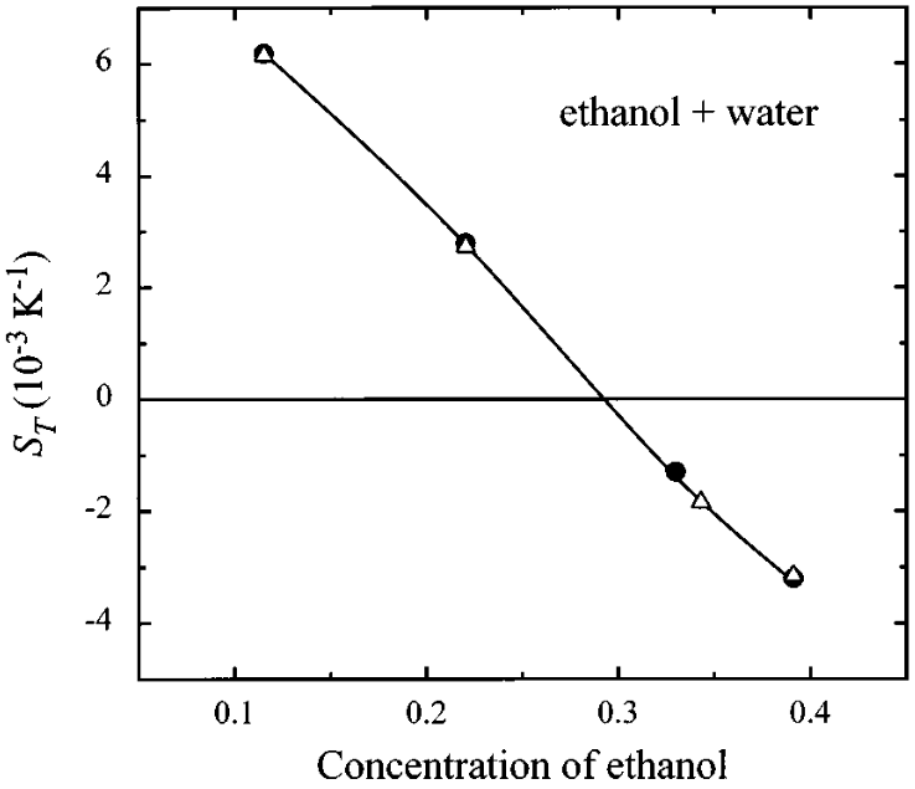

Figure 1.9: *Experimental data for S_T vs composition for a mixture of water and ethanol at the average temperature T = 25 °C. From ref. [45]. Note that the author uses the word "concentration", but in our field this corresponds to the composition, that is to say volume fraction.*

Fig. 1.10 shows that the dependence of S_T with the mass fraction is not trivial. The sign and the magnitude of S_T do depend on the system used. Depending on the solvent composition, the behavior of S_T is very delicate to predict: its magnitude, evolution with volume fraction, does not display any simple trend.

1.3.3 Case of dilute regime - Early subject of interest: Salts

Here we go progressively to our topic of interest: the dilute regime. First we illustrate a case of dilute regime by presenting Soret's experiment in aqueous solution of salts. Then we show how composition gradient and temperature gradient are linked. Then we present the origin of the Soret coefficient in terms of currents of matter.

Soret conducted experiments with sodium chloride and potassium nitrate in tubes, heated at one extremity and cooled at the other. Soret was wondering if the concentration of a solute would remain uniform if the temperature was varying spatially. Soret published his work in 1879 [1], in which he used straight and U-shaped tubes with extremities at 78 and 15 °C. A schematic view of his setup is provided in fig. 1.11. The two salts have very different variations of solubility with temperature. Soret observed that the concentrations of salts are different at the hot side and at the cold side.

However, Soret found a difference between tubes of different shapes. Indeed the way to empty it differs: the straight tubes are emptied from the bottom, and the solution is collected in three parts: cold (first to exit), medium and hot as water goes down, so the hot portion is the last collected. Fortuitously, the hot portion was quite the same in terms of volume and

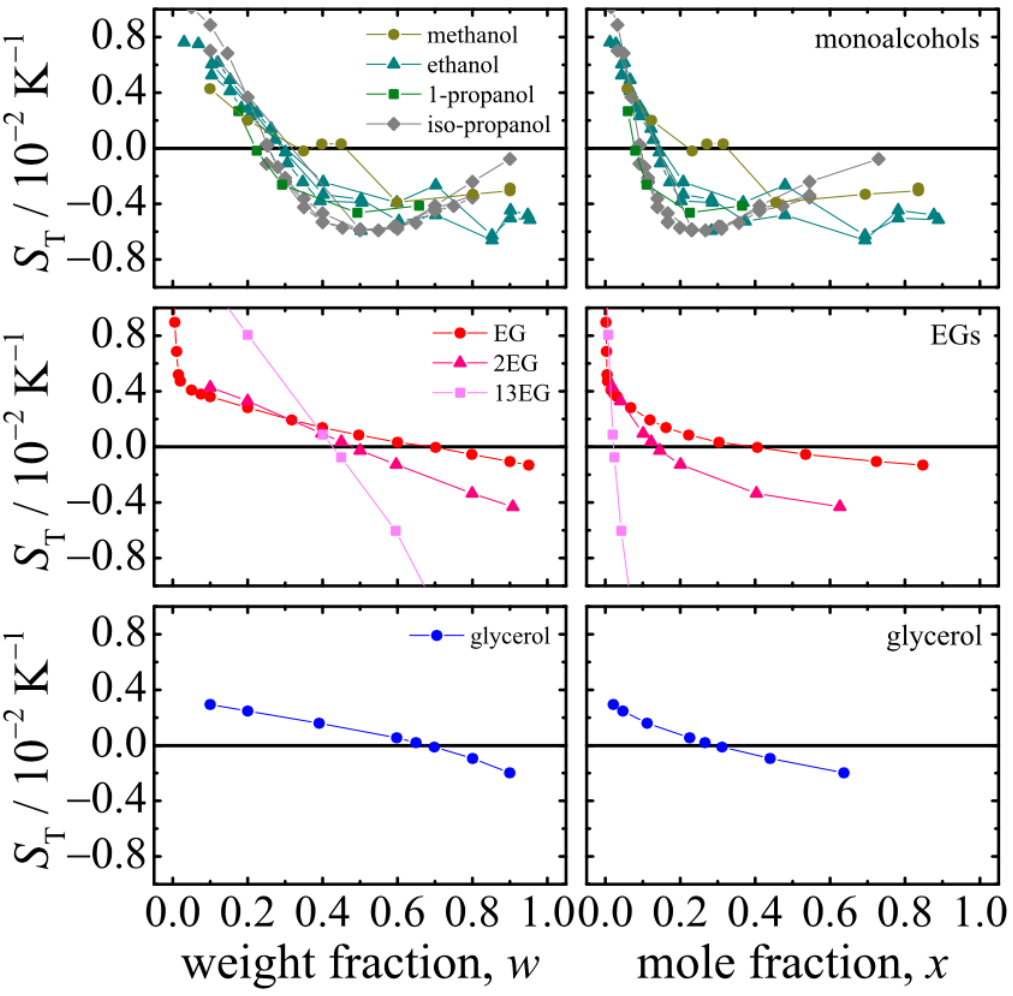

Figure 1.10: *Soret coefficient as a function of the weight fraction (left) and the mole fraction (right) of aqueous solutions of monoalcohols, EGs (Ethylene Glycols), and glycerol at 25 °C. Image taken from ref. [13].*

salt concentration in the different attempts, so it was considered as the concentration reference. Concerning U-tubes, some of the cold water was leaving the tube when extracting the hot portion, so cold portion remained the purer, and was the reference to compare with the mean concentration. Despite this disparity, he concluded that the two salts on which he operated tend to concentrate in the cold part, and that this effect was getting more significant with a larger initial concentration. So Soret exposed the fact that in a temperature gradient, solute can migrate towards the cold side of the environment. This highlights the existence of matter currents generated by a thermal field.

We introduce those currents in the frame of the dilute regime. The volume fraction is thus negligible before one, and since concentration c is directly proportional to volume fraction (in this dilute regime), one can adapt eq. 1.2 to link concentration gradient and temperature gradient:

$$\frac{\nabla c}{c} = -S_T \nabla T. \tag{1.3}$$

Some authors use eq. 1.3 with the mass fraction instead of the concentration. One must notice that if S_T was independent from T, one would directly integrate eq. 1.3 and find a familiar

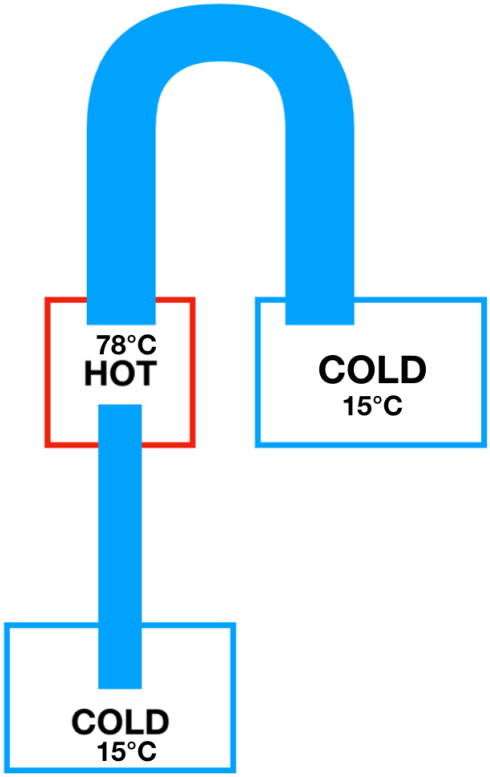

Figure 1.11: *Schematic view of the experiment conducted by Soret, where he exposed salts solution contained in tubes of different forms. Soret tried two different geometries for his tubes, one straight, the other one U-shaped.*

profile: $c(T) \propto \mathrm{e}^{-S_T T}$. In a solution featuring a concentration gradient and a temperature gradient, the total current of matter is given by [46]:

$$\vec{j} = -D\vec{\nabla}c - D_T c\vec{\nabla}T, \tag{1.4}$$

where j is the total current of matter, which has two contributions arising from the two gradients. The first term is the usual quantity given by Fick's law, resulting from collective Brownian motion, and the second term comes from the temperature inhomogeneity. D is thus the diffusion coefficient of the solute, and D_T is called *thermodiffusion coefficient*. This quantity holds a central role in our work.

Following the paradigm of fluid mechanics, we can establish some links between current, velocity, and transport coefficients. The matter current due to thermodiffusion is given by: $j_{TD} = -cD_T\nabla T$, and knowing that some currents are linked to the corresponding velocity of particles by: $j = du$, with d a density (like the mass density and the mass current, or the charge density and the electric current), and u the drift velocity. So, if we identify j_{TD} as cu (c holds the role of the density), the quantity $D_T\nabla T$ is a particle velocity. Thus, we can directly link the thermal field to a velocity, with the relation:

$$\vec{u} = -D_T\vec{\nabla}T. \tag{1.5}$$

So D_T is proportional to the velocity of the particle. We see that if D_T is positive, the velocity is directed toward cold area and vice versa.

In the stationary state, the overall current vanishes ($j = 0$), leading to the definition of S_T:

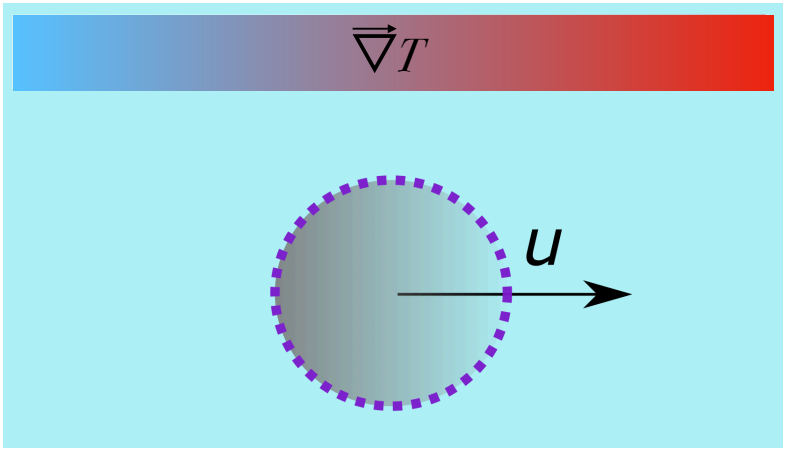

Figure 1.12: *A molecule moving in a temperature gradient.*

$$S_T = \frac{D_T}{D}. \tag{1.6}$$

S_T reflects the competition between two rival phenomena: the drift caused by thermodiffusion that creates a composition gradient, and the Brownian motion, which tends to make this gradient disappear. If the effect of thermodiffusion outmatches Brownian motion, molecules accumulate in a small retention length on one side of the temperature gradient. In the opposite case, the Fickian diffusion tends to make concentration uniform, and in the stationary state the concentration gradient is relatively small.

1.4 Out of equilibrium situations in gaseous medium

Here we present some situations that happen out of equilibrium in gaseous media. We evoke notably the behavior of gas at a solid interface in a thermal field, and the behavior of aerosols.

We offer to start with a brief historical retrospective. In 1870, Tyndall [2] observed the motion of smoke and dust particles repealed by a heated surface. Some years latter, Crookes [47] designed his *lightmill*, supposed to rotate because of radiation pressure but was not successfully describes by theories at first. In 1879, Reynolds submitted a paper to the Royal Society presenting what can be called *thermal effusion*, where he observed a flow of gas through porous plates sparked by a temperature gradient without any initial difference of pressure. Eventually, Maxwell [4] developed the same year a model highlighting the existence of a creep flow of gas at a solid interface in a temperature gradient. This enabled to shed some light of the aforementioned phenomena.

1.4.1 Creep flow of gases at solid interfaces induced by a temperature gradient

The particle motion is sparked by the tangential shear stress induced by the temperature gradient. This is the consequence of two phenomena: first, the thermal momentum is not the same whether the molecule hits from the hot side or from the cold side. Then, the diffusion on the surface is not specular: the tangential component is not conserved. This component is on average zero after collision (non specularity), and its magnitude after collision is smaller than before,

because of the exchange of momentum with the surface. As a result gas molecules provide momentum to the wall [4]. Chapter 3, devoted to theories existing to describe thermodiffusion, features more detailed elements.

Then Maxwell interested himself to the theory of the radiometer, trying to provide a new explanation. The radiometer is described at the end of the section. Fig. 1.13 provides a schematic view of collisions of gas molecules against the solid surface of a channel.

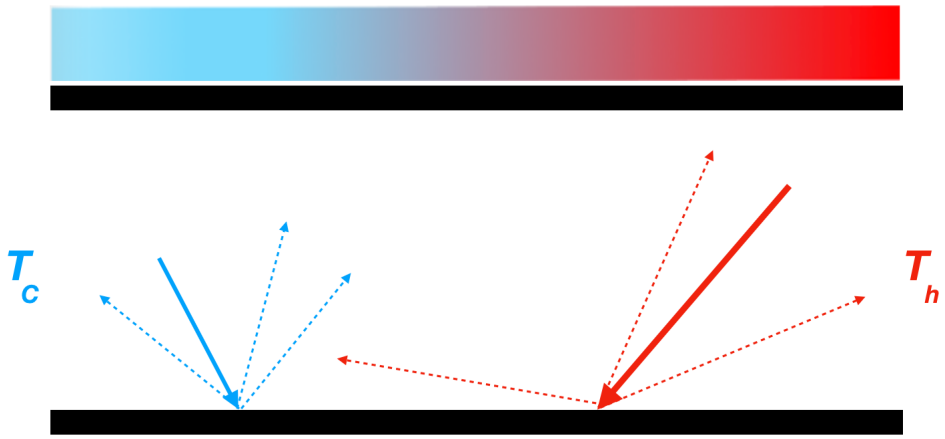

Figure 1.13: *Gas filling a micro-channel in a temperature gradient. T_c is the temperature of the cold side, T_h the temperature of the hot side. Gas is denser but molecules have smaller velocities compared to the hot side, where velocities are larger but the gas is less dense. Bounces of molecules at the surface are not specular, so on average the momentum of the gas molecule after collision is zero. But the incoming momentum, given by gas molecule during collision to the surface, is larger. This induces an overall momentum of the solid towards the cold side, which propels the gas by counter-action to the hot side, resulting in a creep flow oriented towards higher temperatures.*

This creep flow is driven without any difference of pressure imposed. In his theoretical approach on Reynolds' work, Maxwell [4] ended up with an expression connecting the creep velocity of the gas v_c to the temperature gradient, given by:

$$v_c = \frac{3}{4}\frac{\eta}{\rho}\nabla \ln(T). \tag{1.7}$$

where η is the gas viscosity and ρ the gas density. If the pressures are initially the same on the two sides, the gas goes from the colder to the hotter side. This intriguing result is due to tangential forces between the gas molecules and the sides of the narrow pores in the plates. For a system opened on both sides, the pressure remains the same at the cold and the hot sides. However, if the extremities of the channel are closed, this leads to an accumulation of gas on the hot side. As the result, pressures on cold and hot sides will become different, and an opposite flow arises. When both flows are equal, the system reaches a stationary state, and the pressure gradient is linked to the temperature gradient. For a micro-channel of radius a, the gradients are linked by [4]:

$$\nabla P = \frac{6\eta^2}{a^2 \rho T}\nabla T, \tag{1.8}$$

In this part we have introduced the emergence of a creep flow of a fluid at a solid interface (more precisely in a channel here) in a temperature gradient, resulting in the passage of the

gas from the cold to the hot side. This is the basic definition of *thermo-osmosis*. When a temperature gradient is applied parallel to a solid-fluid interface, the phenomenon of *thermo-osmosis* occurs. In general, *Osmosis* is the result of a liquid flow through a semi-permeable membrane caused by a concentration gradient. It is a well known effect with various application, one being the desalination of seawater. Thermo-osmosis works in a similar way, except that the flow is due to a temperature gradient and not a concentration gradient.

1.4.2 Particle thermophoresis of aerosols

Now that we have introduced thermo-osmosis of gas, we provide some direct applications, the case of aerosols and the solution to a physical problem: Crookes radiometer.

As we have evoked it earlier, the displacement of matter due to a temperature gradient has notably been observed with the example of smoke molecules depleted away from a hot spot, as reported Tyndall [2]. Smoke molecules are aerosols, solid molecules suspended in a gaseous medium. In that case, those are small carbon molecules. At a microscopic level, those molecules are very large compared to gas molecules. The solid surface of smoke molecules is thus comparable to the walls of the micro-channel similar to the previous description. In the temperature gradient, there is, as we exposed it previously, a creep flow of gas molecules, flowing toward the hot areas that propells the surfaces to the cold side. As a result, smoke molecules are depleted away from a heated surface.

More quantitatively, the thermodiffusion coefficient for aerosols is given by [48]:

$$D_T \propto \frac{\eta}{\rho}\frac{1}{T}, \tag{1.9}$$

One must compare to eq. 1.7 since thermodiffusion coefficient and velocity of particles are linked. The two expressions are in good agreement, since v_c is opposed to the solid's motion.

Now we illustrate the understanding of gas thermophoresis with another example: Crookes' radiometer. In 1872, Crookes [47] developed a special kind of radiometer, an instrument that could measure radiant energy of heat and light. It consists of four vanes, each of which is blackened on one side and silvered on the other, as illustrated on fig. 1.14. The vanes are fixed to the arms of a rotor that is balanced on a vertical support, in such a way that it can turn with very little friction. The mechanism lies inside a clear glass bulb where a high vacuum has been made, in the order of magnitude of a few hPa. This vacuum is high, but not perfect, which will hold a central role in the following.

When exposed to the sunlight, the radiometer turns, which gives it the name of *lightmill*. At first it was believed that the phenomenon making the mill turn was radiation pressure. But this explanation predicts the opposite rotation direction. The black side is heated by absorption of IR radiation, a temperature gradient perpendicular to the vane is generated. But any attempt trying to resort to pressure difference cannot work: no net force can be generated by normal forces on the faces of the vanes, because pressure would quickly equalize to a steady state with just a flow of heat through the gas.

The vanes of a radiometer are not porous, so thermal transpiration cannot be relevant. To explain the radiometer, one must focus attention not on the faces of the vanes, but on their edges. The temperature gradient on the surface of the edges, makes gas creep along the surface, as we have previously described. So on the edges, gas creeps tangentially to the warm side,

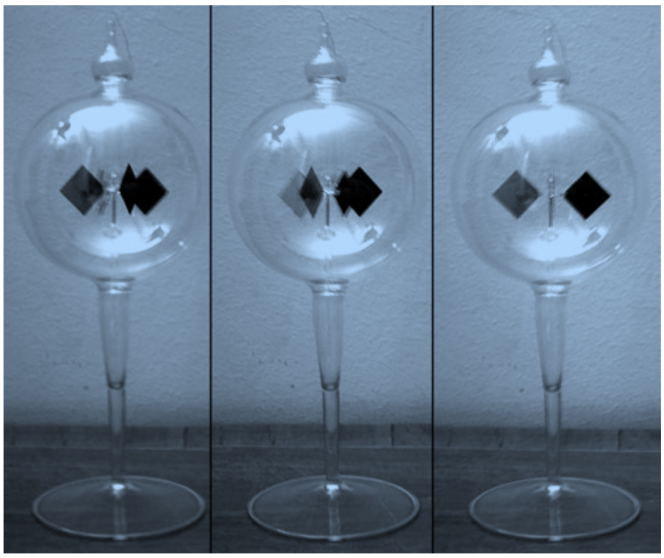

Figure 1.14: *The light mill of Crookes. Image source: public domain.*

which pulls the solid to the cold by reciprocal action. So the mill turns as if the blackened face was moving because of light, but the explanation comes from gas thermo-osmosis and not from radiation pressure.

Chapter 2

Thermophoresis of colloids in aqueous medium

In this chapter, we present the context of colloids in aqueous medium. We will see that the temperature dependences of both Soret coefficient S_T and thermodiffusion coefficient D_T are universal for the systems studied. We will highlight the specificity of protein thermophoresis.

2.1 Position of the problem

As evoked before, modern thermophoresis experiments are often conducted with biomolecules. By biomolecules we mean DNA, proteins, sugars, micelles. Those molecules have in common a size between few nanometers to a few micrometers, i.e. the colloidal range. They feature a complex structure that adapts to water, and are mainly composed of carbon, hydrogen, nitrogen and oxygen atoms. Those systems often have key roles in biological processes. We will also present industrial colloids, such as synthetic polymers, like polystyrene.

Now let us quickly introduce:

- Micelles (see fig. 2.1) are structures made of amphiphilic molecules, that is to say molecules that have both hydrophilic and hydrophobic parts. In general, the hydrophilic area is relatively compact, commonly composed of oxygens, and other groups susceptible to establish hydrogen bonds with water. This is designated as *head*. The hydrophobic part, the *tail*, is commonly a carbon chain. If left alone surrounded by water, this system is frustrated, since the contact hydrophobic tail-water represent an energetic cost. At high concentration of amphiphilic molecules, they can gather in spherical structures, protecting the hydrophobic tails from water and exposing the heads towards the exterior of the micelle.

- Carbohydrates, commonly referred as *sugars*, are biomolecules that holds several roles in biochemistry, such as storage of energy (like starch ore glycogen molecules) or as a structural component (like cellulose in wood). These molecules are polymers. The elementary monomer is called monosaccharide. Glucose or fructose are probably the commonly known monosaccharides. Those are cyclic molecules (see fig. 2.2 for the example of glucose) that connect by a covalent bond called *glycosidic bond* to form polymers.

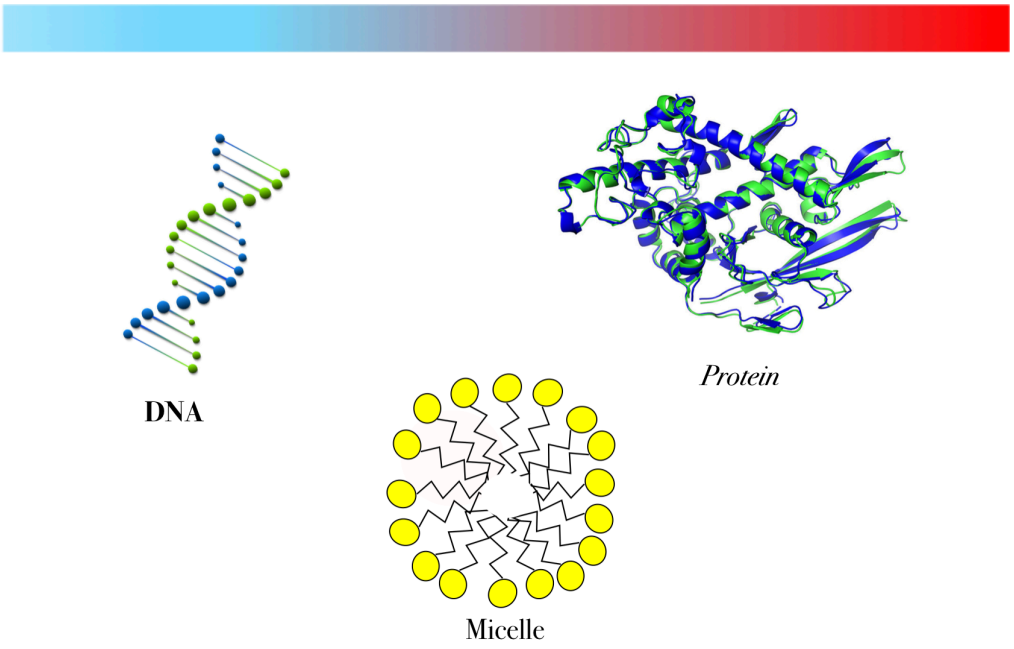

Figure 2.1: *Some examples of studied systems: DNA, micelles and proteins in a temperature gradient. The positions of systems images in the temperature gradient does not indicate the place where molecule tend to accumulate.*

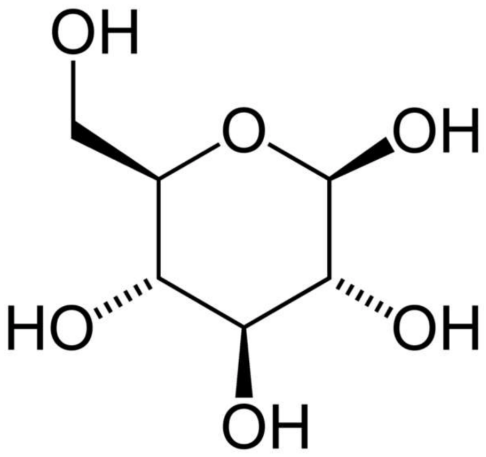

Figure 2.2: *Structure of a glucose molecule. We see the cyclic pattern. Image source: Public domain.*

The assembly of two monosaccharides results in a disaccharide. Sucrose, lactose and maltose are notorious disaccharides. A sugar, deoxyribose is even the starting component of the backbone of DNA, which is another system investigated in thermophoresis experiments.

- DNA (Deoxyribonucleic acid) (see fig. 2.1) is a macromolecule present in almost every cells and virus. It has a famous structure in double helix. The two DNA strands are polymers of *nucleotides*, see figure 2.3. Those monomers are made of three subunit molecules: a nucleobase, a five-carbon sugar and a phosphate groupe. The four nucleobases are A T G C (Adenine, Thymine, Guanine and Cytosine), encoding the genetic instructions.

Nucleotides are connected by a covalent bond between the phosphate group of a first monomer and the sugar of the next one. The two strands are connected to each other via their nucleobases that establish hydrogen bonds between each other, with G-C or A-T pairs. In water, DNA coils into tight loops, and exposes to water different functional groups.

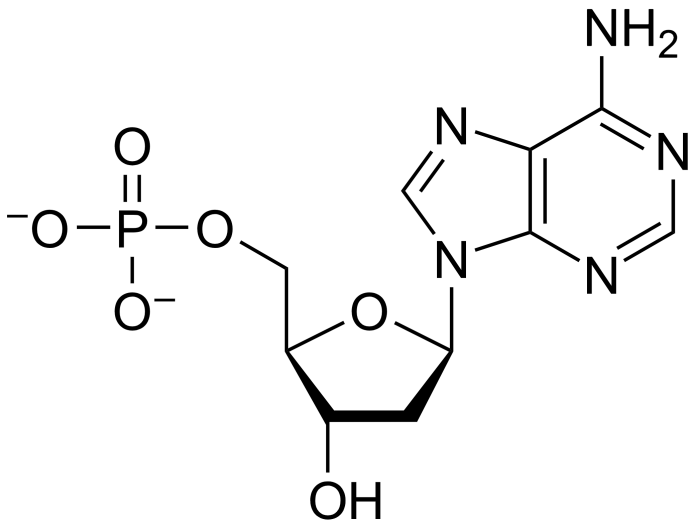

Figure 2.3: *Structure of a nucleotide, the monomer of a single strand of DNA. We identify the five-carbon sugar at the center (deoxyribose), connected to a phosphate group (on the left) and a nucleobase (on the right), here adenine. Image source: Wikipedia.*

- Amino-acids (AA) (see fig. 2.4) are organic molecules that basically bears three components: an acid group, an amine group, and a carbon radical that differs from one amino-acid to another. There are about hundreds different AAs in nature. However, only about twenty are present in proteins, the *L-α-amino-acids* (see fig. 2.4). AAs are the monomers that can be polymerized to synthesize proteins. AAs establish a covalent bond between the carboxyl group of an AA and the nitrogen atom of the other, resulting in a *peptidic* bond. The formed molecules are called *polypeptides*. This denomination is used for polymers of less than a hundred AAs, and the term *protein* is usually reserved for molecules of more than a hundred AAs, yet this definition is arbitrary.

- Proteins are macromolecules, more precisely bio-polymers of about a hundred AAs. In water, under normal conditions of temperature and pH, they coil and adopt a globular shape, with a typical radius of gyration of a few nanometers. This globular structure is determined by the sequence of AAs [49]. This comes from inter AAs interactions, such as hydrogen bonds. Disulfide bonds for instance, are capable of giving the protein a 3D structure that feature a hydrophobic core at the center, the part the less exposed to water. Sometimes sub-structures are present, such as α-helix and β-sheets, stabilized by hydrogen bonding. The overall structure is determined by whether AAs are hydrophilic or hydrophobic, which has drawn the scientific attention [50–56]. More recently (2020), protein folding appeared to be predicted thanks to artificial intelligence [57].

In our work, all those species are in aqueous solution, in dilute regime. So the relationship between the concentration gradient and the temperature gradient will be modeled by eq. 1.3.

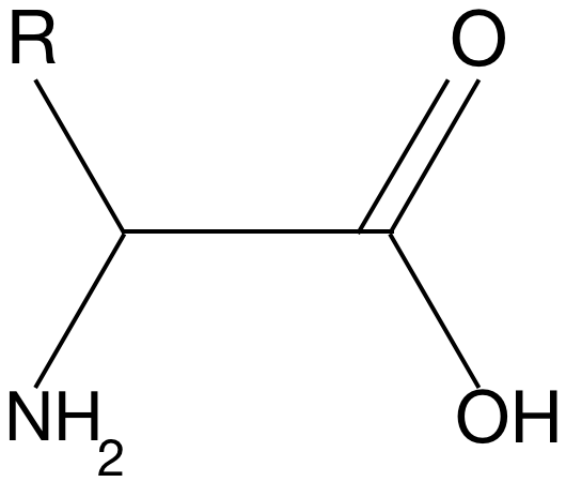

Figure 2.4: *Structure of an α-amino-acid (AA). We identify the COOH group, that makes the molecule an acid, and the carbon in position α bears the amine NH_2 and the radical R, which characterizes every different amino acid.*

2.2 Intriguing dependence on temperature

Here we introduce the central point of our work: the dependence of the thermodiffusion coefficient, D_T, with temperature. In water, this dependence behaves in a way that was not predicted by theories. We see on fig. 2.5 that thermodiffusion coefficient of polystyrene beads in toluene is quasi constant with temperature in the investigated range. However, in water, the Soret coefficient depends significantly on temperature. One can witness a huge difference in thermophoresis if we compare an apolar solvent, such as here toluene, or benzene, to water, which is a polar solvent.

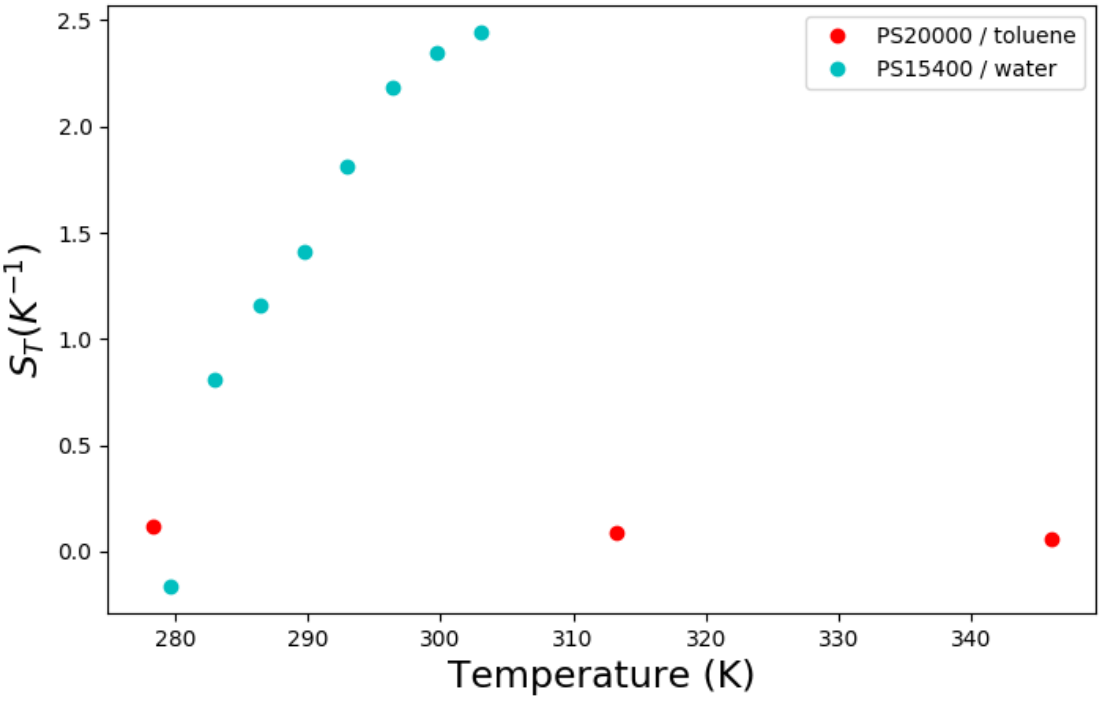

Figure 2.5: *Experimental data for polystyrene in toluene and in water, for different molar weights. Notice that S_T in toluene is decreasing and varies very slowly with T compared to S_T in water. Data from ref. [58] and [7].*

One expects to find $S_T \propto 1/T^2$. Indeed, the thermodiffusion coefficient D_T is predicted to be roughly inversely proportional to the temperature [5], which implies a small variation of S_T over the temperature range considered. We shall introduce polystyrene. Polystyrene (PS) is a synthetic polymer obtained by polymerization of styrene (see fig. 2.6), resulting in long chains of about some hundreds of units. The molecules have a typical radius of 30 nm.

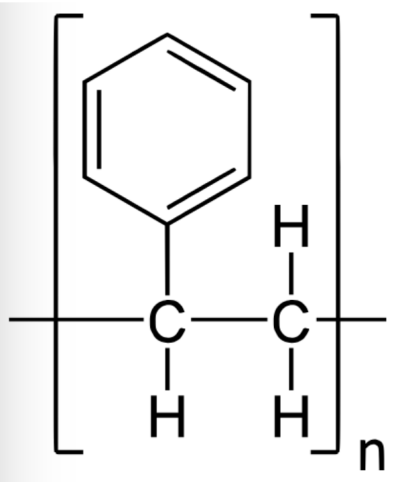

Figure 2.6: *Polystyrene. We can see the monomer styrene with the aromatic cycle.*

A striking feature that can notably be observed on fig. 2.5 is the sign change of S_T in water at lower temperatures. Caldwell [59] also studied thermophoresis of salts in 1973. In good agreement with Soret's observation, he observed a positive thermophoresis for salts solutions at room temperature. However, if Soret would have performed his experiments at lower temperatures, he would have observed a different behavior, as we can see it on fig. 2.7. Indeed, if the average temperature is below a temperature threshold, the Soret coefficient becomes negative.

This sign change of S_T with temperature is the central question of this work. One could think that the sign of the Soret coefficient would be utterly system dependent: in gases, for aerosols the Soret coefficient is positive; while polyvinyl alcohols [60] and poly-ethylene oxide [61] in water were reported to have a negative Soret coefficient. Thermophoresis's direction has sometimes been qualified of *erratic* or *unpredictable* [7, 62]. But we see that the value of temperature itself can change the direction of the thermophoresis. The thermophoresis can be tuned in some cases from thermophobic behavior to thermophilic by simply decreasing the temperature.

Piazza *et al.* have investigated the thermophoresis of several colloidal systems, and provide the image of *macromolecular tourists*. Suspended particles act like a vacationer (or a migrating bird): "when it is hot, they drift to colder regions, while when it is cold, they look for warmer places" [7].

Piazza and coworkers [8] notably studied thermophoresis of egg-white lysozyme, a globular protein of about 130 amino-acids present in egg-white. They observed a characteristic concave curve for the evolution of thermophoresis with temperature, as displayed on fig. 2.8, and fit the data for the temperature dependence of S_T with the equation:

$$S_T(T) = S_T^{\infty}\left(1 - \exp\left(-\frac{T - T^*}{T_0}\right)\right). \tag{2.1}$$

S_T^{∞} the high temperature value, T^* the sign change temperature, and T_0 an amplitude that

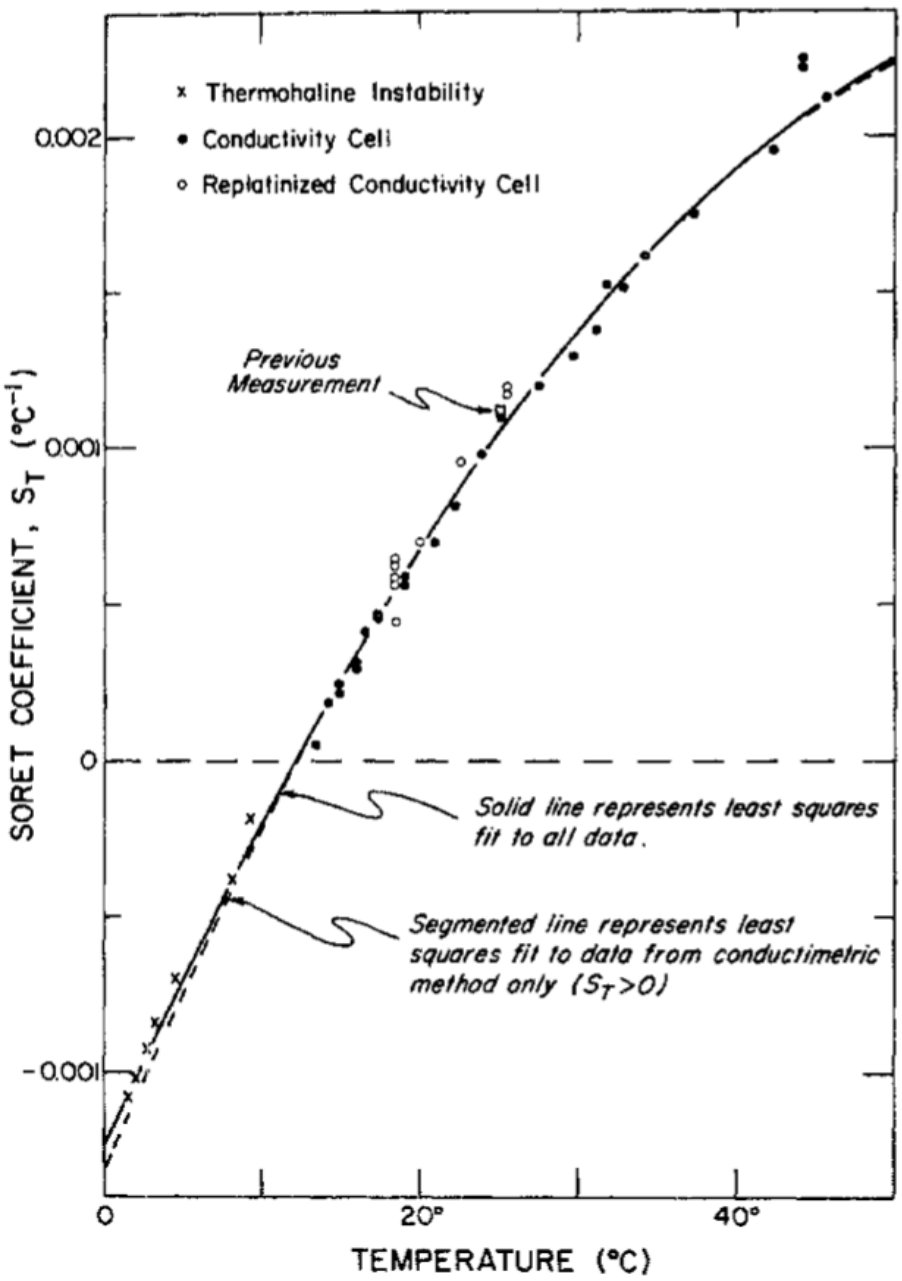

Figure 2.7: *Soret coefficient for some salt solutions. This study confirms Soret and Ludwig observation of a positive thermodiffusion at room temperature. However we observe in a certain range of temperatures a negative thermophoresis. Image taken from ref. [59].*

embodies the temperature effects [8]. It is worth noticing that T_0 sets a characteristic energy scale $k_B T_0$ which is about 5 to 10 percents of the thermal energy. Piazza's work also indicates that the sign-switching temperature T^* is surprisingly always about 20 °C for polypeptids and DNA, but about 5 °C for PS and NaPSS (Sodium Polystyrene Sulfonate, a molecule with a structure similar to PS), so these molecules virtually always display $S_T > 0$. One should note that these values indicate the strong thermophilic behavior of DNA at 4 °C, just like marine deep-water temperature, compatible with the idea provided before that hydropores can concentrate DNA evoked in chapter 1. Eq. 2.1 is however an empirical function, which is not based on any theoretical model.

Piazza *et al.* show that this temperature dependence is universal for a large class of macromolecular and colloidal systems [7], as we can observe it on fig. 2.8: polypeptides, such as

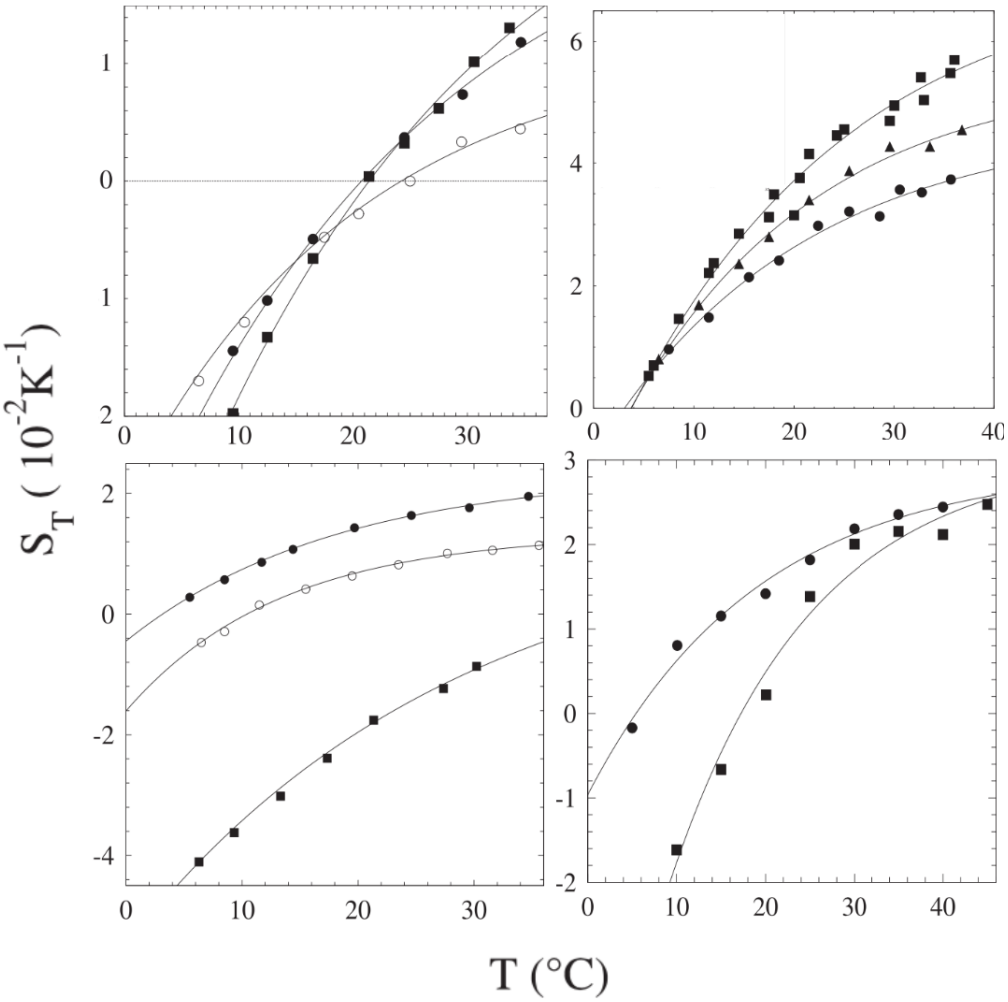

Figure 2.8: *Experimental data for S_T vs T for various systems. Upper left: Polypeptides: BLGA (black dots), PLL (squares), and lysozyme (open dots); upper right: NaPSS for different molar weights: M_W = 15200 g/mol (dots), M_W = 32 900 g/mol (triangles), M_W = 74 000 g/mol (squares); bottom left: pure SDS micelles (black dots), DM micelles (squares), mixed micelles of an equimolar mixture SDS/DM (open dots); bottom right: PS (dots) and DNA (squares). From ref. [7].*

lysozyme, β-lactoglobuline-A (BLGA),and poly-L-lysine (PLL), polymers like NaPSS and PS, micelles, and DNA.

Since $S_T = D_T/D$, the sign change observed for S_T must be related to the temperature dependence of D_T. On fig. 2.9 we can observe the temperature dependence of D_T for the same systems. $D_T(T)$ is linear for all systems studied, despite their differences in nature.

So the thermodiffusion coefficient D_T can be expressed:

$$D_T(T) = A(T - T^*), \tag{2.2}$$

with A a system-dependent amplitude, and T^* the same sign switching temperature observed with $S_T(T)$. A has the same order of magnitude for PS, SDS or NaPSS despite the large size difference between colloids. This observation is confirmed by other groups [14, 63].

We have highlighted so far two striking behaviors for colloids in water: the Soret coefficient displays a sign change at a temperature T^*, and the thermodiffusion coefficient is linear with temperature. Those rather universal behaviors adopted by various macromolecular and particle

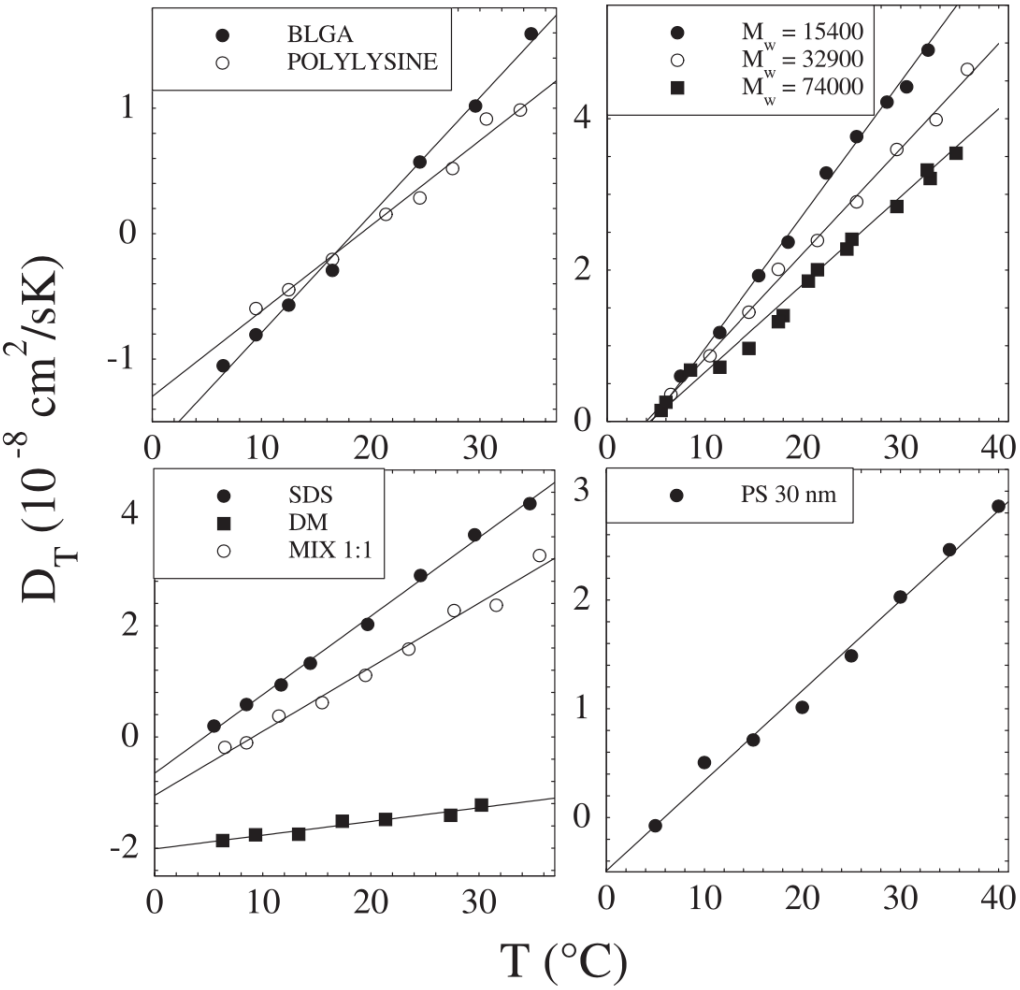

Figure 2.9: *Strikingly linear dependence of D_T on temperature, observed for different classes of systems: polypeptides (upper left graph), NaPSS (upper right), SDS/DM micelles (lower left) and polystyrene latex particles (lower right). Full lines are linear fits to the data. From ref. [7].*

suspensions suggest common origins.

2.3 Dependence on molecular weight

We present the impact of the molecular weight (and the size) of the solute on Soret and thermodiffusion coefficient. We illustrate this with the example of a molecule already mentioned, the NaPSS. Sodium Polystyrene sulfonate (see fig. 2.10) is a polymer with a large hydrophobic group (the aromatic cycle) and an ionic group composed of sulfur and oxygen. Its elementary motif is composed of styrene with a sulfonate group. We see on fig. 2.8 that S_T is always positive. This observation, and the fact that NaPSS is poorly hydrophilic will be discuss later.

We see on fig. 2.8 that the Soret coefficient increases with the molar weight. On the other hand, T^* and T_0 in eq. 2.1 are weakly affected by NaPSS molecular weight [7], which mainly influences the high temperature limit S_T^∞. The Soret coefficient is found for polymers to be proportional to the square root of the molecular mass [64]. Since for polymers the radius of gyration is proportional to the square-root of the polymerization degree (and *a fortiori* the molar mass), S_T in the long-chain regime is proportional to the radius of the colloid. With $D_T = S_T D$, it is expected that D_T does not depend on colloid size. Indeed, for a given polymer-

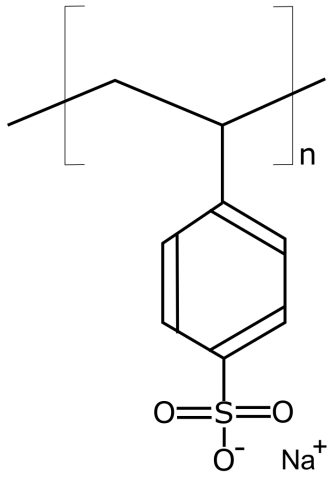

Figure 2.10: *Sodium Polystyrene sulfonate.*

solvent system, D_T is essentially independent of the polymer molecular weight [12,26,27,65,66]. As we have evoked it with relation 2.2, the amplitude remains of the same order of magnitude for the different systems, despite the large disparity in colloids size.

Stadelmaier *et al.* [67] have investigated the Soret effect for different lengths of polystyrene in different solvent. A first remarkable result (see fig. 2.11) is that for a typical size of the polymer, D_T becomes constant with respect to the molar mass, independently of the solvent. Another feature is that the short-size regime D_T increases with the molar mass. This result is confirmed by other studies [68]. The thermodiffusion of polymer is independent from length of chain and branching configuration. This implies that the polymer chain moves at the same velocity as an individual monomers units, at least for homopolymers, that is to say a polymer made of only one kind of monomer [69].

So thermodiffusion of colloids does not depend on their size for most systems studied.

2.4 Electrical effects from the solvent

Now we evoke the effects of ions in the solvent, with the ionic strength and the pH. We display two very different cases: thermophoresis of micelles and thermophoresis of proteins.

The ionic strength I is a quantity that characterizes the concentration of all ions present in a solution, taking into account the electrical charge carried by the ions in solution. It is defined as $I = \frac{1}{2}\Sigma_i c_i z_i^2$, z_i is the ion charge of the salt and c_i is the salt concentration, for each ion i. We illustrate the situation with Sodium dodecyl sulfate (SDS). SDS is an anionic surfactant featuring a C_{12} carbon tail (See fig. 2.12). Ìt is broadly used as a component for engine cleaning, but can be found in shampoos or soaps. If the concentration of SDS molecules is superior to the critical micelle concentration, it assembles in charged micelles with typical radius of about 2.5 nm [62]. SDS is virtually always thermophobic (S_T positive) as we see on fig. 2.13, because its T^* is relatively low, between 0 and 5 °C.

Piazza and Guarino [9] have studied thermophoresis of SDS solutions. Here the temperature was fixed at 25 °C, and the surfactant concentration was varying between 2.5 and 25 g/L (equivalent to a mass fraction of 0.25 to 2.5 percents).

We can also see on fig. 2.13 a key parameter for the thermophoresis of charged micelles.

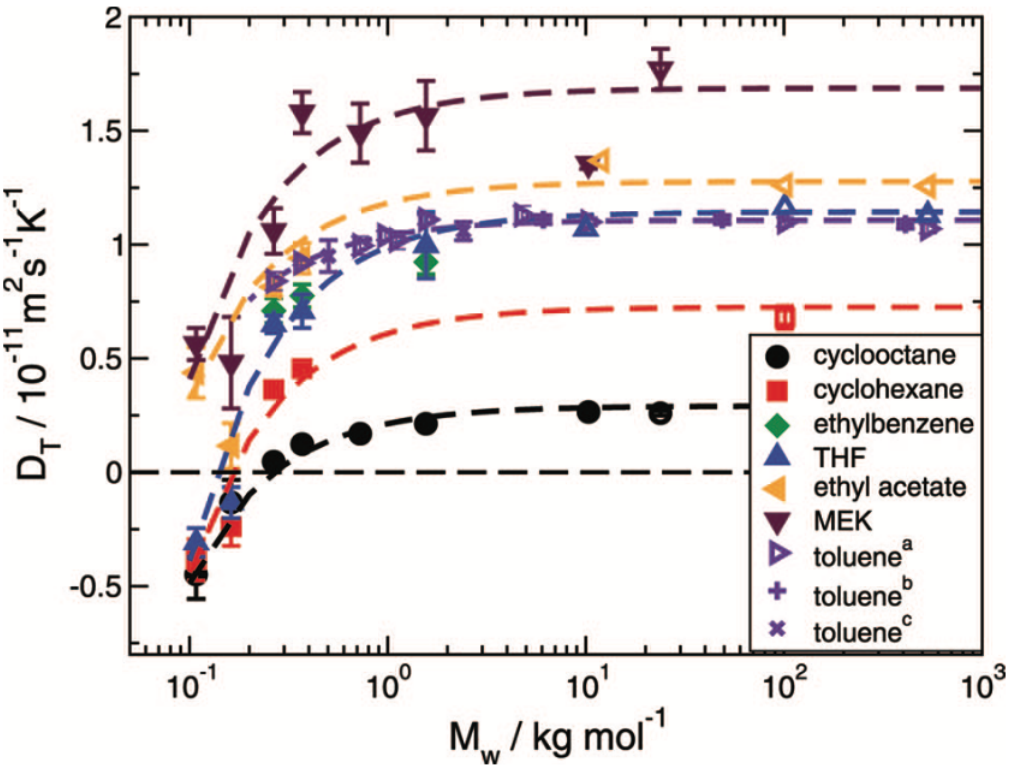

Figure 2.11: *Thermal diffusion coefficient D_T as a function of molar mass for PS in different solvents at the constant $T = 295$ K. From ref. [67].*

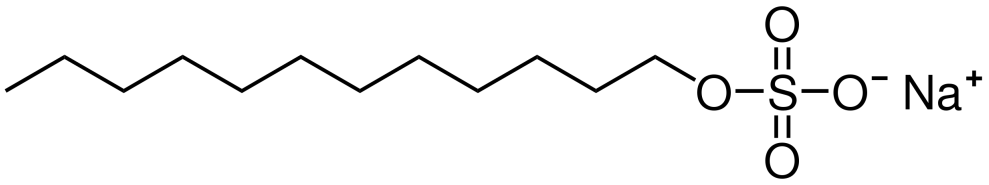

Figure 2.12: *Sodium dodecyl sulfate (SDS).*

Indeed, in the dilute regime, Piazza and Guarino have shown [9] that the Soret coefficient of SDS solutions strongly decreases with the solution ionic strength. Fig. 2.14 shows the evolution of the inverse of the Soret coefficient as a function of SDS concentration for different NaCl concentrations added in solution. As shown in the figure, the Soret coefficient increases with an increase of added salt. It increases at low NaCl concentration, but decreases at high NaCl concentration. In their work, SDS is always assembled in micelles, and the concentration is the one of micelles.

The inverse Soret concentration is linear with the solute concentration, and by taking into account both single particle effects and collective effects, it can be expressed [9]:

$$S_T = \frac{S_T^0}{1 + k_s c}. \tag{2.3}$$

$1/S_T^0$ is the intercept on fig. 2.14. Since it does not depend on the concentration c of molecules, it embodies the single particle behavior. k_s is the ratio of the slope and the intercept, and scales as the inverse of the ionic strength. We can see on fig. 2.14 that the intercept $1/S_T^0$ is modified by the addition of salt, being multiplied by an order of magnitude when changing

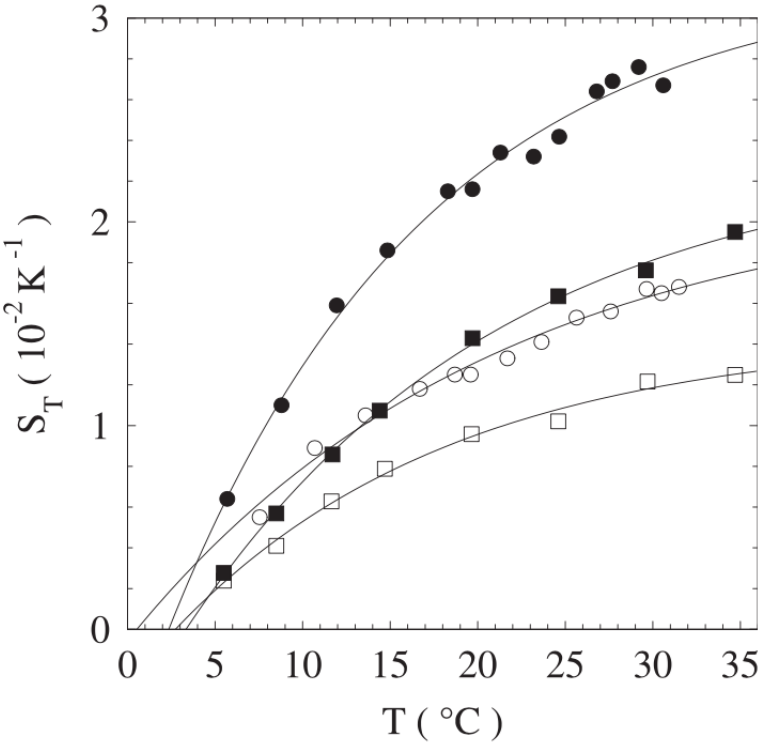

Figure 2.13: *Temperature dependence of the Soret coefficient S_T for SDS ionic micelles at concentration c = 10 g/l (full symbols) and 20 g/l (open symbols), in the presence of 10 mM (squares) and 20 mM (circles) NaCl. Image from ref. [7].*

the NaCl concentration from 10 to 500 mM. This indicates that when the ionic strength is reduced, the Soret coefficient increases significantly. Electrostatic interactions appear to play a crucial role in micelles thermophoresis. Indeed, S_T^0 depends on the ionic strength. On fig. 2.15 we can see that S_T^0 scales as the square of the Debye-Hückel length, which is a screening length in aqueous solutions caused by the presence of ions. It depends on solvent properties such as dielectric permittivity or ionic strength: $\lambda_{DH} = \left(\frac{\epsilon k_B T}{2I}\right)^{1/2}$. At the individual micelle scale, the Soret effect increases with the Debye-Hückel screening length.

However, interactions between micelles exert an opposite effect. The denominator in eq. 2.3 is proportional to the inverse of the ionic strength. Repulsive electrostatic interactions between particles oppose the emergence of concentration gradients, so S_T decreases by increasing SDS concentration. Adding salt reduces those interactions and increases the collective contribution to thermophoresis. Fig. 2.14 shows that even at low SDS concentration, the trend gets totally reversed, and S_T now increases with salt concentration, as highlighted on fig. 2.13.

Now we must compare with the situation of proteins thermophoresis. As already mentioned, the motion of proteins can be tuned from thermophobic to thermophilic by setting the temperature below T^* (about 20 - 25 °C for a lot of polypeptides, as one can see on fig. 2.8. This feature was not observed with SDS micelles, which remained thermophobic.

Lysozyme received a lot of attention in the early 2000's once again from Piazza and coworkers [7, 8, 62]. It was one of the first observation of a molecule which, for a fixed system (solvent composition constant), features this dual thermophoretic behavior that can be either thermophobic or thermophilic depending on the temperature. Fig. 2.16 and 2.17 show that the dependence on the ionic strength is weaker than in the case of SDS micelles.

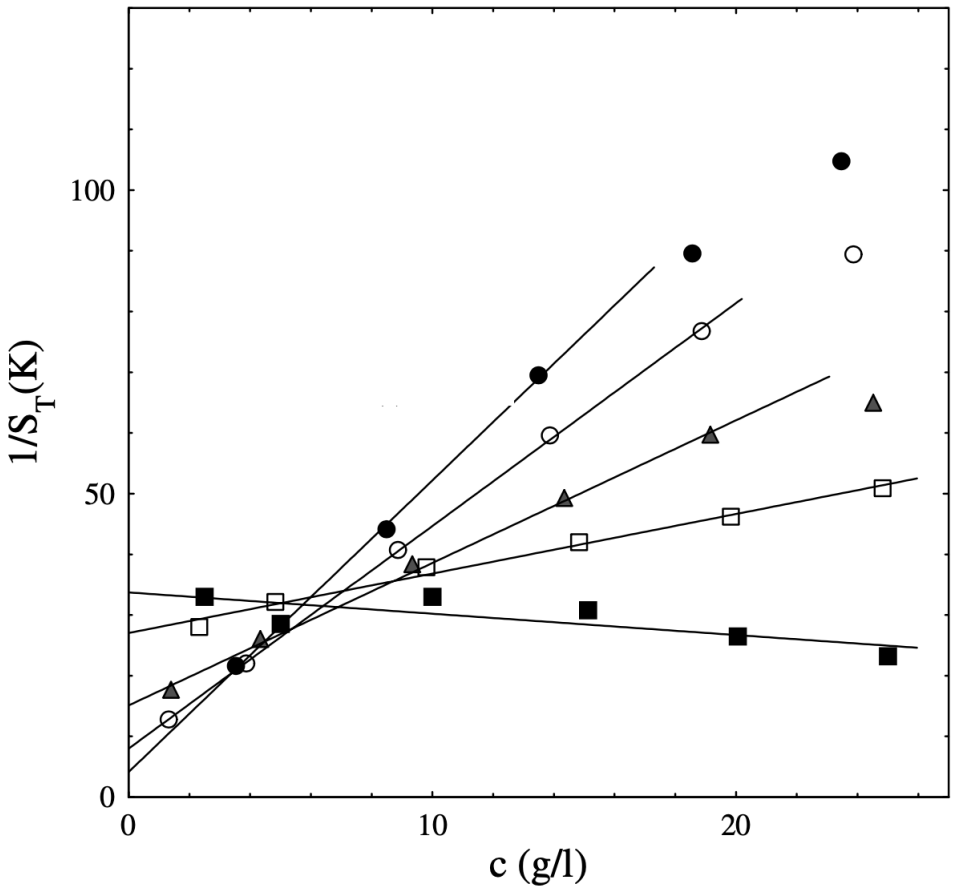

Figure 2.14: *Reciprocal Soret coefficient S_T versus SDS concentration in the presence of 10 (full circles) , 20 (hollow circles), 50 (triangles), 200 (empty squares), and 500 mM (full squares) added NaCl concentration. Fig. from ref. [9].*

We can see that T_0 and S_T^∞ display a decrease with the ionic strength [8], and T^* barely changes. Despite multiplying the NaCl concentration by a factor 40, the temperature dependence of the Soret coefficient of lysozyme is not significantly affected. The evolution of S_T with the ionic strength can be immediately observed on fig. 2.17, in which it is plotted for two different temperatures. The curve of positive value is at 35 °C, the behavior is definitely thermophobic. The curve of negative value is at 5 °C, where lysozyme is thermophilic. We see that there are no notable effects for $I > 0.1$ M. Protein thermophoresis experiments are usually performed in *salting-out* conditions, that is to say with a concentration of salt that is high enough to prevent solubilization of proteins. Otherwise some effects appear at low ionic strength (< 100 mM) [10].

One could think that pH can hold a role. Like a lot of proteins, lysozyme feature a *zero point charge* (ZPC), that is to say the net charge carried by the molecule depends on pH. For a pH inferior to the ZPC, the charge is positive, since the solvent is acid and can give protons to the molecule. If the pH is superior to the ZPC, the protein bears a negative charge, since the solvent has taken protons from the protein surface. So one can expect lysozyme thermophoresis to depend on pH. Moreover, the dependence of thermophoresis on pH has been reported [70] for PS spheres with different surface functionalities.

Parameters T_0 and S_T^∞ display a dependence on pH, as we can see on the inset of fig. 2.18. T^* on the other hand remain constant with respect to pH. This variation is barely observable

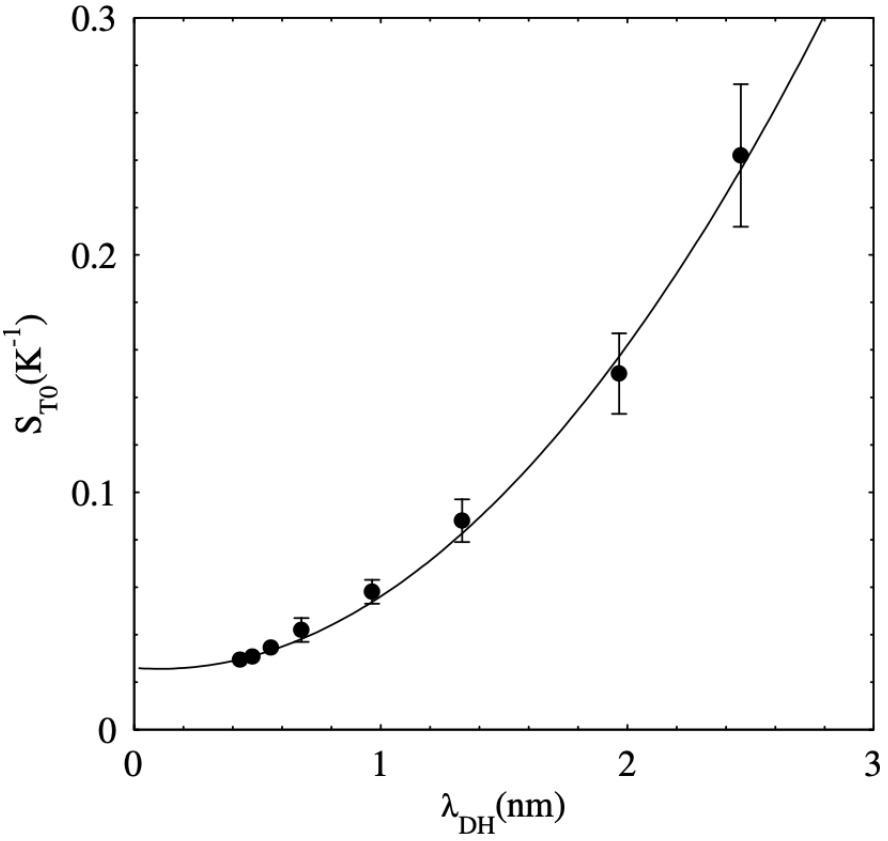

Figure 2.15: *Single-particle Soret coefficient S_T^0 as a function of the Debye-Hückel screening length. Image from ref. [9].*

as we consider the overall thermophoretic behavior. As we can see on fig. 2.18, in the pH range from 3 to 9.3, with every other parameters fixed, the curve $S_T(T)$ seems to be only shifted vertically, and the shape of the curve is not modified.

The electrical charge carried by the protein, tuned by the change of pH, does not seem to be a major parameter for the lysozyme thermophoresis. Putnam *et al.* [71] also reported that changing the formal charge of lysozyme using mutants of the protein does not change much its thermophoretic behavior. Finally, the crucial temperature dependence of S_T on one hand, and the weak sensitivity to ionic strength and particle charge on the other lead to think that unlike charged micelles, the overall features of lysozyme thermophoresis are not set by electrostatic forces.

Now that we have presented the context of the experimental observation of both Soret and thermodiffusion coefficients, that displays unexplained behaviors notably for proteins, we offer to introduce theories developed to explain thermodiffusion in different contexts, that enabled a better understanding of thermodiffusion.

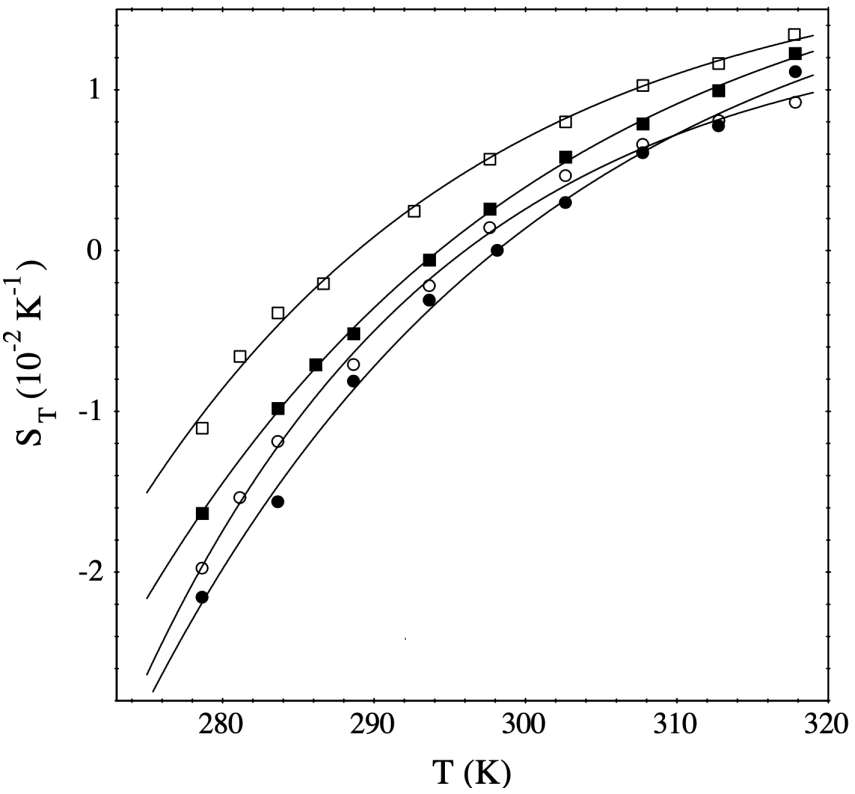

Figure 2.16: *Soret coefficient vs temperature for c = 7 g/l lysozyme solutions at pH = 4.65, in presence of 7.5 (white squares), 20 (black squares), 100 (black dots), and 400 mM (white dots) NaCl. Adding NaCl screens electrostatic interaction, yet does not modify the concave behavior of $S_T(T)$. Taken and adapted from ref. [8].*

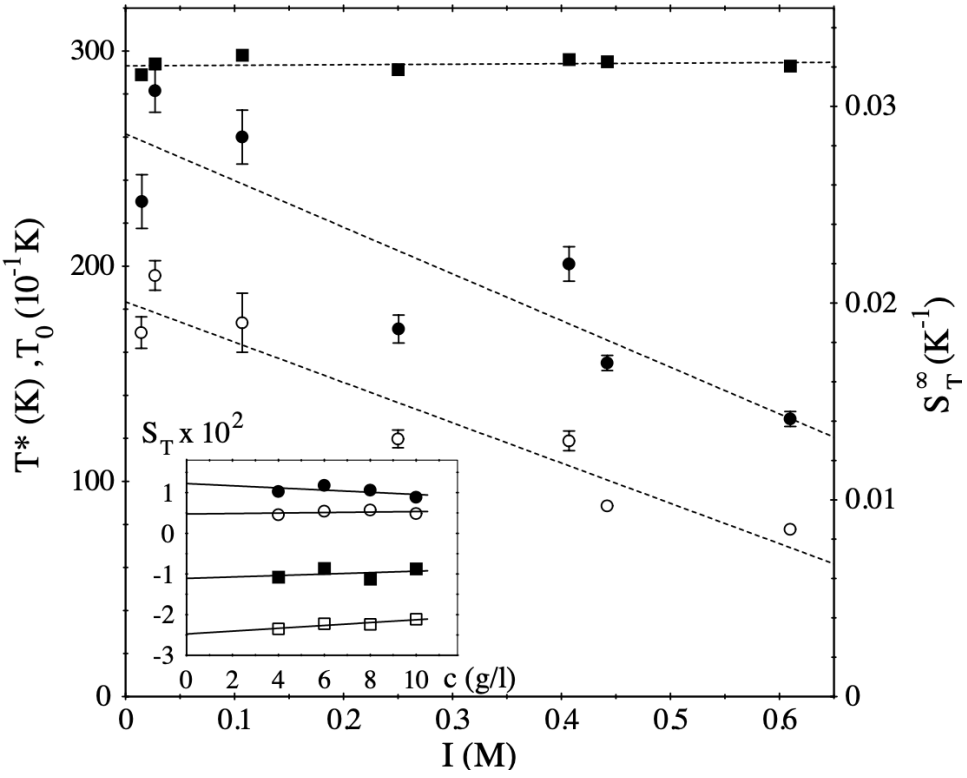

Figure 2.17: *Parameters of equation 2.1: T_0 (full dots, left axis), T^* (squares, left axis), S_T^∞ (open dots, right axis), evolution with ionic strength I. Inset: concentration dependence of S_T at T = 35 (circles) and 5 °C (squares) in presence of 7 (full symbols) and 100 mM (open symbols) NaCl. Taken from ref. [10].*

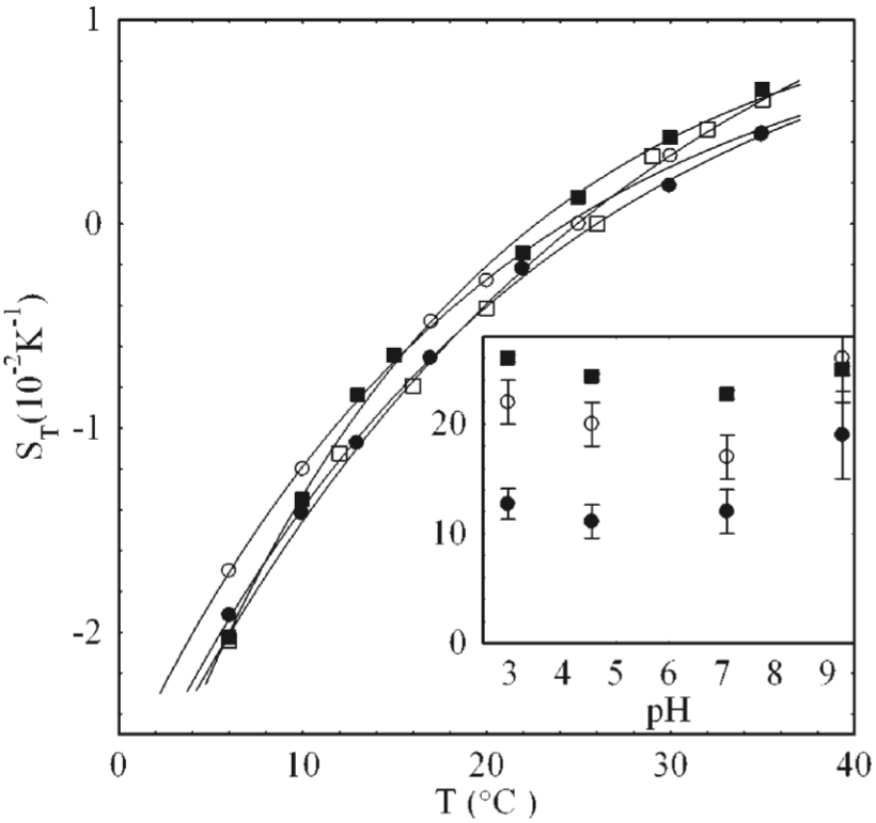

Figure 2.18: *Temperature dependence of S_T for c = 10 g/L lysozyme solutions at pH = 3 (full dots), 4.55 (open dots), 7.1 (full squares) and 9.3 (open squares), fitted with eq. 2.1. Inset: pH dependence of T^*, T_0 and S_T^∞ fitting parameters of eq. 2.1. Image taken from ref. [7].*

Chapter 3

Elements of Theoretical Understandings of Thermophoresis

Here we expose theories developed to explain different experimental observation of thermophoresis. First, we explain the case of gaseous medium, presenting Maxwell's work that highlighted the existence of a creep velocity at a solid surface in a temperature gradient. Then we present *thermo-osmosis* in the boundary layer in liquids, and display theories developed for thermophoresis of charged particles, that successfully explain the thermophoretic motion in some cases.

3.1 Resort to gas kinetics theory to explain thermodiffusion in gases

In his article of 1879, Maxwell [4] aimed at explaining Crookes' *radiometer* [47] and Reynolds' work [3] on *thermal transpiration*. Reynolds's method established the existence of the phenomenon, and Maxwell wanted to be quantitative. In an homogeneous gas, in volume, a temperature gradient does not result in a drift velocity of gas molecules. But in presence of solid surface a creep flow appears, what we call in modern language *thermo-osmosis of gases*.

3.1.1 Corrected distribution of velocities

The method used by Maxwell is purely statistic, it never attempts to trace the motion of a molecule. The attention is on average values of velocity components. A major assumption here is that the space-variations within distances comparable to the mean free path are small enough to allow limited developments. We define the mean free path:

$$\ell = \tau v_T, \tag{3.1}$$

$\tau = \frac{\mu}{P}$ being the relaxation time of the medium due to elastic collisions between molecules, and $v_T^2 = \frac{k_B T}{m}$ the thermal mean value of each component. μ is the viscosity of the gas, P the pressure, and m is the gas molecular mass. τ is supposed independent from temperature [72].

The properties of the medium are supposed constant over distances comparable to the mean free path. So, the number density of gas n, as well as the mass density $\rho = mn$, are supposed constant in all calculations led here. In this section ξ, η, ζ are reversely components of velocity

along x, y, z in the frame of the center of mass of the gas. In equilibrium, in a homogeneous gas, the velocities follow the Maxwellian distribution p_0, which is gaussian:

$$p_0(\xi,\eta,\zeta) = \frac{1}{\sqrt{2\pi v_T^2}^3}\exp\left(-\frac{\xi^2+\eta^2+\zeta^2}{2v_T^2}\right), \tag{3.2}$$

The mean values in equilibrium $<\xi>_{eq}$,$<\eta>_{eq}$ and $<\zeta>_{eq}$ are all zero, as the center of mass of velocity (u, v, w), the gas is at rest.

But out-of-equilibrium, in presence of a temperature gradient, the pdf is no more p_0 and must account for dissipative processes induced by the temperature gradient. It becomes $p(\xi, \eta, \zeta, y, T)$, the non-equilibrium pdf in the bulk. Maxwell worked in an elementary volume of gas $dxdydz$, located at a given position y at the temperature T. He supposed that p only depends on velocity components (which depend implicitly on spatial coordinates). The exponential in the pdf in eq. 3.2 is now supposed to feature extra terms proportional to the temperature gradient, arising from correlations between η and the other velocity components. For a temperature gradient applied along y, in the stationary regime:

$$\begin{aligned} p(\xi,\eta,\zeta) = \frac{1}{\sqrt{2\pi v_T^2}^3}\exp\Bigg(&-\frac{\xi^2+\eta^2+\zeta^2}{2v_T^2} + \frac{1}{v_T}C_{010}\eta \\ &+\frac{1}{v_T^3}\left(C_{210}\frac{\xi^2\eta}{2!} + C_{030}\frac{\eta^3}{3!} + C_{012}\frac{\eta\zeta^2}{2!}\right)\Bigg). \end{aligned} \tag{3.3}$$

Maxwell has limited this development to the third order. The dimensionless coefficients C_{XYZ} are all proportional to the spatial derivatives of the temperature. The indexes refer to the powers of the components (*eg* C_{012} weighs the $\eta\zeta^2$ term). F denotes the sum of the corrections in the exponential in eq. 3.3. Since the gradient is supposed relatively small, its successive powers are all neglected, F is small compared with unity. Eq. 3.3 is linearized:

$$p(\xi,\eta,\zeta) = (1 + F(\xi,\eta,\zeta))p_0(\xi,\eta,\zeta). \tag{3.4}$$

The temperature inhomogeneity's impact lies now in this correction factor $1 + F$. In equilibrium, there is no correlation between the different velocity components: all the C are zero, so does F. Eq. 3.4 is fully consistent with expressions findable in other works [73, 74]. which suggest at first order $F = k\eta\left(\frac{5}{2} - \frac{m(\xi^2+\eta^2+\zeta^2)}{2k_BT}\right)$, with k the normalization constant that we find to be: $k = \frac{3}{2}\frac{\mu}{TP}\frac{\partial T}{\partial y}$.

To find the mean values of any function of ξ, η, ζ, or any quantity Q combination of those for the molecules in the elementary volume, one must multiply this function by p, and integrate over the right domain of ξ,η, ζ. The mean value of Q is thus:

$$\langle Q\rangle = \iiint d\xi d\eta d\zeta\, p\, Q. \tag{3.5}$$

This allows to compute all correlation functions between velocity components. The method used by Maxwell to determine the coefficients C is presented in Appendix A. However, we still find that even out-of-equilibrium $\langle\eta\rangle = 0$ in the bulk. But a different situation occurs in presence of a solid surface, leading to a creep flow of gas toward the hotter places.

3.1.2 Model for the solid surface

The following is the computation of relations between mean values engaged in the gas-surface interaction, which makes directly emerge the expression of the creep velocity. The model developed by Maxwell takes place in the frame of small Knudsen numbers, that is to say when the mean free path of gas molecule is small before the characteristic length of the system. We have seen that the solid surface of a micro-channel holds the role of the surface of a solid particle suspended in a gas. So the characteristic length here is the radius of the solid particle, infinite in the case of the wall of a micro-channel, which makes the small Knudsen number regime appropriated.

Now the elementary volume $dxdydz$ of gas considered previously is in contact with a solid surface. The temperature gradient is parallele to this surface, which is a plane yz. We present the solid surface that will experience collisions from the gas, as modeled by Maxwell. The surface is not specular, that is to say an incident molecule is repealed in a random direction. To account for this, Maxwell chose to mixture between two opposite configurations: the surface perfectly reflects a portion $1-f$ of incident molecules of gas hitting it, and adsorbs and reemits a portion f, as illustrated on fig. 3.1. Maxwell showed previously that a perfectly reflecting surface (specular reflexion) cannot lead to a tangential stress, since the tangential difference of momentum is systematically zero for every molecule. Mixing the two situations should result in a equiprobable non-specular reflecting surface. Thus, on average, after collision, the tangential velocity of a gas molecule is zero.

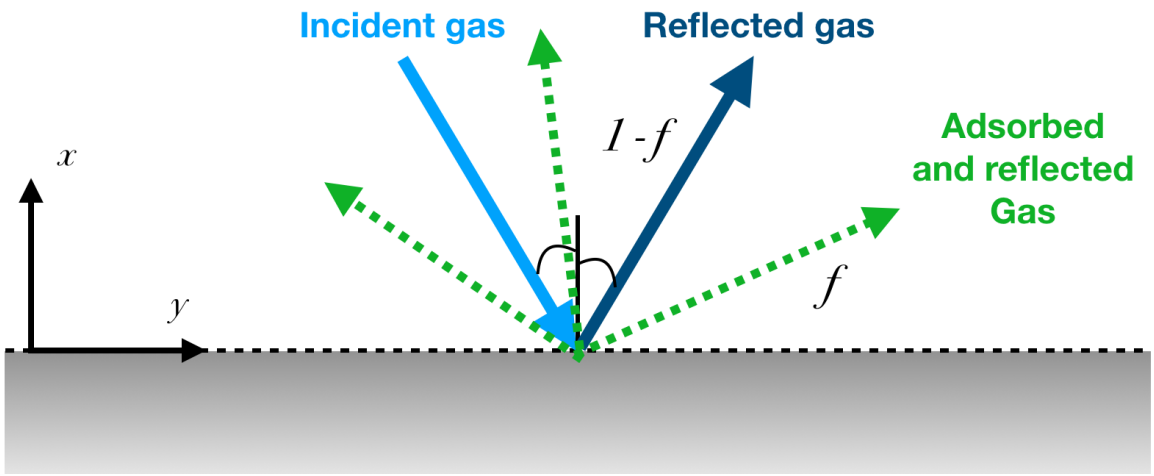

Figure 3.1: *Surface experiencing gas collisions. A fraction f is absorbed, and a fraction $1-f$ is perfectly reflected. The adsorbed molecules hits the network of solid molecules and thermalize with the solid surface, then they are evaporated and released to positive x.*

The fraction f of gas that is adsorbed has on appearance the same properties as if it was coming from the inside of the solid. This "gas" is called *adsorbed and evaporated gas*. Those molecules are at rest, have the temperature of the solid and their density is so that the incoming number of particles of gas hitting the surface per unit of time is equal to the absorbed gas leaving the surface. This enables to recover the conservation of the current of mass, expressed by eq. 3.7. Molecules are reemitted without memory of the incoming state.

Incident molecules are in the region $x > 0$, and are denoted with an index 1. For them, and only them, ξ is negative. Rebounded molecules (reflected and evaporated) are referred with an index 2, their ξ is positive. The *adsorbed and evaporates* molecules bear an index 2 and an

apostrophe, and no index refers to any molecule from the whole gas.

We must remember, however, that since there is a discontinuity at the surface, the expression for the pdf in eq. 3.4 does not fit as well the gas close to the surface than in the bulk. Maxwell's approach of the behavior of the gas at the boundary is thus an approximation. A treatment pointed out by Würger is to modify the pdf $\hat{p}(\xi, \eta, \zeta)$ in the boundary layer of gas, with the bulk pdf $p(\xi, \eta, \zeta)$ presented earlier for incident and reflected molecules, and the gaussian pdf p_0 for adsorbed molecules that have thermalized with the solid. For this, it is useful to consider the gas immobile and the surface moving with the velocity $-v$. This way, the pdf can be adapted:

$$\begin{aligned} \hat{p}(\xi, \eta, \zeta) &= H(-\xi)p + (1-f)H(\xi)p + fH(\xi)p_0 \\ &= (1 - H(\xi))p(\xi, \eta, \zeta) + fH(\xi)p_0(\xi, \eta - v, \zeta), \end{aligned} \tag{3.6}$$

where H is the Heaviside function. For our work, we have proceeded as Maxwell suggested by integrating over the right domain for ξ and approximating that the pdf is p in any case [4]. The same result is obtained by taking into account the perturbation in the pdf brought by the boundary.

3.1.3 Computation of the creep velocity

Maxwell computed the mass current, and did the same with the current of momentum. He aimed at linking the mean incident momentum along y to the mean leaving momentum along y. Note that density and velocity-components are independent. So, averaging with the pdf p with eq. 3.5 is independent from density, so ρ can be factorized, and then simplified. The mean incident quantity of gas, namely the current density of mass, is thus $-\rho \langle \xi \rangle_1$. This quantity is divided between reflected molecules and evaporated molecules. By conservation of number of molecules, we must have on average: $-\langle \xi \rangle_1 = \langle \xi \rangle_2$. Now we link incident and evaporated molecules. All absorbed molecules are evaporated. So, simplifying by f and ρ, we get:

$$\langle \xi \rangle_1 = -\langle \xi \rangle'_2 . \tag{3.7}$$

This expression is the consequence of the conservation of the current density of molecules. Absorbed molecules are all evaporated, there is no accumulation. Thus, for rebounding molecules (index 2), we get:

$$\langle \xi \rangle_2 = -(1-f)\langle \xi \rangle_1 + f \langle \xi \rangle'_2 . \tag{3.8}$$

Eq. 3.8 indicates the contributions of the rebounding molecules from reflection and absorption. The mean current of momentum in the y direction (tangential to the surface and parallel to the temperature gradient) from the incident gas is $\rho \langle \xi\eta \rangle_1$. Since impacting molecules are not specularly reflected (outgoing molecules have a partially random momentum distribution, due to thermalization with the surface), each molecule transfers a momentum to the wall. In the following, we compute this average transfer of momentum. We have $< \eta >= -v$, which is namely the velocity of the surface with respect to the gas in contact with it (the opposite of the velocity of the center of mass).

Following the same procedure than for eq. 3.8, the computation of the current of momentum leaving the surface along y, $\rho \langle \xi\eta \rangle_2$, after simplification with ρ, leads to:

$$\langle \xi\eta \rangle_2 = -(1-f)\langle \xi\eta \rangle_1 - fv\langle \xi \rangle'_2 . \tag{3.9}$$

Inserting eq. 3.7 in eq. 3.9, and simplifying the terms from adsorbed and evaporated gas, we get:

$$(1-f)\langle \xi\eta \rangle_1 + \langle \xi\eta \rangle_2 + v[\langle \xi \rangle_2 + (1-f)\langle \xi \rangle_1] = 0. \tag{3.10}$$

Eq. 3.9 now links correlations functions and the creep velocity of the gas. Then we must compute all the correlation function in eq. 3.9.

The mean values $\langle \xi \rangle_1$ and $\langle \xi \rangle_2$ are obtained by integrating $\xi p(\xi, \eta, \zeta)$ according to eq. 3.5 over the right domain: for incident molecules (index 1) ξ from $-\infty$ to zero, η and ζ from minus to plus ∞; for rebounding molecules (index 2) ξ between 0 and ∞. Same process for the quantities $\langle \xi\eta \rangle_1$, with ξ in range $-\infty$ to 0; and $\langle \xi\eta \rangle_2$ with ξ from zero to ∞.

$$\langle \xi \rangle_1 = \int_{\xi=-\infty}^{0}\int_{\eta=-\infty}^{\infty}\int_{\zeta=-\infty}^{\infty} d\xi d\eta d\zeta p\xi, \tag{3.11a}$$

$$\langle \xi \rangle_2 = \int_{\xi=0}^{\infty}\int_{\eta=-\infty}^{\infty}\int_{\zeta=-\infty}^{\infty} d\xi d\eta d\zeta p\xi. \tag{3.11b}$$

If the non-exponential factor of any term contains an odd power of any of the variables, the corresponding part of the integral gives 0. Limiting to terms of dimension three and less, we find:

$$\langle \xi \rangle_1 = -\frac{v_T^2}{\sqrt{2\pi}}\left(1 + \frac{C_{200}}{2}\right), \tag{3.12a}$$

$$\langle \xi \rangle_2 = \frac{v_T^2}{\sqrt{2\pi}}\left(1 + \frac{C_{200}}{2}\right), \tag{3.12b}$$

$$\langle \xi\eta \rangle_1 = -\frac{1}{\sqrt{8\pi}} v_T^2 C_{210}, \tag{3.12c}$$

$$\langle \xi\eta \rangle_2 = \frac{1}{\sqrt{8\pi}} v_T^2 C_{210}. \tag{3.12d}$$

Now we inject eq. 3.12a 3.12b 3.12c and 3.12d in eq. 3.9. C_{200} is neglected before unity, and using the expression for C_{210} calculated by Maxwell [4]:

$$C_{210} = -\frac{3}{2}\frac{\mu}{P}\frac{v_T}{T}\frac{\partial T}{\partial y}, \tag{3.13}$$

we find an expression for v the creep velocity of the gas, using its physical parameters:

$$v = \frac{3}{4}\frac{\mu}{\rho T}\nabla T. \tag{3.14}$$

Using the form $\frac{1}{T}\frac{dT}{dy} = \frac{d\ln(T)}{dy}$, we recover eq. 1.7. This expression for the gas velocity highlights a contribution of the inhomogeneity of temperature to the velocity of the gas close to the surface. This shows the existence of a force urging the gas from colder to hotter places.

Then Maxwell made a direct application of this expression to the case of a capillary tube. He aimed at linking the gas flow to temperature and pressure gradients. The capillary is assimilated to a cylinder of axis y and radius a. For the sake of simplicity he assumed that

the motion of gas is so slow, and the temperature varies so gradually along the tube, that the temperature can be supposed uniform throughout any one section of the tube. Starting from Euler equation, he showed [4]:

$$\frac{\Phi}{\pi\rho a^2} + \frac{a^2\rho^2}{8\mu}\frac{dP}{dy} - \frac{3}{4}\frac{\mu}{\rho T}\frac{dT}{dy} = 0. \tag{3.15}$$

Φ is the gas mass flow which passes through a section of the tube in unit of time. The viscosity of the fluid holds a role, as we see in eq. 3.15. Eq. 3.15 gives the relation between the quantity of gas which passes through any section of the tube, the rate of variation of pressure, and the rate of variation of temperature along the axis of the tube. If there is no difference of pressure, like the case of an open system, there will be a gas flow from the colder to the hotter end of the capillary. If there is no flow of gas, the pressure increases from the colder to the hotter end of the tube, and in the stationary state, we recover eq. 1.8 displayed in chapter 1.

3.1.4 Explanation of Reynolds' result

Now we cease dealing with the creep flow of a gas in a capillary described by Maxwell to provide elements of explanation of Reynolds' result [3]. Maxwell pointed out the difference that Reynolds used a porous plate instead of a capillary. Maxwell assumed that the plate used by Reynolds features holes, which geometrical characteristics, that is to say the diameter and the thickness, are small before the mean free path. In other words, this corresponds to a high Knudsen number regime, the Knudsen number being defined as the ratio of the mean free path and the characteristic length of the system studied. A low density gas amplifies this aspect. The flow of gas is thus more similar to a flow through a small hole in a thin plate, and not a capillary. This is why the term *thermal transpiration* does not seem appropriated here. Collisions between molecules are very unlikely, and the concept of viscosity becomes here irrelevant. So this is a different phenomenon in the case studied by Reynolds, that can be referred as *thermal effusion*, which features a gas on the two sides of the plate is of the same species but at different temperatures, as illustrated on fig. 3.2.

The velocity is proportional to the square root of the temperature, yet the quantity that passes through the hole is proportional to temperature and density. Then, depending on the side where the product of the density and the square root of the temperature is the larger, more molecules will pass from that side than from the other through the hole, and this until equality of $v\rho$ on both sides of the hole. So the condition of equilibrium is:

$$\rho_c T_c^{\frac{1}{2}} = \rho_h T_h^{\frac{1}{2}}. \tag{3.16}$$

Since we have $\rho = \frac{mP}{k_B T}$, with m the mass of a molecule, we can express eq. 3.16 via the ratio of pressures:

$$\frac{P_c}{P_h} = \sqrt{\frac{T_c}{T_h}}. \tag{3.17}$$

So Maxwell pointed out [4] that there are two distinct regimes. If pores of a porous plate are thin, and the gas which effuses through the plate is rare, the process is *effusion*, and depends poorly on the viscosity of the gas. This corresponds to the very small Knudsen number scenario. If the pores of the plate are coarse and the gas is dense, the phenomenon is no more simple

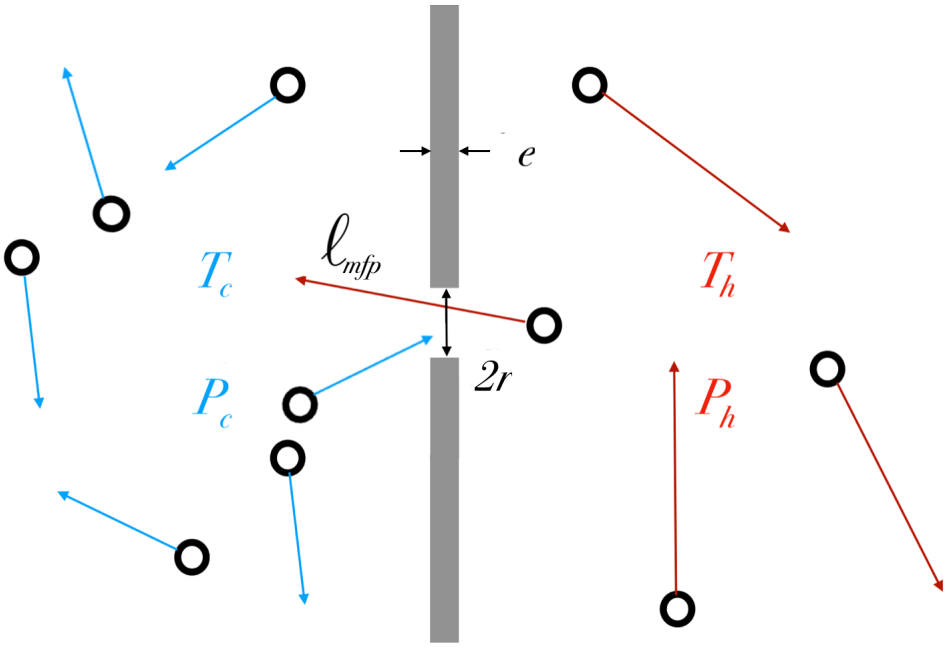

Figure 3.2: *Schematic view of the the phenomenon of thermal effusion in the stationary state. A plate separates two assemblies of molecules at different temperatures T_c and T_h. The mean free path of molecules (circles) ℓ_{mfp} is large before the diameter of the hole $2r$ and the thickness of the plate e. So a molecule passes through the hole with little chance of collision. It is as if, from the point of view of molecule about to go through the hole, there were vacuum on the other side of the hole. Here we describe the stationary state, when the currents of matter between the two assemblies are equal. The pressures, initially equal, are now different and given by equation 3.16.*

effusion, and becomes similar to transpiration through a capillary tube, depending altogether on viscosity. So the appellation *thermal transpiration* proposed by Reynolds appeared wrong to Maxwell. Yet in both regimes, the phenomena are satisfactory explained with gas kinetics theory.

Thanks to a correction to the velocity distribution function, adapted to the temperature inhomogeneity, Maxwell was able to highlight the existence of a creep velocity of gas at the solid interface induced by a temperature gradient.

3.2 Theories for thermo-osmosis in liquids

Now we illustrate thermo-osmosis in liquids. Fluid mechanics is the relevant approach to describe the fluid, resorting to continuous fields instead of discrete quantities used for gas kinetics. First we present how a creep flow emerges from the application of a temperature gradient at a solid interface. In a temperature gradient surface-solvent interactions induce thermo-osmotic flows [5]. Then we present some physical mechanisms that have been studied and understood.

3.2.1 Frame: boundary layer approximation

We consider a spherical particle of radius a. There are interactions between the particle surface and solvent molecules, that can be of different nature: electrostatic, van der Waals, applied

fields etc. In any case, interactions are exerted on the fluid through volume forces f, come from the solid boundary and vanish in the bulk, with a range B from the surface.

The Bjerrum length is defined as the distance where thermal agitation is comparable to electrostatic energy. Namely, $l_B = \frac{e^2}{4\pi\epsilon k_B T}$, with e the elementary charge, and ϵ the dielectric permittivity of the solvent. In our situation l_B is about few angstroms. On the other hand, there is no relevant long-range interaction that could be exerted on the fluid. Van der Waals interaction, electrostatic interaction or hydrogen bonds are not significant beyond some nanometers, especially compared to thermal agitation. If a is very large before B, the particle surface may be considered as flat in the range where the force f is significant. Colloids and proteins are relatively large objects, with typical radii about some dozens of nanometers. So, we only consider cases where the particle radius a is much larger than B, closely following Anderson [75]. Fig. 3.3 enables to locate the frame and the different geometric quantities used here. The position at the surface of the particle is located thanks to the polar angle θ, z is the axis perpendicular to the surface, and x is the direction tangential to the surface.

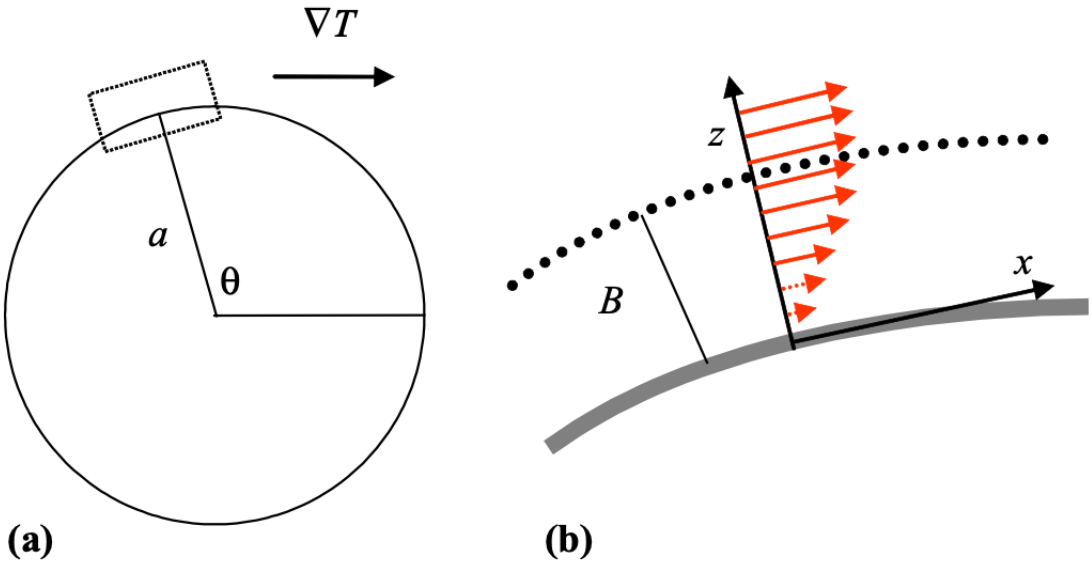

Figure 3.3: *(a) Schematic view of a spherical particle of radius a in a temperature gradient (b) zoom at the surface in the frame of the boundary layer approximation. The temperature gradient modifies solute-solvent interactions, which generates a creep flow with a plug profile. The fluid velocity relative to the particle surface increases and attains the value v_B at distances beyond the interaction range B. From ref. [76].*

Typical velocities are of the order of some μm/s, and the typical length of our system is of the order of a nanometer. Considering water's density and viscosity, the Reynolds number is very small before unity. So the fluid velocity field surrounding the particle is governed by Stokes equation:

$$\eta\vec{\nabla}^2 v = \vec{\nabla}P - \vec{f}. \tag{3.18}$$

η is the viscosity and P the hydrostatic pressure. Stokes boundary condition imposes: $v_x(z=0) = 0$ and the velocity takes a constant value v_s for $z > B$. So, In the vicinity of the surface, the fluid creeps at the surface, so $v_z = 0$, and the velocity depends only on the distance from the surface, so $v = v_x(z)$.

Since $\frac{\partial v}{\partial z}\Big|_{z=B} = 0$, we get, from eq. 3.18, the expression of the slip velocity v_s reached for the fluid beyond the interaction range B is:

$$v_s = \frac{1}{\eta}\int_0^B dzz\left(f_x - \frac{dP}{dx}\right). \tag{3.19}$$

For a homogeneous surface both the force density f_x and the pressure derivative $\frac{\partial P}{\partial x}$ vary with the sine of the polar angle θ, and so does the boundary velocity: $v_s = \bar{v_s}\sin\theta$, $\bar{v_s}$ being the maximum velocity, when the temperature gradient is perfectly tangential to the surface, reached for $\theta = \pi/2$.

The velocity of the particle u is opposed to fluid'one. Anderson [75] links the particle velocity u to the fluid velocity by averaging $\vec{u} = -\langle v_s \vec{e_x}\rangle$, and finds:

$$u = -\frac{2}{3}\bar{v_s}. \tag{3.20}$$

This enables us to link the thermodiffusion coefficient D_T to the forces exerted on the fluid by the temperature gradient and the particle.

3.2.2 From excess enthalpy to thermo-osmosis

The first observation of thermo-osmosis was made by Derjaguin and Sidorenkov [5] through porous glass. They provided a theoretical analysis [5, 77]. Their work was based on *Non-equilibrium thermodynamics* of De Groot and Mazur [46]. If an originally isothermal layer of liquid flows within an "excess" enthalpy area, this results in an "excess" heat flux. This sparks a temperature gradient parallel to the flow. By the laws of non-equilibrium thermodynamics [46], the reverse effect must also exist. Namely, a flow of the liquid due to a temperature gradient, without any difference of pressure imposed must exist.

The thermodynamic force $f = -T\nabla\left(\frac{\mu}{T}\right)$ [78], with μ the specific chemical potential of a solvent particle, can be written, thanks to the Gibbs-Helmholtz relation:

$$f = -\delta h\frac{\nabla T}{T}. \tag{3.21}$$

Eq. 3.21 links an extra enthalpy of excess δh to an applied temperature gradient. In the bulk, the liquid in a temperature gradient reaches a non-equilibrium stationary state, but there is no matter flow. The solid boundary layer however, provides this enthalpy of excess δh through interactions between solvent and particle. δh is a priori negative, since the forces we consider are attractive. Plugged into Stokes equation, this creates a creep flow parallel to the surface, and gives the fluid an effective slip velocity:

$$v_s = -\frac{1}{\eta}\int_0^B dzz\delta h\frac{\nabla T}{T}. \tag{3.22}$$

Fig. 3.4 displays the velocity profile in the vicinity of the solid boundary. It satisfies Stokes' non-slipping condition and reaches a constant value beyond the interaction layer. The two volume forces, viscous stress and enthalpy transfer have the same magnitude and opposite direction as illustrated on fig. 3.4, satisfying Stokes' equation 3.18.

In a micro-channel, the velocity profile is symmetrical with respect to the channel's axis, and is qualified of *plug-profile velocity*. This is illustrated on fig. 3.5.

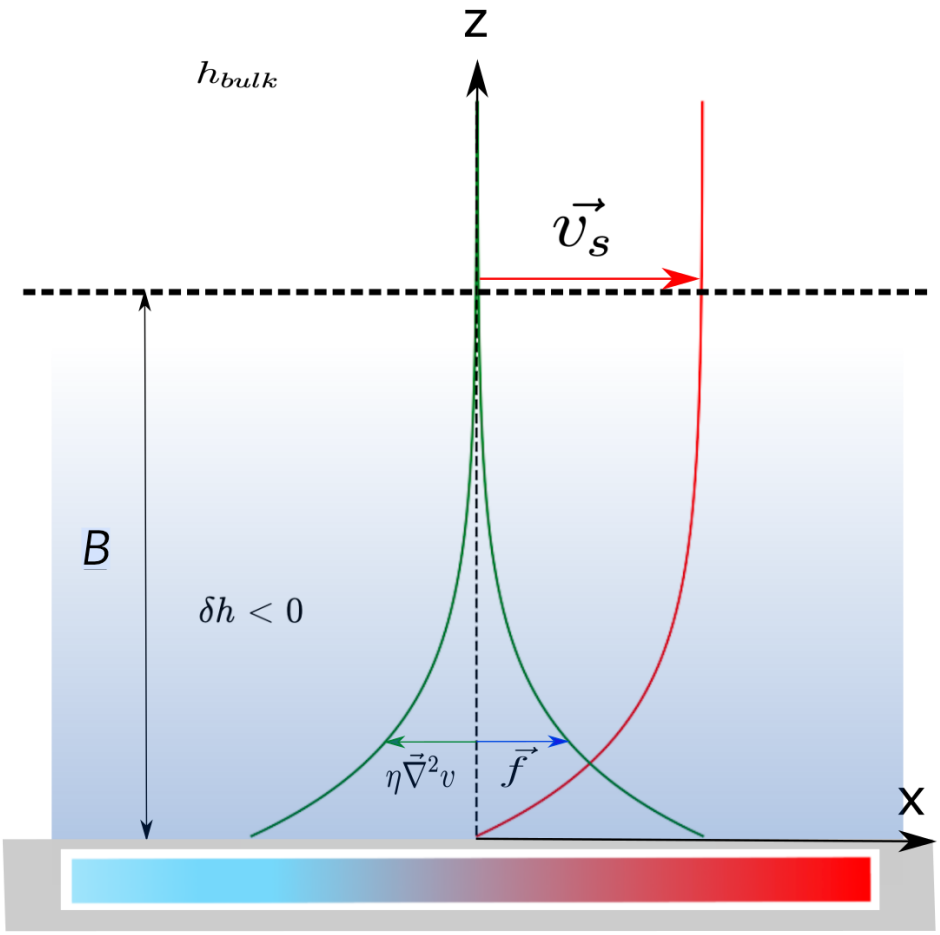

Figure 3.4: *Schematic view of forces at the interface. Here the excess density of enthalpy δh is negative inside the interaction layer (shades of blue), and vanishes beyond the range B where the enthalpy is the one of the bulk and there is no excess of enthalpy. The green lines indicate the profiles of the thermodynamic force f and the viscous force $\eta\nabla^2 v$ which vary along z, and cancels each other, satisfying the Stokes' equation. The red line indicate $v(z)$, the resulting velocity field. The fluid is dragged towards the hot side.*

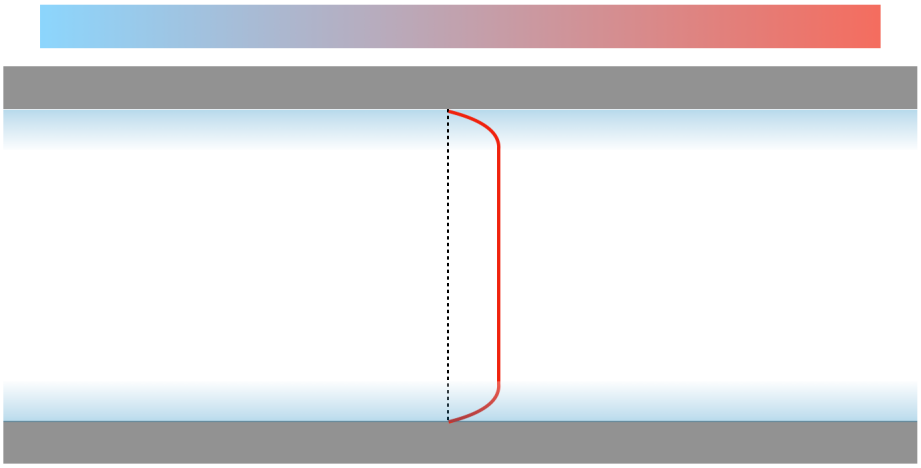

Figure 3.5: *Plug-profile velocity in a micro-channel. The red line is the velocity profile. On both edges the fluid reaches its maximum velocity beyond the interaction range.*

The force f in eq. 3.21 pushes the fluid to hot areas if the enthalpy is smaller in the boundary layer. This expresses the second law of thermodynamics, that affirms that heat in a temperature inhomogeneity moves from the hot to the cold to make temperature uniform, and maximize entropy. Conversely, if the excess enthalpy is positive, the fluid particle is carried to the cold side.

Using eq. 3.21, 3.22 and 3.20, we can link the thermodiffusion coefficient D_T to the enthalpy excess δh. This leads to $D_T \propto -\frac{1}{\eta T}\int dzz\delta h$. Since $\delta h < 0$ in the cases we consider, one expects: $D_T > 0$. So, any interaction providing a negative enthalpy of excess can be expected to result in a positive D_T. We must notice the inverse dependence of D_T on viscosity.

We consider the dispersion forces, that is to say the van der Waals interaction between the suspended particle and the solvent. This interaction is attractive for solvent molecules. The computation of the thermophoretic contribution of dispersion forces results in:

$$D_T^{vdW} \propto \frac{H}{\eta T d_0}, \tag{3.23}$$

Where H is the Hamaker constant of the solute–solvent interaction, and d_0 is a molecular length scale. Thus D_T^{vdW} is positive. This expression does not feature any dependence on the particle size for D_T, which is in good agreement with the observation evoked in chapter 2.

3.2.3 Physical origins of thermo-osmotic flows in the electric double layer

Here we discuss in detail the physical origin of thermo-osmotic flow in a the electric-double-layer of charged colloids, and present the resulting particle velocity. We evoke different transport mechanisms, and show that a temperature gradient brings companion fields.

Colloidal particles in liquid suspension interact with the solvent essentially via electric-double-layer (EDL) and dispersion forces. The EDL is made of two layers at the immediate vicinity of the particle surface in contact with a fluid. The first electric layer is made of charges at the surface of the colloid. This layer attracts by electrostatic interaction counter-ions present in the fluid, which are screening the first layer. The hydrodynamic and electrostatic treatment of colloidal particles that are going to be presented rely on the boundary layer approximation presented previously, which is valid here because of the short-ranged solute–solvent forces. Since most solute and solvent properties depend on temperature, a thermal gradient affects the EDL in several aspects.

Consider a spherical particle of radius a and surface charge density $e\sigma$. The following takes place in the frame of Gouy-Chapman theory. The electrostatic potential ψ and the corresponding electric field $E = -\nabla\psi$ are screened through the accumulation of mobile counter-ions in the solution, as illustrated on fig. 3.6. In the Poisson–Boltzmann mean-field approximation, the excess densities with respect to the bulk of cations (n_+) and anions (n_-),at least the monovalent, are given by:

$$n_\pm = n_0(\mathrm{e}^{\mp\frac{e\psi}{k_BT}} - 1), \tag{3.24}$$

where n_0 is the bulk salinity. The accumulation of counter-ions combined with the depletion of co-ions because of electrostatic repulsion provides the fluid with a charge density ρ in the boundary layer, and an excess density n of mobile ions. Those are respectively given by [76]:

$$\rho = e(n_+ - n_-), \tag{3.25}$$

and

$$n = n_+ + n_-. \tag{3.26}$$

This excess ion density in the EDL increases the hydrostatic pressure by $P = nk_BT$ [76].

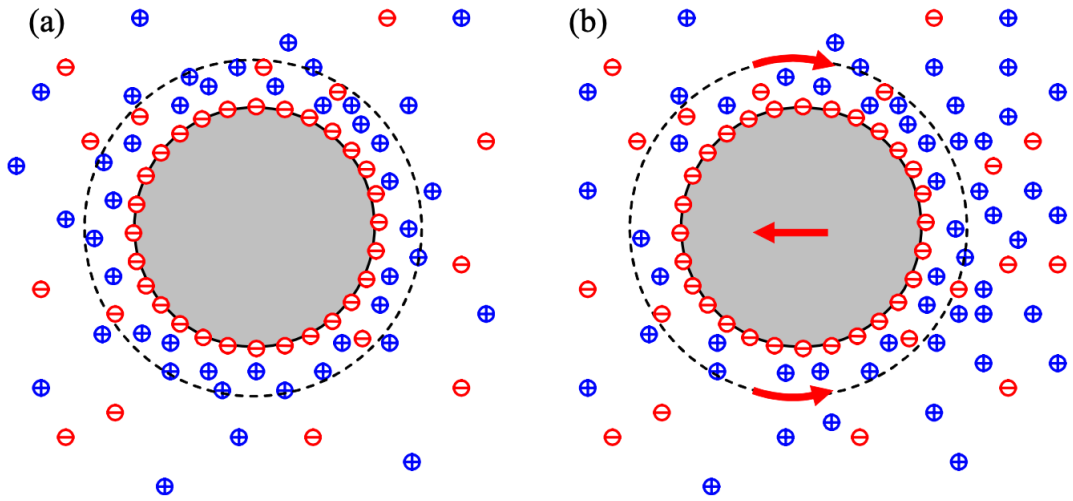

Figure 3.6: *(a) Charged particle with its screening cloud; the dashed line indicates the Debye length. (b) Polarization of the electric double layer. An electric field or interface forces drive the charged liquid along the surface to the right; the particle moves in the opposite direction. The surface flow leads to an accumulation of counter-ions at the right end of the sphere, and to depletion at the left. Picture taken from ref. [76].*

In an isotropic system, EDL properties depend only on the distance from the particle. Applying a temperature gradient breaks the spherical symmetry, sparking lateral forces on the ions in the EDL. This induces a motion of the fluid with respect to the particle surface. Indeed, the temperature gradient generates companion fields: solvent permittivity gradient, solvent salinity gradient and thermo-electricity [76, 79]. As a result, those gradients provide the thermodynamic forces acting on the EDL. Würger [76] has shown that at the first order of external fields, the sum of the volume force and the pressure gradient acting on the fluid in the EDL is given by:

$$f - \nabla P = \rho\bar{E}_0 - (\rho\psi + nk_BT)\frac{\nabla T}{T} - \frac{E^2}{2}\nabla\epsilon - nk_BT\frac{\nabla n_0}{n_0}. \tag{3.27}$$

The first term $\rho\bar{E}_0$ accounts for the *thermo-electric effect* [79]. When a finite temperature gradient is applied to an initially uniform electrolyte, an electric field $\bar{E}_0$ companion of ∇T appears, resulting from the electrolyte properties. The temperature gradient drives cations and anions at different strengths or even in opposite directions, depending on their size and solvation energy [79]. A difference of electrostatic potential between the hot and cold sides of the solution appears. This difference difference, called *thermopotential*, is expressed $\psi_0\frac{\Delta T}{T}$, where ψ_0 is a constant depending on electrolyte properties [76] and ΔT is the temperature difference brought by the temperature gradient. This results in a macroscopic field $\bar{E}_0$. The bar indicates

the deformation due to the permittivity jump at the particle–fluid interface. Because of the different material properties of particle and fluid, the external fields are modified close to the interface. The permittivity of water being much larger than that of the particle. As a result enhances the parallel component of the electric field is enhanced by a factor $\frac{3}{2}$. Then, the first term in eq. 3.27 is the volume force coming from the coupling of the charge density to this external thermo-electric field $\bar{E}_0$.

The quantity $\rho\psi + nkBT$ in eq. 3.27 can be identified as the double-layer enthalpy density δh as displayed in the previous part. This strengthens the idea developed by Derjaguin in eq. 3.21 suggesting that thermo-osmosis along a charged surface corresponds to an enthalpy flow [5].

The two last terms feature the gradients of ϵ and n_0, respectively solvent permittivity and salinity. The salinity is defined by: $n_0 = \frac{1}{2}\Sigma_i n_i$, with n_i the different salt ions number densities. Those are also companions fields of the temperature gradient.

To satisfy the one-dimensional Poisson–Boltzmann eq. $\epsilon\frac{\partial^2\psi}{\partial z^2} = -\rho$, ψ is:

$$\psi(z) = \zeta \mathrm{argth}(\mathrm{e}^{-z/\lambda}) \tag{3.28}$$

ζ is the surface potential, and λ is the Debye length. Plugging eq 3.27 into 3.19, the fluid velocity becomes:

$$v_B = -\frac{\epsilon\zeta}{\eta}\bar{E}_{0x} + \frac{\epsilon(\zeta^2 - 3\zeta_T^2)}{2\eta T}\frac{dT}{dx} - \frac{\epsilon\zeta_T^2}{2\eta}\left(\frac{1}{\epsilon}\frac{d\epsilon}{dx} + \frac{1}{n_0}\frac{dn_0}{dx}\right), \tag{3.29}$$

with the shorthand notation: $\zeta_T^2 = \left(\frac{2k_BT}{e}\right)^2 2\ln\cosh\left(\frac{e\zeta}{4k_BT}\right)$ used in reference [76]. Finally, using expression 3.20, we can have the particle's contributions to the velocity:

$$\vec{u} = \epsilon\frac{\zeta}{\eta}\vec{E}_0 - \epsilon\frac{(\zeta^2 - 3\zeta_T^2)}{3\eta}\frac{\vec{\nabla}T}{T} + \epsilon\frac{\zeta_T^2}{3\eta}\left(\frac{\vec{\nabla}\epsilon}{\epsilon} + \frac{\vec{\nabla}n_0}{n_0}\right). \tag{3.30}$$

This is the general expression for a charged particle subject to gradients of the solvent parameters T, ϵ, n_0.

The first term comes from thermo-electric effect. Since the thermo-electric electric field E_0 is given by: $E_0 = -(\psi_0/T)\nabla T$, a term proportional $\zeta\psi_0$ appears. This brings a dependance on the sign of the surface potential ζ of the molecule [76]. For a negatively charged particle ($\zeta < 0$), if ψ_0 is high enough the velocity can change sign and result in a negative D_T.

We discuss the physical origin of the second term, proportional to ∇T. A lateral force along the particle surface arises since the EDL in ∇T is not isotropic. The excess pressure and the electrostatic energy density vary along the particle surface, and result in thermo-osmotic flow in the EDL toward higher temperatures. This quasislip velocity gives rise to an overall flow to the hot side, whereas a mobile particle is dragged in the direction opposite to ∇T.

A detailed comparison [76] indicates that the velocity contributions proportional to ζ^2 and ζ_T^2 come respectively from $\rho\psi$ and nk_BT, in eq. 3.27. In the highly-charged particles regime, $\zeta_T \ll \zeta$ [76], which simplifies eq. 3.30. On the other hand, from the Debye-Hückel approximation for weakly charged surfaces one has $\zeta_T = \zeta/2$ [76], which leads to the same simplification than for highly charged surfaces but with a factor 1/4.

This term proportional to ζ^2 was first derived by Ruckenstein [80] in 1981. Ruckenstein has shown that the stationary drift velocity induced by an electric potential, ion concentration, or

a temperature gradient can be written: $U = -\ell\nabla\gamma/\eta$, η is the viscosity of the solution and ℓ is a characteristic length of the order of λ_{DH}. Ruckenstein suggested in his model that a generalization can be made to any case where the particle interfacial free energy γ depends on T. According to this view, thermophoresis can be envisaged as a "microscopic Marangoni effect": attractive (respectively repulsive) solvation interactions "pull" particles along ("push" particles down) ∇U, because of unbalanced γ. The electrostatic contribution to the interfacial tension between a charged colloidal particle and a solvent of dielectric constant is given, for low surface potential ψ_s by: $\gamma_{el} = -\epsilon\psi_s^2/8\pi\lambda_{DH}$. Since λ_{DH} depends on T, a temperature gradient will induce an effective interfacial tension gradient because of the unbalance of electric stresses on the particle. Temperature gradients on the scale of λ_{DH} induce electric stresses in the double-layer, leading to creep flow and thermophoretic motion.

The third term in eq. 3.30 highlights the companion fields of the temperature gradient. First, it indicates that the fluid in the boundary layer moves to regions of low ϵ, so the particle moves in the area of higher permittivity. On the other hand, in water, the permittivity gradient is linked to its father temperature gradient by: $\frac{\nabla\epsilon}{\epsilon} = -\tau\frac{\nabla T}{T}$ [76]. At room temperature in water, $\tau = 1.4$ [76]. Thus the areas of higher permittivities are in colder places, so this contribution makes particle move to the cold side.

Then, the term proportional to the salinity gradient corresponds to Anderson's chemiophoretic contribution [75]. A higher salinity reduces both the surface potential and the Debye length, thus lowering the EDL energy. In this picture, the particle is attracted toward the region of higher salt concentration. For several common ions, such as $H^+, Li^+, K^+, Na^+, OH^-$ or Cl^-, the salinity is higher at lower temperature [76]. This is totally consistent with Soret's measurements performed on sodium chloride and potassium nitrate [1]. As a result, this contribution leads the particle once again to the cold side.

As a conclusion, the positive thermophoresis observed for aerosols and charged colloids has received attention from the scientific community and theoretical treatments, that have successfully explained the thermophoretic motion towards the cold side of a temperature gradient.

Chapter 4

Thermophoresis and hydrogen bonds

In this chapter we link thermophoresis and hydrogen bonds. We start from the central point of our problem: the behavior described for proteins in water presented in chapter 2 is not successfully explained by theoretical backgrounds evoked in chapter 3. We present elements that seem to highlight a role of hydrophilicity in thermophoresis of some systems. Then we present how hydrogen bonds work, and why it could be a clue to negative thermophoresis observed notably with proteins in water.

4.1 Motivation: experimental observations

Here we display some experimental elements that expose the limits of the current theoretical understanding of thermophoresis, in particular in our situation. This enables to discard most of known interactions as mechanisms leading to the behavior observed with proteins.

4.1.1 Major issue: temperature dependences

We have presented earlier the understandings of thermophoresis for charged colloids. Electrostatic interaction in the EDL made emerge different stresses urging the fluid to hot areas, in agreement with the observed motion of the particle towards cold areas. However, electrostatic (ES) interaction is unable to explain the behavior of proteins in water. As we see on fig. 4.1 for lysozyme, if salts are added to the extent that ES interaction is screened, the behavior of $S_T(T)$ remains well described by Piazza's formula. So lysozyme thermophoresis overall features are not set by ES forces [51].

Moreover, Putnam *et al.* [71] observed that the variation of lysozyme electric charge hardly modifies the thermophoretic behavior of the molecule. This tends to dismiss the ES interaction as an explanation of the observation reported by Piazza *et al.* So the dependence on the surface potential sign presented in chapter 3 does not successfully describe the observation. Eventually, ES interactions do not explain the negative thermophoresis observed with proteins in water.

4.1.2 Sign change

We remind that a sign change for D_T, and a fortiori S_T, is observed for a lot of different system, as presented in chapter 2. This sign change is not successfully explained by the theories mentioned in chapter 3. All expression for D_T presented so far only accounts for a positive expression

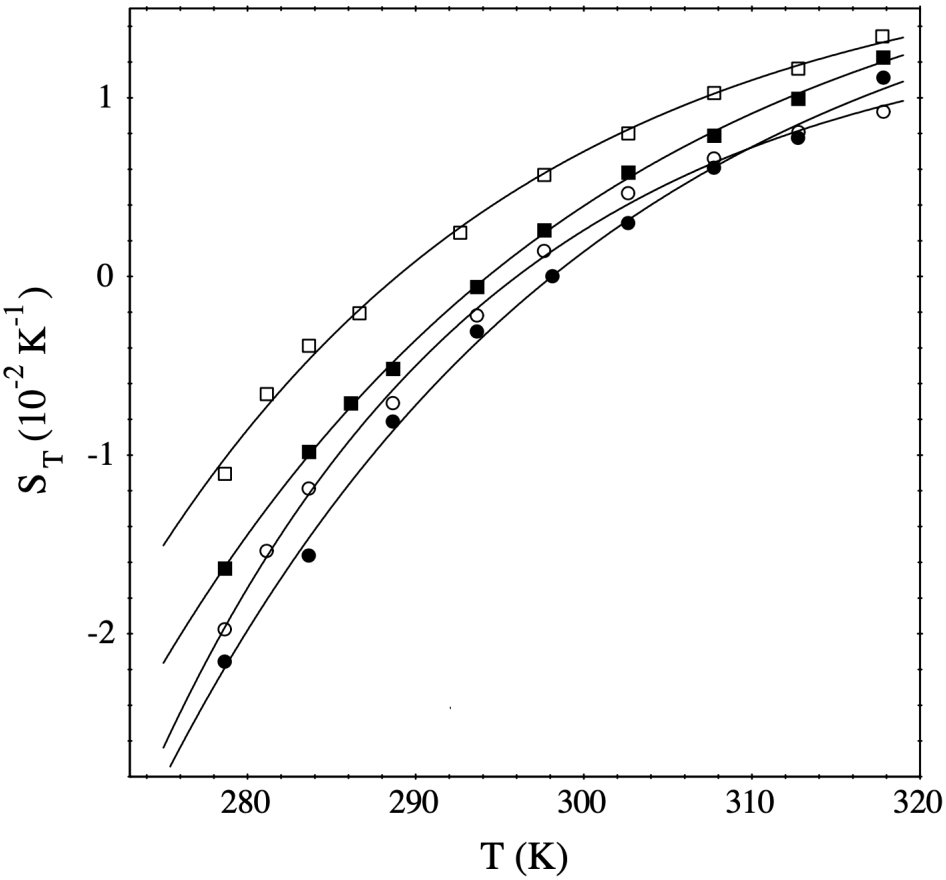

Figure 4.1: *Soret coefficient vs temperature for c = 7 g/l lysozyme solutions at pH = 4.65, in the presence of 7.5 (white squares), 20 (black squares), 100 (black dots), and 400 mM (white dots) NaCl. Adding NaCl screens ES interaction, yet it does not modify the concave behavior of $S_T(T)$. Figure taken from ref. [8].*

for D_T, which successfully explains a motion of particles towards cold, but the thermophilic behavior lacks theoretical development. Nothing explains the behavior switch reported with temperature. Moreover, D_T is a transport coefficient, and therefore is expected to be proportional to the inverse viscosity, as displayed in chapter 3. On the investigated temperature range, especially in water, the viscosity displays a non-linear dependence on temperature. Assuming that the main temperature dependence of D_T comes from the exponential one of viscosity, D_T would be written: $D_T = \frac{A_{D_T}}{\eta}$, with A_{D_T} assumed to be constant with temperature. The Soret coefficient would have the form: $S_T = \frac{6\pi A_{D_T} R}{k_B T}$, with R the hydrodynamic radius. So S_T would be proportional to the inverse temperature. No sign change when decreasing the temperature would be observed, and there should be no link between the Soret coefficient and the temperature dependence of viscosity. This is in disagreement with the observation presented in chapter 2. Something seems to be missing in D_T.

We can see on fig. 4.2 that S_T appears to follow a linear dependance with the viscosity.

One shall notice that the slope is always negative and similar for a vast majority of systems. So, neglecting all temperature dependence before the exponential one of the viscosity, S_T can be written:

$$S_T = S_T^0 + A_{S_T}\eta(T). \tag{4.1}$$

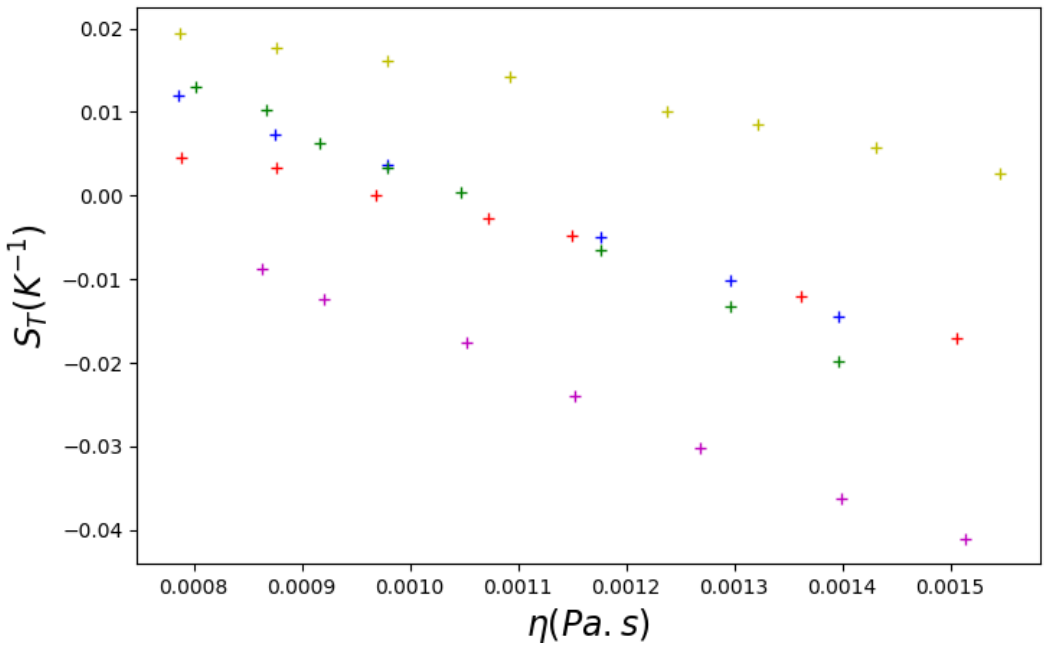

Figure 4.2: *Experimental data of S_T vs η of water for some systems. Data from ref. [7]. Temperature is a parameter (we plot $S_T(T)$ vs $\eta(T)$). The values for $\eta(T)$ are obtained using eq. 4.6, with parameters from tab. 4.3.*

S_T^0 and A_{S_T} are respectively the intercept and the slope on fig. 4.2. Using typical values estimated form fig. 4.2, we retrieve the typical convex curve for S_T vs T, as illustrated on fig. 4.3.

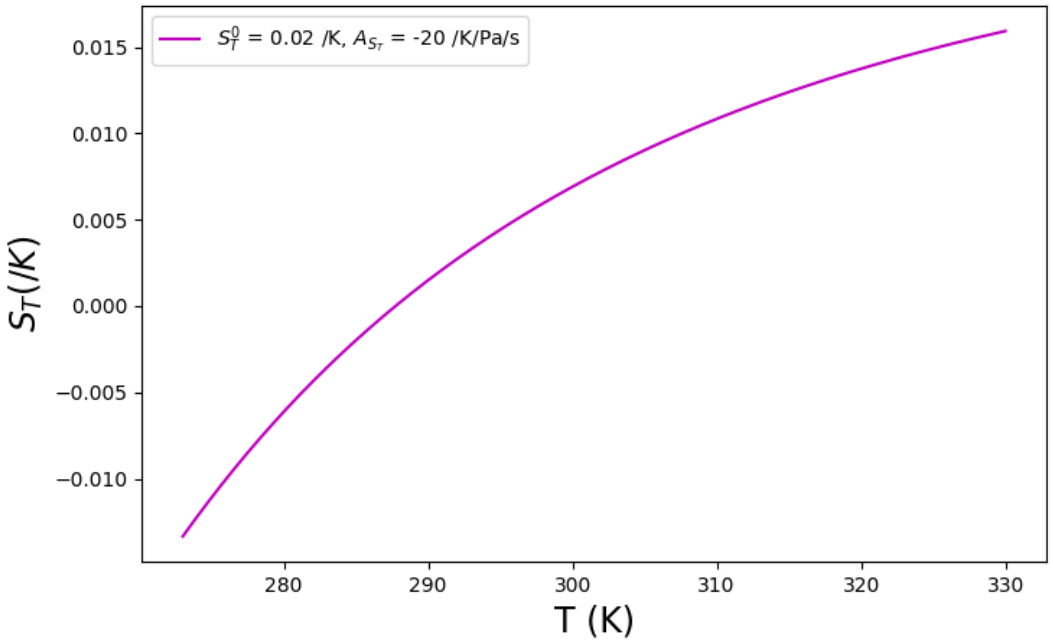

Figure 4.3: *Plot of S_T using eq. 4.1.*

Since $D_T = S_T D$, and because D is proportional to $1/\eta$, we must have:

$$D_T = D_T^0 + \frac{A_{D_T}}{\eta}. \tag{4.2}$$

D_T^0 is a term independent from viscosity. So we expect D_T to have two contributions,

one independent from viscosity, and one inversely proportional to η. Thermo-osmosis brings a contribution inversely proportional to the viscosity, but something seems to be missing to fully account for the viscosity dependence. In this paradigm, the development of a term D_T^0 could bring the expected behavior.

We have ruled out ES interaction to account for the thermophoretic behavior of proteins. One could think about van der Waals (vdW) interactions as a possible clue, however they do not depend significantly on temperature [81]. Only the Keesom term for the potential of energy between two permanent dipoles features a weak reciprocal temperature dependence. This has already been presented in eq. 3.23. Anyway, this contribution is positive and cannot explain Piazza's observation, in particular the sign change for D_T. Hydrophobic interactions can also be dismissed: the temperature dependence of the Soret coefficient for poly-L-lysine, which is the least hydrophobic polypeptide, is compatible with eq. 2.1 [82]. So any major impact of hydrophobic interactions is dismissed.

Finally, we want to build a theoretical model explaining thermophoresis of proteins in water, which has to satisfy a linear dependence of the thermodiffusion coefficient D_T with a sign change. D_T has to be the sum of two terms, with one independent from viscosity and the other proportional to the inverse viscosity, as suggested by most theoretical studies. Thus, in this work we aim at building D_T in the form:

$$D_T = D_T^0 + D_T^{OS}, \tag{4.3}$$

D_T^0 being negative and strongly dependent on temperature compared to D_T^{OS}, which is the term coming from thermo-osmotic contributions and proportional to the inverse viscosity. D_T^0 must come from an interaction between the particle and the solvent, which is neither ES, vdW nor hydrophobic interactions, and once again independent from viscosity. An interaction that has not received attention so far is hydrogen bonds (HBs) between solvent molecules and the solute. Proteins share many traits in common with amphiphilic molecules: their folded tertiary structure is indeed the outcome of a delicate balance between the hydrophobic and hydrophilic properties of the constituent amino-acids. Moreover, hydrophilic regions may cover a large extent of the exposed area (up to 50–60 percents for lysozyme).

4.1.3 Partition coefficient

Here we display some interesting effects that make HBs a relevant candidate to explain negative thermophoresis at low temperature. Niether and Wiegand [17] suggest that the temperature dependence of S_T could be strongly linked to the hydration layer, which is modified by a ligand or a rise in temperature [15]. Sign change in S_T has rarely been observed in non-aqueous systems, so one can question the particular properties of water, namely the strong presence of HBs. HBs are strongly linked to hydrophilicity [81], and hydrophilic interactions are temperature dependent, and are likely to play a primary role. So one can seek for a relation between thermophoresis and hydrophilicity, which has been studied by Niether *et al.* [13,15–17].

A parameter is introduced: P the partition coefficient between 1-octanol and water. P characterizes the hydrophilicity of a molecule. To determine the partition coefficient of a given solute (*eg* a sugar), a biphasic mixture of water and 1-octanol (or another immiscible organic solvent) is made. A small amount of solute is put in a shaking flask containing water and 1-octanol. After shaking the mixture, the aqueous and organic phases are allowed to separate

and the concentration of the solute in each phase is measured. Some sugar molecules will accumulate in the water phase, some in the octanol phase. $c_{octanol}$ is the concentration of the solute in the organic phase and c_{water} the concentration in the aqueous phase. P is defined as the ratio of those concentrations:

$$P = \frac{c_{octanol}}{c_{water}}. \tag{4.4}$$

If P is large, this means that the species prefers to be in the 1-octanol phase rather than in water, thus the species is poorly hydrophilic. If P is small, the species is hydrophilic. Indeed, 1-octanol is a long carbon-chain of eight carbon atoms with an OH tail, so it does not establish several HBs with a solute. On the other hand, water established a maximum of HBs with an hydrophilic compound. This way, P characterizes quantitatively if a species is rather hydrophilic or hydrophobic.

Niether *et al.* [16, 17] have measured the difference between the Soret coefficient at 20 and 50 °C ($\Delta S_T = S_T(50) - S_T(20)$) for different compounds, have plotted it versus log$P$. Fig. 4.4 shows that the more hydrophilic the species (more negatives values of log$P$), the larger the increase in S_T with temperature. We also notice that for poorly hydrophilic species (the least negative values of log$P$), S_T can even be decreasing with T. This leads us to consider a contribution coming from hydrophilicity within S_T, corresponding to D_T^0 in eq. 4.3.

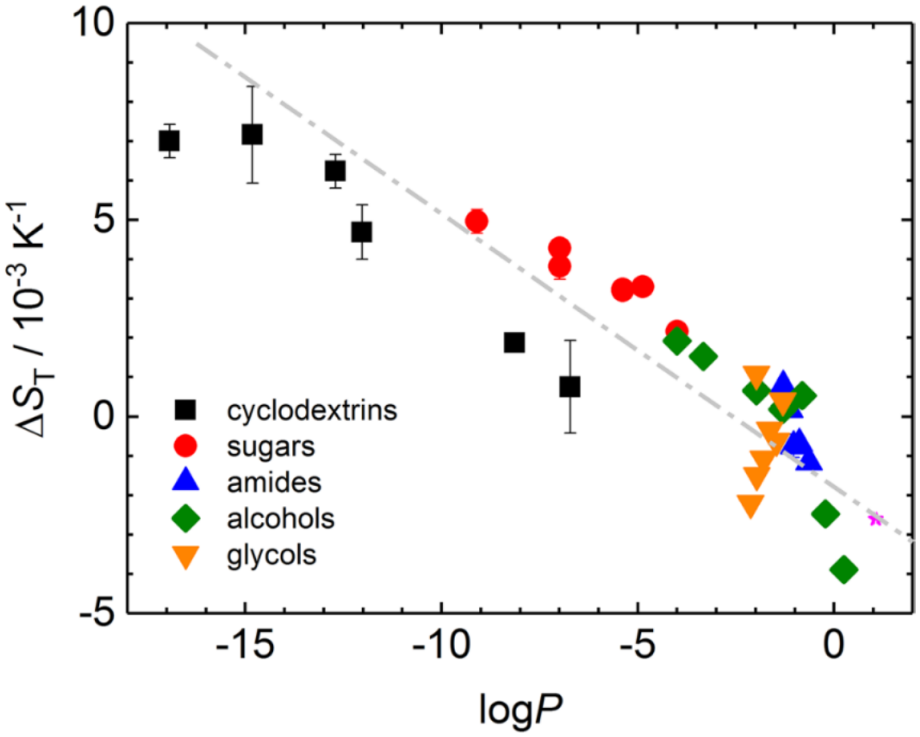

Figure 4.4: *ΔS_T, the difference between S_T at 20 and 50 °C, against the partition coefficient log P for cyclodextrins (1%), sugars (10%), alcohols (25%), and glycols (1%). The percentages in the brackets are the concentration in weight fractions. Figure taken from ref. [17].*

Maeda *et al.* have shown [13] that at constant temperature, the molar fraction for a sign change of S_T is proportional to log$P$. Another criterium evoked in ref. [13] can be used to determine whether a molecule is hydrophilic or not. This one is based on the chemical structure: the ratio of the number of hydroxyl groups over to the number of carbon featured on a molecule.

Hydrophilic spots like nitrogen or carbonyl can be envisaged too, alongside OH groups. When this ratio decreases, a molecule is less hydrophilic [83]. Maeda *et al.* reported that the molar sign change concentration showed a clear linear correlation with this ratio [13].

4.1.4 Number of hydrogen bond donors and acceptors

Maeda *et al* [14] also found that for ethylene glycols and crown ethers, the difference between the number of HB donor and acceptor sites is linearly correlated to the temperature dependence of their Soret coefficients. They suggest that the Soret coefficient at the fixed temperature of 25 °C can be written as the sum of two terms:

$$S_T(N_{don}, N_{acc}) = S_T^{\Delta} + \beta_0(N_{don} - N_{acc}). \tag{4.5}$$

$S_T(N_{acc}, N_{don})$ is the value of S_T at 25 °C. The first term S_T^{Δ} is independent from the hydrophilicity of the solute, and β_0 describes the strength of the HB effect for Soret coefficient due to the difference of N_{don} and N_{acc}. Here $S_T^{\Delta} = (8.1 \pm 0.3)10^{-3}K^{-1}$ and $\beta_0 = -0.0012K^{-1}$. The result indicates that the difference between donor and acceptor groups has a notable impact on the magnitude of S_T, and highlights the role of HBs in thermophoresis in water.

Maeda *et al.* also showed [14] the direct contribution of the difference $\Delta N = N_{don-}N_{acc}$ to the Soret coefficient. Expressing S_T as $S_T(T) = S_{T0} + S_{T1}T$, the authors showed a linear dependence of the intercept S_T^1 on ΔN, as illustrated on fig. 4.5.

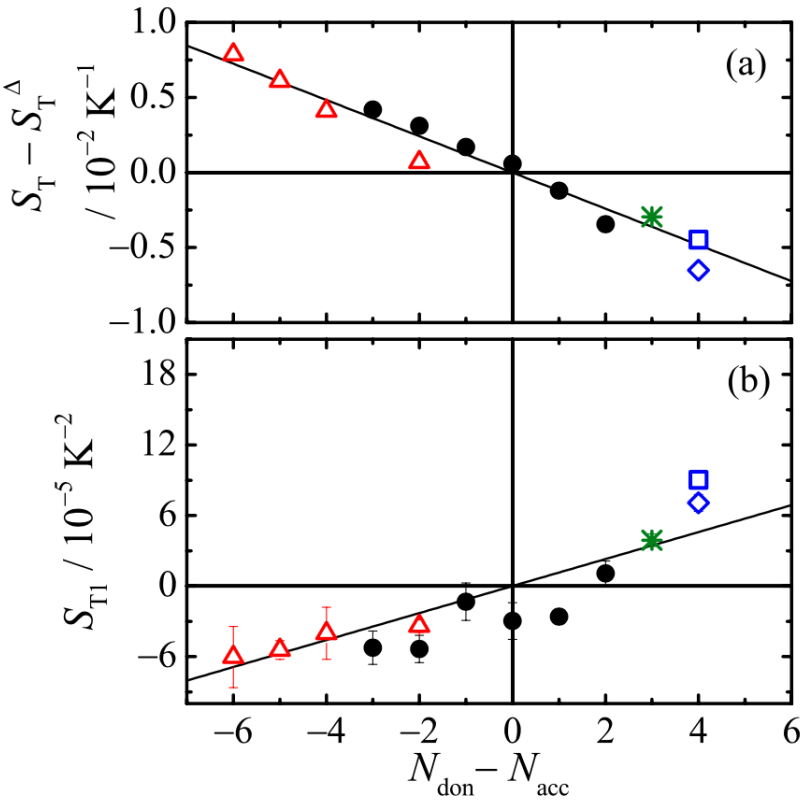

Figure 4.5: *S_T - S_T^{Δ} and the slope S_{T1} as function of $N_{don} - N_{acc}$ for ethylene glycol oligomers (dot), crown ethers (red triangle), and glycerol (green asterisk). Square (blue square) and diamond (blue diamond) refer to the solutions of glucose in water as their mass fraction of 1.0 percent and 20 percents. From ref. [14].*

The presence of donor sites of HBs seems to strengthen the dependence of the Soret coefficient on temperature, while the presence of acceptor sites seems to weaken it, as we can see it on fig. 4.5. Focusing on D_T, with a similar expression $D_T(T) = D_{T0} + D_{T1}T$, the slope of the temperature dependence D_{T1} shows also a linear dependence with ΔN, as illustrated on fig. 4.6.

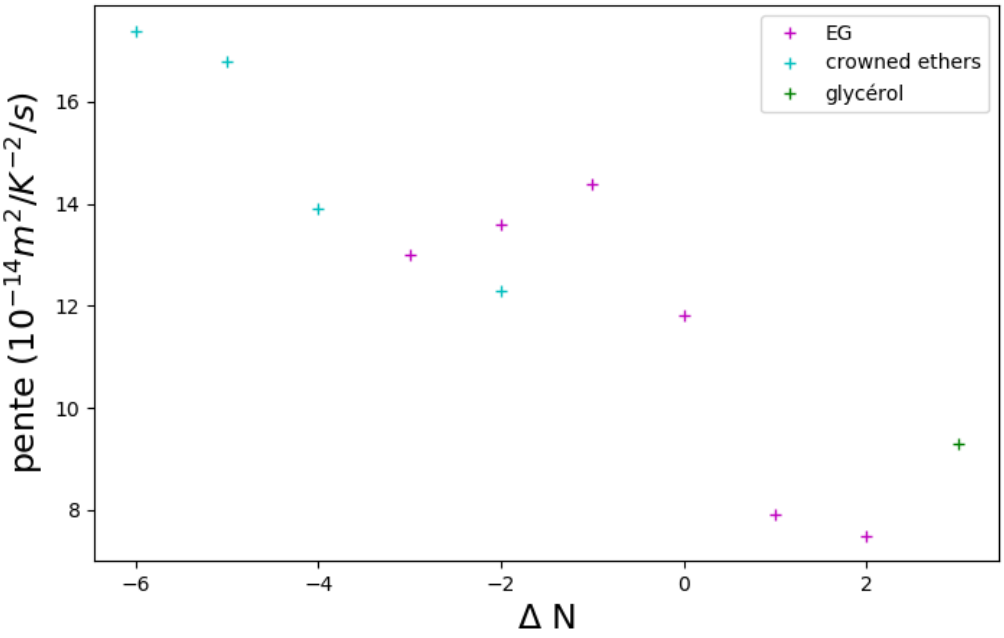

Figure 4.6: *Slopes of $D_T(T)$ vs the difference between the number of donor and acceptor sites on different molecules. Data from ref. [14].*

It is worth noticing that here the slopes S_{T1} and D_{T1} have opposed signs. This is because the systems used here have a huge sensibility of the diffusion coefficient D with respect to temperature, through the dependence of the hydrodynamic radius on temperature. This results in a decreasing S_T with temperature in the range considered. This has been also reported for poly(N-isopropylacrylmide) [84, 85].

The HB effect is highlighted here by the impact of difference of number of donor and acceptor sites $N_{don} - N_{acc}$ on S_T and D_T, a larger number of acceptor sites seems to indicate a larger slope for the thermodiffusion coefficient D_T.

4.1.5 Glucose rings contribution

Another clue in favor of hydrophilicity and HBs is the net thermophilic behavior displayed by sugars. As briefly presented in chapter 2, there are systems for which the Soret coefficient is always negative. This is the case of β-dodecyl-maltoside, shortened DM. DM is a sugar that carries a large hydrophilic head, composed of two glucose rings, as illustrated on fig. 4.7. It forms micelles of about a hundred molecules, and is nonionic. We can see on fig. 4.8 that its S_T is always negative, even at room temperature. Its sign change temperature T^* is shifted to much higher temperatures, about 43 °C [7]. The full S_T curve for SDS/DM mixtures can actually be obtained from that of SDS by adding a constant negative value $-0.008K^{-1}$ [7], comforting in the idea of a contribution coming from hydrophilicity.

DM is a good example to introduce the peculiar behavior of biomolecules in the field of thermophoresis. Sugars feature an increase in thermophilicity as the number of glucose units

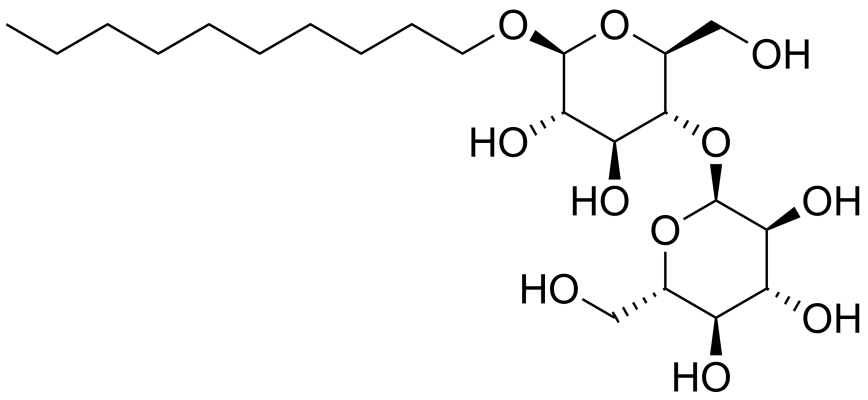

Figure 4.7: *β-dodecyl-maltoside (DM). We can see the maltose group, consisting of two glucose units, that compose the hydrophilic head.*

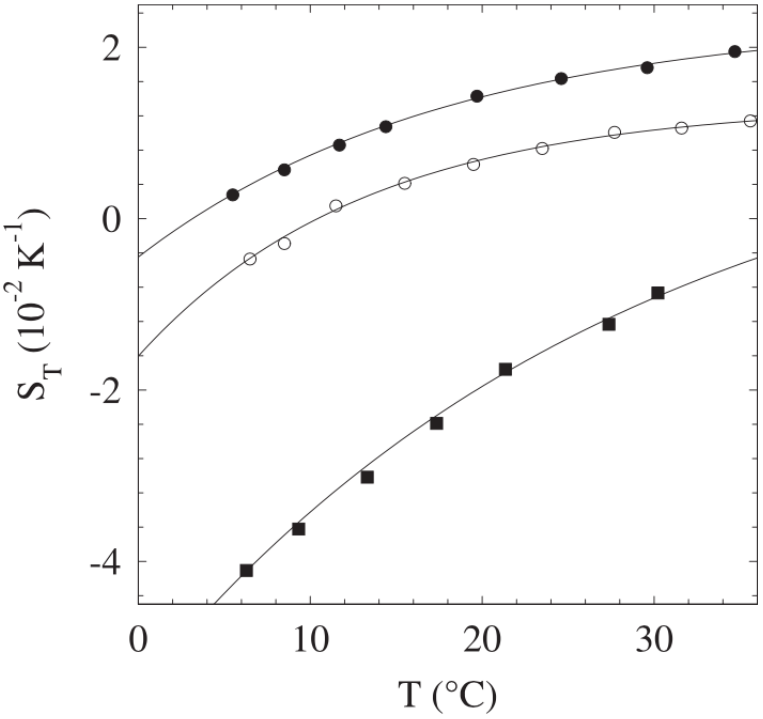

Figure 4.8: *Temperature dependence of S_T for DM (black squares) and SDS (black dots). The central curve is a mixture of the two species. The mixture gives birth to mixed micelles, that feature an in-between thermophoretic behavior. We see that micelles which feature glucose groups migrate more towards the hot spot at low temperature than those who do not. Fig. taken and adapted from ref. [7].*

gets larger [20]. Indeed, polysaccharids are a sequence of glucose units (maltose is two rings, maltotriose three, maltohexaose six...), and we can observe that the more glucose rings, the more thermophilic the molecule. Fig. 4.11 shows thermophoresis of sugars, such as maltohexaose, dextran, pullalan 4k and pullalan 440 k. Dextran is a ramified polymer of glucose of high molecular mass, about 60000 to 70000 g/mol. Pullalan is a polymer of maltotriose, which formula is given on fig. 4.10. Those molecules are all basically polymers of glucose.

We have already discussed the molar mass dependence of both Soret and thermodiffusion coefficient. However, we can notice on fig. 4.11 that all curves of D_T vs T share a relatively similar slope, but the longer the polymer chain, the more negative the intercept. The shorter

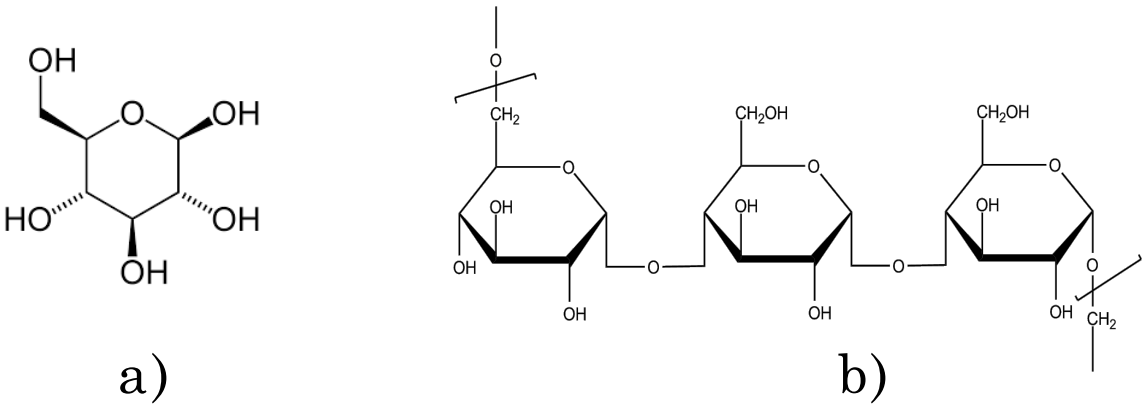

Figure 4.9: *a) glucose ring, elementary unit of several polysaccharids and b) pullulan, polymer of maltotriose.*

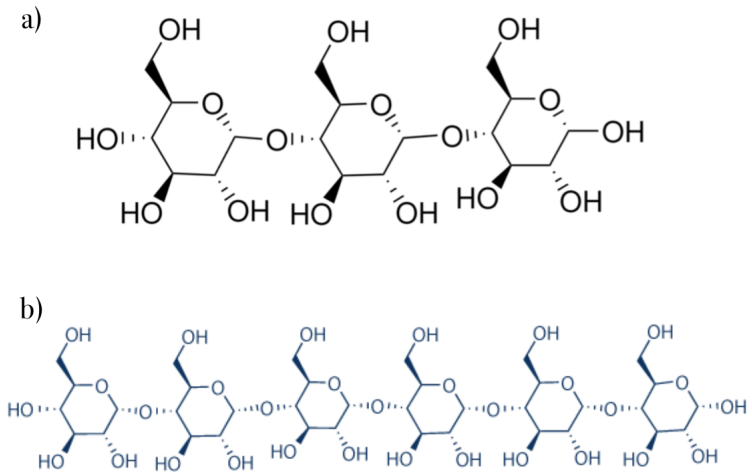

Figure 4.10: *Topologic formulas of a) maltotriose and b) maltohexaose. Pullalalan is a polymer of maltohexaose.*

chain of the monomeric glucose displays an ever positive D_T over the studied temperature range. But increasing the polymerization degree seems to add on offset shifting the curve downwards.

While we have seen that for long chains D_T barely depends on molar mass, here it seems that adding glucose rings adds a negative contribution to the thermodiffusion coefficient over the temperature range. It happens as if glucose rings are pulling the molecules to the hot side. It is interesting to notice that glucose rings are highly hydrophilic, establishing a lot of HBs with water.

We have different clues that allow us to consider that hydrogen bonds could be an interaction that could explain protein thermophoresis. In the following we will present different aspects of HBs.

4.2 Anomalies of water

Since colloid thermophoresis in water features a very distinctive behavior than in apolar solvent, one can legitimately ask what makes of water a unique liquid. Water notably features a strong presence of HBs, which are responsible for a lot of its particular properties. In this section we present anomalies of water, that directly come from HBs.

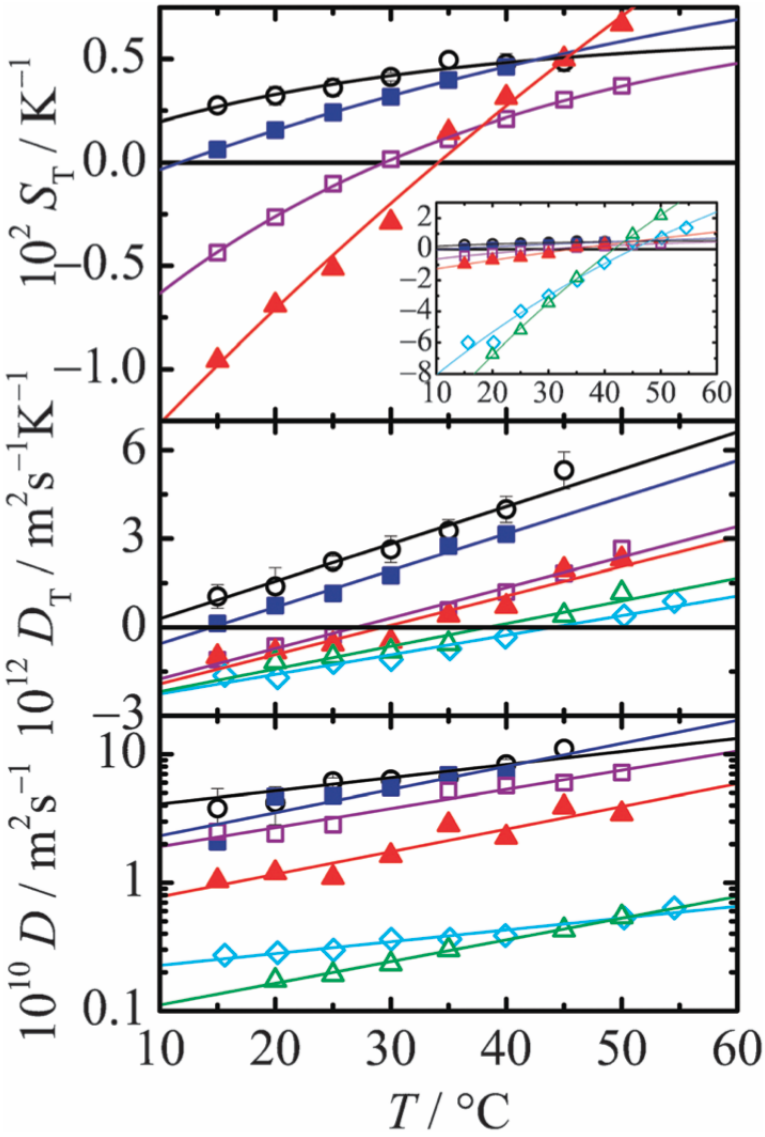

Figure 4.11: *Thermophoretic behavior of different polysaccharids. Soret coefficient S_T, thermal diffusion coefficient D_T, and mutual diffusion coefficient D for aqueous solutions of glucose (open circles), maltotriose (blue squares), maltohexaose (purple squares), pullulan-4k (red triangles), dextran (cyan diamonds), and pullulan-440k (green triangles). The curves in S_T are fitted using eq. 2.1, and in D_T and D the lines are obtained with linear regression. S_T of dextran and pullulan(440k) is only shown in the inset. Figure from ref. [20].*

4.2.1 Thermodynamical properties

The melting and boiling temperatures of water are much higher than those of other usual liquids, as we can see it on fig. 4.12 and 4.13. The presence of HBs between water molecules increases the cohesion in the liquid. So the energy needed for the thermal agitation to separate molecules is higher in the presence of HBs.

This observation could be *a priori* surprising, since water is a small and light molecule, especially compared to the carbon molecules presented. One could have expected water to be easier to bring from solid to liquid, notably because of smaller inertia. But the presence of HBs in water provides an extra cohesion and an enhanced network, leading to a higher melting temperature.

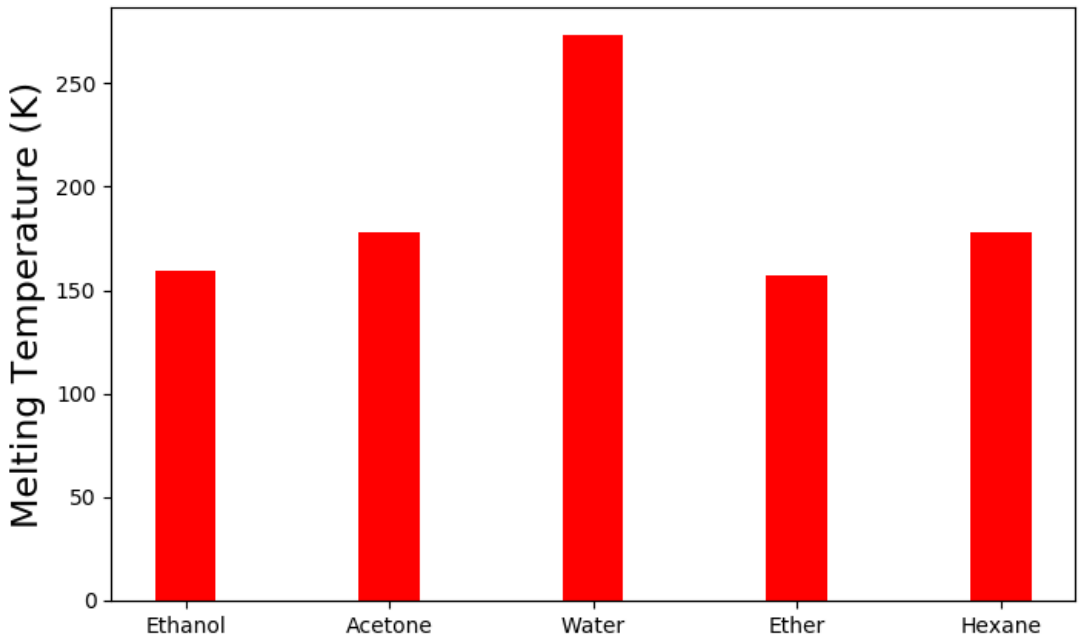

Figure 4.12: *Melting temperatures for some common liquids. We see that despite the small size and mass of the H_2O molecules compared to carbon-chained molecules, water has a higher melting temperature. Data source: Handbook of Chemistry and Physics 95th edition.*

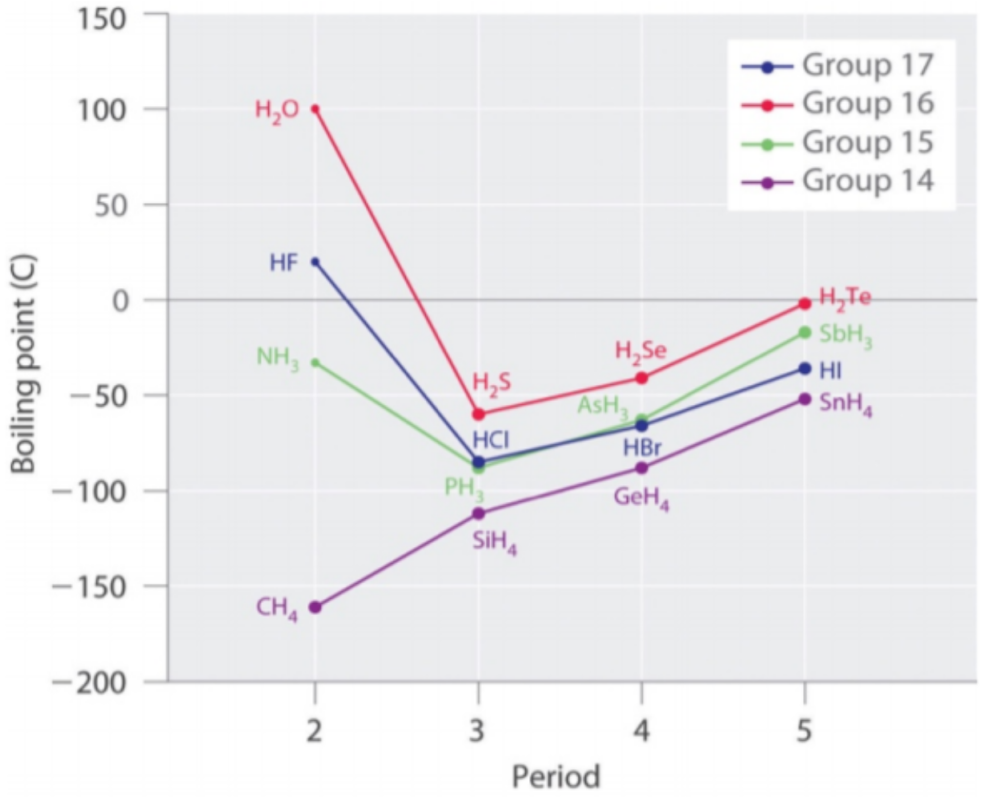

Figure 4.13: *Boiling temperatures for some species, consisting of elements of the periodic table bond with hydrogens. Elements of a same group (ie same column of the periodic table) are sorted by color.*

Fig. 4.13 shows a notable anomaly of water molecule. Most elements usually forming covalent bonds with hydrogen are sorted by boiling temperature. We can see for elements of the column XIV of the periodic classification, the boiling temperature is increasing with

the atomic number. Boiling temperature seems to be, at least to some extent, a function of electronegativity: the higher the electronegativity, the higher the boiling temperature. But this trend does not hold for columns XV, XVI and XVII, where elements of the second line form molecules of relatively high boiling temperature. We can see that this motif is shifted vertically when the column changes, but not in a linear way. We can see that all elements of column XVI have a higher temperature than their homologues from other columns. In particular, water has a boiling temperature significantly higher than other substances. Exception made of HF, which feature a quite high boiling temperature, notably because this species is naturally present as a dimer $(HF)_2$, there is at least a difference of a hundred degrees between water and other molecules.

Since all those molecules can establish to some extent HBs, we must note that HBs are particularly strong in water, illustrated here by its uniquely high melting and boiling temperatures. Another manifestation is the relatively high heat capacity of liquid water, as highlighted by tab. 4.1. Liquid water has one of the highest specific heat capacities among common substances, about 4184 J/K/kg at 20 °C; but that of ice, just below 0 °C, is only 2093 J/K/kg. One kilogram of liquid water requires more energy to be heated than one of solid water, which arises from structural differences.

Substance	water	ice	glycerol	ethanol	toluene	ether
C_P (J/kg/K)	4182	2090	1244	2500	1670	2200

Table 4.1: *Heat Capacity for some substances under normal conditions of pressure and temperature (excepted for ice). Data source: Handbook of Chemistry and Physics 95th edition.*

Speaking about structural differences, another well known anomaly of water is the smaller density of its solid phase compared to its liquid one. Indeed, ice floats over water, which is quite surprising: usually, for a given substance, the solid phase is denser than the liquid one. The density of liquid water is also a non-linear function, as displayed on fig. 4.14. In general, common liquids expand upon heating. But water display a maximum density at 4 °C, as illustrated on fig. 4.14. HBs on the one hand make water molecules more difficult to separate because of cohesive interaction, and on the other hand provide solid and near-zero-water an enhanced tetrahedral network [81, 86]. Rising temperature weakens this structure, molecules get closer and density increases. So two phenomena are competing: thermal dilatation and HB network breakdown, which results in a maximum of density.

Liquid water also features a sensibly higher thermal conductivity than other common liquids, as shown by tab. 4.2. In the daily life, this is notably illustrated by the calorie deficit experienced by a swimmer. Water enables thermal transfer more efficiently than air, which is explained by the difference in thermal conductivity. The only liquid substance having a value larger than water at our knowledge is mercury (8.514 W/K/m), which is metallic so has the usual large thermal conductivity of metals, notably because of metallic bonds present in liquid mercury. Concerning water, the geometric properties of the HB network enable a better propagation of thermal energy [81].

4.2.2 Viscosity

Water also attract attention by a large activation energy for the viscosity. Indeed, the temperature dependence of viscosity can be modeled with:

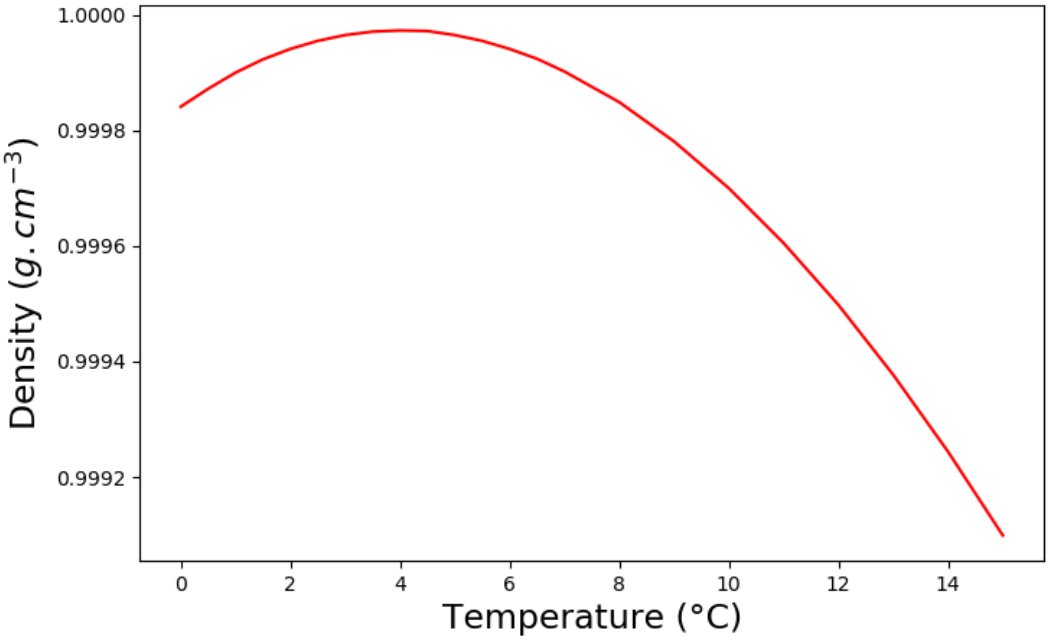

Figure 4.14: *Density of liquid water vs temperature. We see that the density is maximum at the temperature of 4 °C. Data source: Handbook of Chemistry and Physics 95th edition.*

liquid	water	n-heptane	toluene	ethanol	acetone	glycerol
λ (W/m/K)	0.607	0.123	0.131	0.169	0.161	0.292

Table 4.2: *Thermal conductivity at 25 °C for some liquids. Data source: Handbook of Chemistry and Physics 95th edition.*

$$\eta(T) = A\mathrm{e}^{\frac{B}{T}}, \tag{4.6}$$

with A and B two fitting parameters. A is homogeny to a viscosity, and B is a temperature in Kelvin, or more precisely an enthalpy of activation divided by the Boltzmann constant. Eq. 4.6 is a rather simplistic formula for the viscosity, and is similar to Eyring's equation. This expression is a good approximation as long as the temperature of liquid-glass transition of the substance is very low compared to the temperature range studied. In practice, eq. 4.6 is in good agreement with experimental data at ambient temperatures, between 0 and 50 °C, which is the frame of thermodiffusion experiments. There are more involved expressions that describe the temperature dependence of viscosity over a larger range of temperature [87], but eq. 4.6 gives a rather good approximation over the temperature range considered.

liquid	Bromine	Acetone	Ethanol	Toluene	Benzene	Water
A (Pa.s)	4.53×10^{-5}	2.03×10^{-5}	4.5×10^{-6}	1.69×10^{-5}	1.34×10^{-5}	4.54×10^{-7}
B (K)	918	830	1655	1069	1060	2279

Table 4.3: *Estimated parameters for expression 4.6 for some liquids, based on values of viscosity at 0, 25 and 50 °C that can be found in Handbook of Chemistry and Physics 95th edition.*

We can note that B for water is very large, especially considering it is the argument of an exponential. This can be understood as a larger barrier of energy for a molecule to overcome in order to jump from its position to a nearby vacant position in its vicinity. The barrier's origin

being the attraction of other molecules, here HB, that are an extra element compared to other substances. We can see on fig. 4.15 that the relative variation of viscosity with temperature is more significant for water than for other liquids.

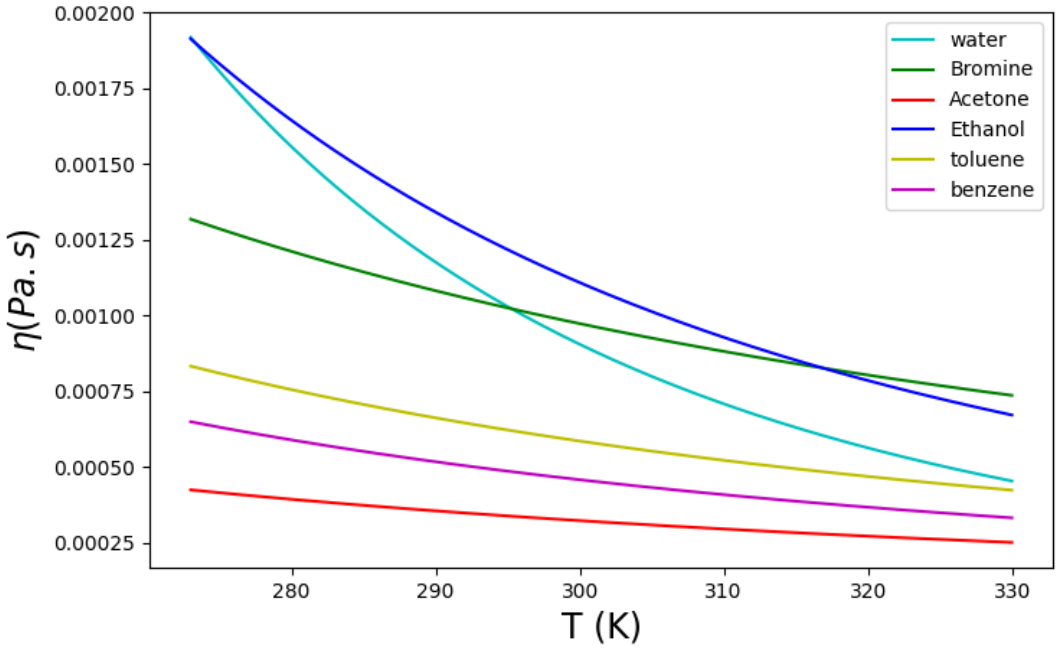

Figure 4.15: *Plots of the evolution of viscosity with temperature for some liquids, according to eq. 4.6, and using parameters of tab. 4.3.*

The resulting Arrhenius law for the diffusion coefficient, that is to say $D \propto \mathrm{e}^{-\frac{B}{T}}$, is confirmed by experiment [58] for the investigated temperature range for different solvents. The temperature dependence of the diffusion coefficient lies essentially in the viscosity's one.

4.3 Geometric and energetic properties of hydrogen bonds

In this section we present how HBs are organized in water, and their energetic properties.

4.3.1 Tetrahedral network

Liquid water is highly disordered, but with more or less tetrahedral local symmetry, with at least three HBs per molecule; and a majority of water molecules are double donors [88]. Unlike covalent bonds, HBs are less constrained by geometry and physical properties, but give water a tetrahedral structure [89–96], like a cage [86]. The tetrahedral structure of water molecules is illustrated on fig. 4.16.

There is no universal and precise definition of a hydrogen bond, any definition of hydrogen bonding in liquid water is essentially arbitrary, and is not any more fundamental for the liquid than it is for gas-phase dimers [88]. There are geometric and energetic definitions, developed more in details in ref. [88]. However, it always implies that two nearby oxygen atoms are separated by a proton. Such a pair of oxygen atoms is said to form an HB if the distance between oxygens, R, is shorter than a cutoff value R_0, of the order of 0.3 nm [97,98]. A strong HB is characterized by $R = 0.27$nm and almost aligned O-H-O bonds [81]. The average number of HBs that each water molecule participates in, which, technically, is twice the average number

of HBs per molecule. This average number is about 3.5 [88]. This means that a water molecule makes two HBs through its hydrogen atoms, as a double donor, and as a double acceptor makes two HBs through its oxygen atom.

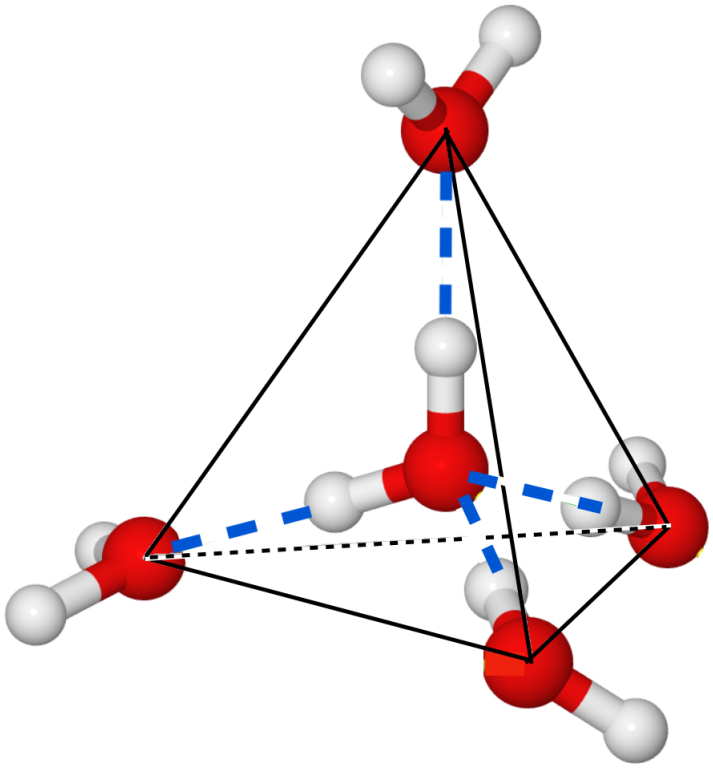

Figure 4.16: *Tetrahedral structure of water. A water molecule establishes four HBs with its closest four neighbors, which form a cage. The black lines mark the tetrahedron.*

A water molecule has less closest neighbors than without HBs, which makes ice lighter. As a result, a water molecule has less, but closer neighbors, due to the attractive HBs. A water molecule is thus engaged in four HBs on average [99], two as a donor and two as an acceptor. This tetrahedral coordination is enhanced with decreasing the temperature [100]. This allows a local three-dimensional network. The average number of HBs that each water molecule participates in, which, technically, is twice the average number of HBs per molecule.

Hydrogen bond is an interaction that depends on temperature [92], which makes it a good candidate for the contribution D_T^0 evoked earlier.

4.3.2 Potential Landscape

HBs have received some attention for a treatment via molecular dynamics (MD) simulations [86, 92, 96, 100–112]. A widely used criterion for determining the HB is a geometry definition for a pair of water molecules, that is to say, a pair of water molecules is considered H-bonded if the intermolecular distance and angle become less than preassigned threshold values. Kumar *et al.* [88] proposed a method to describe the profile for the two-dimensional potential of mean force (PMF), which is also referred to as the free-energy surface, from the distribution function of the intermolecular distance and angle between two water molecules. Those quantities are illustrated on fig. 4.17. α is the relative orientation of two nearby water molecules and defines

relative coordinates, such as the O-O distance R, and β is the O-O-H angle. The stronger the bond the smaller the β angle.

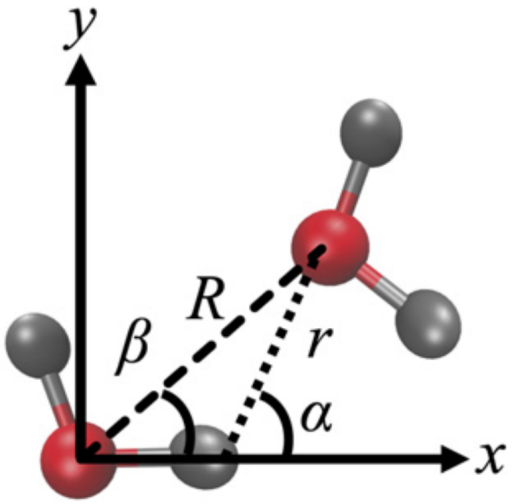

Figure 4.17: *The different coordinates used for the PMF landscape. Figure from ref. [100].*

The potential of mean force W is defined as $W(R,\beta) = -k_B T \ln(g(R,\beta)$., where $g(R,\beta)$ is distance–angle distribution function, namely the ratio of the average number of O atoms in a shell between R and $R + dR$ from a given O atom if the relevant angle is between β and $\beta + d\beta$, to the same number if the molecules were noninteracting. In this case the latter number is $\rho 2\pi sin\beta d\beta R^2 dR$. This represents the averaged number of O atoms found in the partial spherical shell having dR and $d\beta$ at distance R and angle β from one fixed O atom. Here, ρ is the molecular density of the system. The PMF map is illustrated on fig. 4.18. This 2D PMF can be regarded as the free-energy surface using reaction coordinates (R,β).

As we can see on fig. 4.18, there is a valley of potential in the PMF landscape. The coordinates of the map can be explicitly seen on fig. 4.17.Two molecules are considered H-bonded if the distance-angle relationship is (0.24 nm, 0°) < (R, β) < (0.34 nm, 30°) [92]. This suggests that while bonding, a water molecule is dragged to the bonding molecule, passes the saddle point and then falls into the valley of stability. We can note that the saddle point's coordinates are not affected by temperature [92, 100], as illustrated on fig. 4.18.

This is illustrated by fig. 4.18.a) which shows the potential landscape projected on the $R - \beta$-map, as obtained from molecular dynamics (abridged MD in the following) [100]. In the unbounded state the OO-distance is larger than 0.35 nm, whereas a HB corresponds to the low-energy region (blue) at $R < 0.35$ nm and $\beta < 30$. The complementary fig. 4.18.c) shows the same as a function of the distance r of the proton from the acceptor oxygen, and the angle α.

One can see on fig. 4.18 that these states are separated by a barrier, the grey circle indicating the saddle point. Comparison of the data at 300 and 190 K enables to appreciate qualitatively the different enthalpy and entropy contributions. The difference in energy between the saddle point and the bottom of the potential valley is of the order of 3 to $4k_BT$ [86, 92, 100].

In this chapter, we have connected thermophoresis to hydrogen bonds, explaining why it could be a good candidate to explain negative thermophoresis observed notably with proteins in water. We have presented the structural properties of hydrogen bonds, that manifest through different properties of water. In the following we deal with dynamical properties, that would

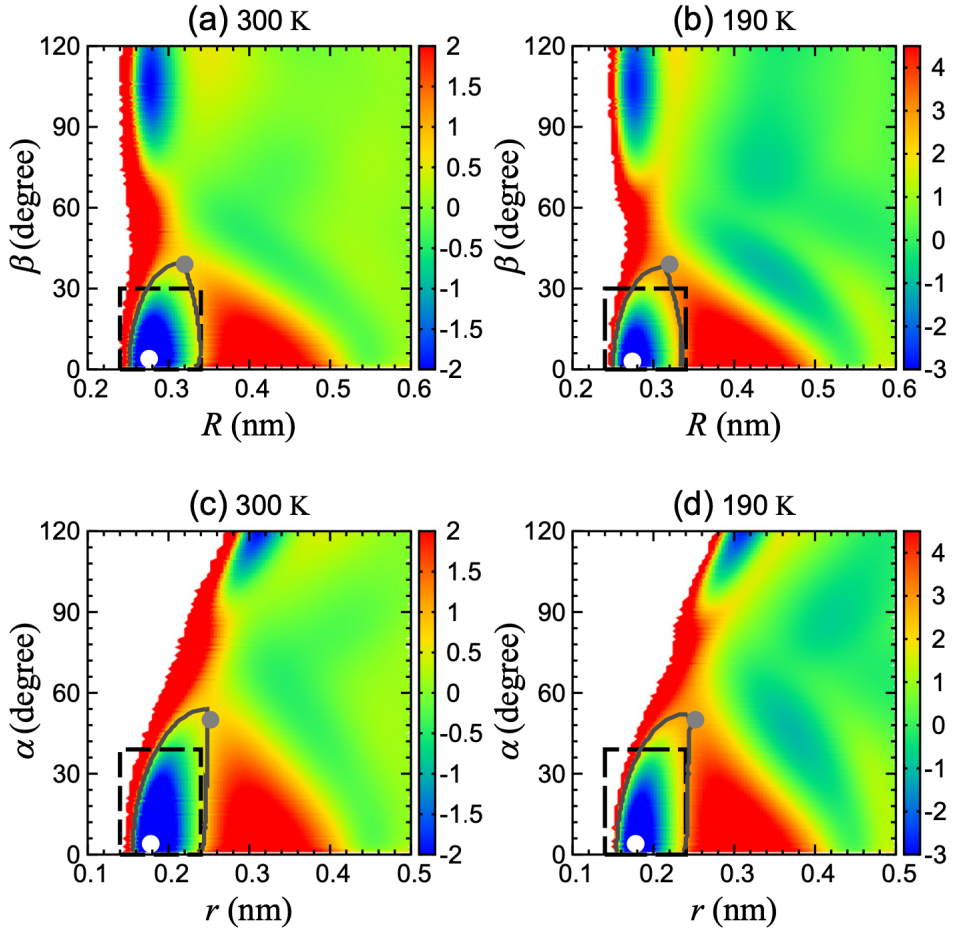

Figure 4.18: *Contour plots of the 2D Potential of Mean Force, W(R, β) at T = 300 (a) and 190 K (b), and W(r, α) at T = 300 (c) and 190 K (d). The value of W represented by the color scale is normalized by k_BT. The global minimum and saddle points are shown by white and gray points, respectively. The gray line represents the equipotential contour line corresponding to the saddle point. The rectangle indicated by the black dashed line stands for the H-bond region. The region with unsampled configurations is depicted in white. From ref. [100].*

be helpful to build a model implying HBs for the thermodiffusion of proteins in water.

Chapter 5

Dynamical properties of hydrogen bonds

In this chapter, we deal with dynamical aspects of HBs. We will see that those dynamics are ruled by a temperature dependence that is very likely to play a major role in our context of colloids in a temperature gradient. We will also display some elements from MD that suggest that the dynamics are altered in a presence of biomolecules.

HB network must not be seen as a rigid structure, but a constantly rearranging network, which forms a dynamical cluster. HBs form and break at a picosecond scale [108]. Here we present experimental results that have highlighted a temperature dependence of the lifetime, then we evoke the different processes that are suspected for the breaking of HBs, and finally we present some elements of the influence of a surface on HB dynamics.

5.1 Experimental observation - Lifetime

The main dynamical feature, the lifetime of the bond, has the similar temperature dependence regardless the process of breaking. We show here that, in the bulk, the HB lifetime must follow an Arrhenius dependence with respect to the temperature. The HB lifetime decreases when the temperature rises, and seems to follow at ambient temperature an Arrhenius equation [86, 92, 92, 96, 100, 102, 113, 114]:

$$\tau_{HB} = \tau_0 \mathrm{e}^{\frac{E_A}{k_B T}}. \tag{5.1}$$

E_A is the energy of activation, evaluated at a few kcal/mol, namely some units of $k_B T$, and τ_0 is of the order of 10^{-14} s [114, 115]. With those parameters we indeed retrieve lifetimes of the order of picosecond. This picture is supported by several studies. Conde and Teixeira [114] measured the depolarized light scattering of water in a temperature range extending from 80°C down to - 17°C, in the supercooled region. The spectrum features two Lorentzians lines whose half-widths differ by a factor about four. The two Lorentzians are associated to a rotational diffusion time and the HB lifetime. Teixeira *et al.* [116] also studied the behavior of liquid water on a temperature range from 38°C to -20°C with incoherent quasi-Elastic neutron scattering (QNES), and confirmed the precedent observation.

Teixeira *et al.* [113] also probed HBs thanks to coherent QENS with heavy water using a three-axis spectrometer. For D_2O, almost all the contributions to the scattered intensity

are coherent [113]. This method measures almost exclusively the correlation function of the positions of individual H atoms, that are time-dependent. This function features contributions due to molecular diffusion and to HB dynamics, which are separated to some extent by a data fit. Thus neutrons scattering can be a method able to directly probe HB dynamics.

Two momentum transfers are studied, $Q_1 = 1.95$ Å and $Q_2 = 3.54$ Å, corresponding to a maximum of scattered intensity and to a local minimum, where the pairs DD dominate the scattered intensity. Once again they observed two absorptions patterns, with very different linewidths, with only one displaying a significant temperature dependence. The linewidths of the peaks are shown of fig. 5.1.

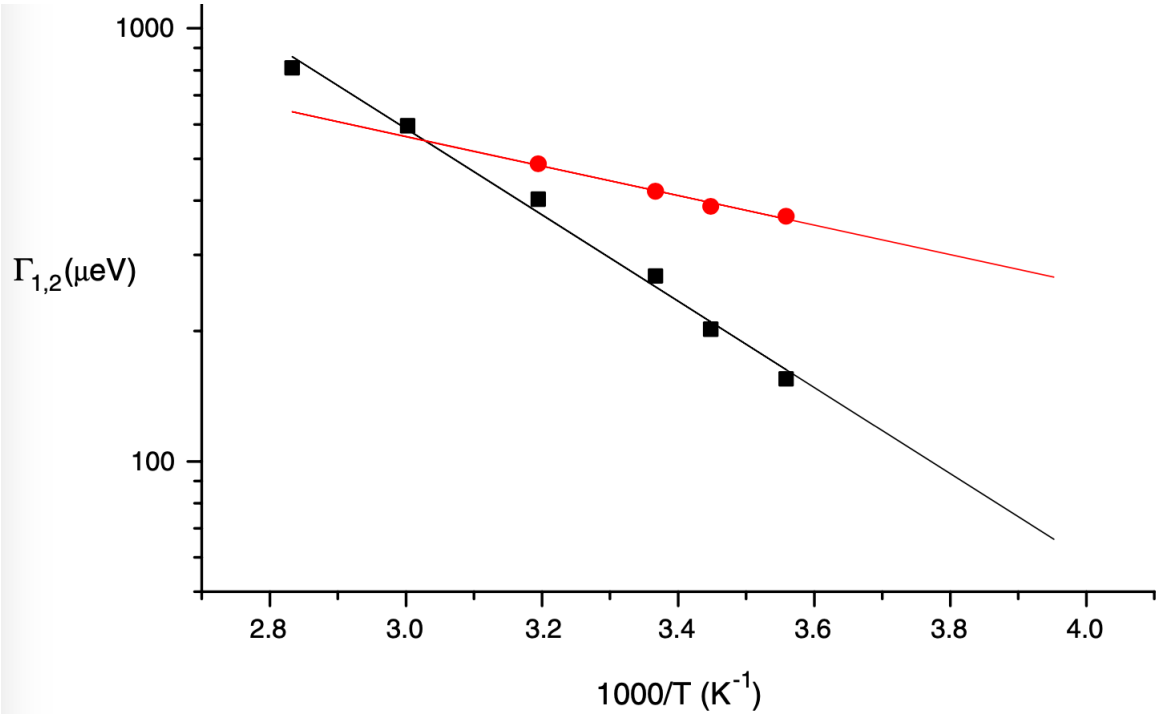

Figure 5.1: *The two linewidths Γ_1 (squares) and Γ_2 (circles) of the quasi-elastic lines at the two different values of the momentum exchange plotted in an Arrhenius plot. The lines are linear fits with slopes of 7.74 and 19.1 kJ/mol. Figure taken from ref. [113].*

The first linewidth Γ_1 is interpreted as a contribution from molecular motions. The second, Γ_2, is associated to the HB lifetime, confirming the precedent work [116]. Teixeira *et al.* suggested that rotational motion is the main way of HB breaking, and that those motions follow an Arrhenius temperature dependence with an activation energy of the order of 10 kJ /mol. Figure 5.2 gives the Arrhenius plot for HB dynamics obtained with several experimental techniques. This experiment has shown that the dynamics of liquid water must take into account the HB network and its dynamical properties. At very short timescales, (some ps), water must be seen as a percolated network of HBs forming an instantaneous gel. Thus, to some extent, a parallel can be made between the dynamical behavior of water and the one obtained with polymer melts. The first linewidth is associated to the ensemble motion of groups of water molecules as a whole, while the second one is associated to motions of individual bonds.

In contrast with the case of polymer melts, the global dynamics of water at very low temperature is determined by the second process [113], which corresponds for water to the dynamics of intermolecular bonds, that is to say individual HBs. Even if not strictly Arrhenius, the temperature dependence of the hydrogen bond lifetime is much weaker than that of the transport

properties displayed by the first linewidth. The second component that results from the fitting procedure was attributed to the rotations of hydrogen atoms around the centre of mass of the molecules.

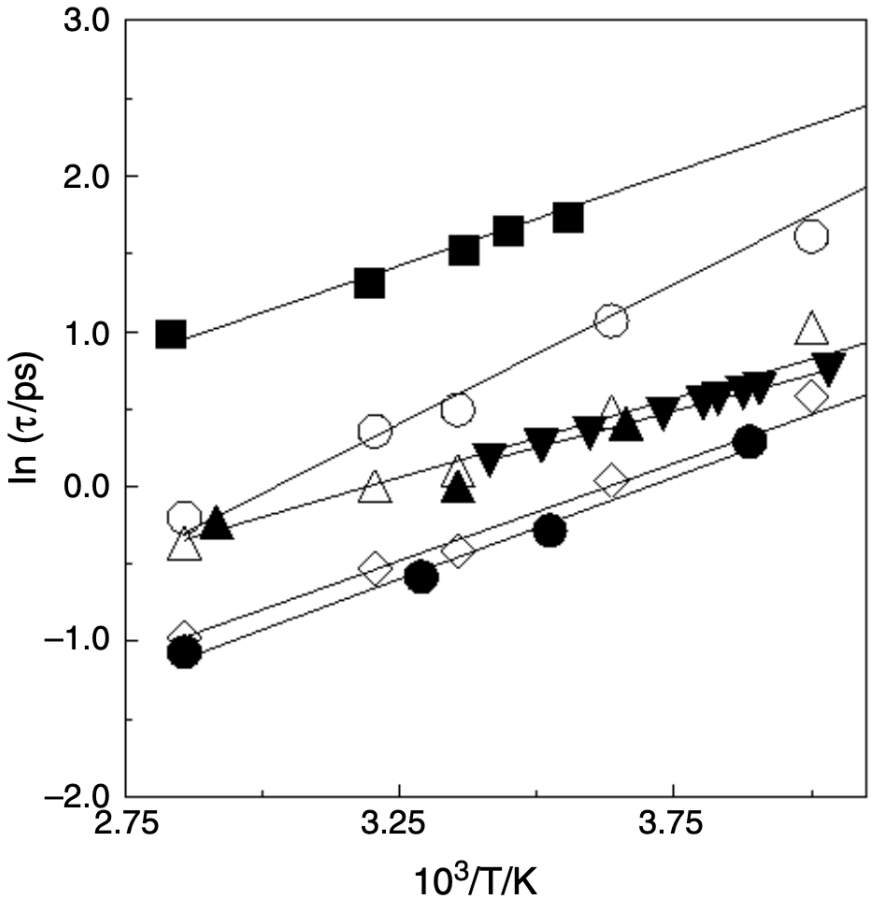

Figure 5.2: *Arrhenius temperature dependence of the HB dynamics determined by several different experimental techniques (filled symbols) and theoretical calculations (open symbols); experimental points: coherent QENS [113] (squares), incoherent QENS [115] (triangles down), IR transient hole burning [117] (triangles up), depolarized Rayleigh light scattering [114] (circles). Theoretical points obtained by means of MD and the reactive flux correlation function approach [103], using the SPC model of water: HB lifetime (circles), HB reforming time (triangles up), time of switching hydrogen bond partners [118]. Slopes represent activation energies between 8 and 11 kJ/mol. From ref. [113].*

MD simulations also confirm the Arrhenius behavior for the HB lifetime [86,92,100,107], as fig. 5.2 starts to mention. The procedure is to compute the relaxation time of the correlation function $c(t) =< h(t)h(0) > / < h(t) >$ corresponding to the average lifetime of a single HB. $h(t)$ denotes the HB operator. At time t, $h(t) = 1$ if two water molecules are bonded, while $h(t) = 0$ in the absence of HB. $c(t)$ is the conditional probability that the HB between a tagged pair of water molecules is intact at time t; $h(t) = 1$, given the bond was intact at time zero, $h(0) = 1$. Those methods have been used to perform simulations for the processes that are going to be presented, and do confirm the Arrhenius dependence of the HB lifetime [103].

5.2 Processes of breaking

Now we have to evoke how HB are suspected to break and form. There some controversy about which one is the principal process of breaking, though we have found interesting to evoke some of them. Here we display different mechanisms that can occur: rotational jumps and translational diffusion of water molecules.

5.2.1 Rotational jumps and partner change

Rotational jumps, according to some authors, could be the principle way of HB breaking. Laage *et al.* [112] suggest that HBs break by large angular jumps, exchanging HB partners. This way, the rotating water molecule (donor) does not lose any HB, but changes partner. This process is backed up: MD simulations [86, 92, 100, 108, 110, 112], nuclear spin relaxation [119] and neutron scattering experiments [113] [116] [115]. So rotational jumps of water molecules can be the main way of breaking of HBs. This picture is illustrated on fig. 5.3.

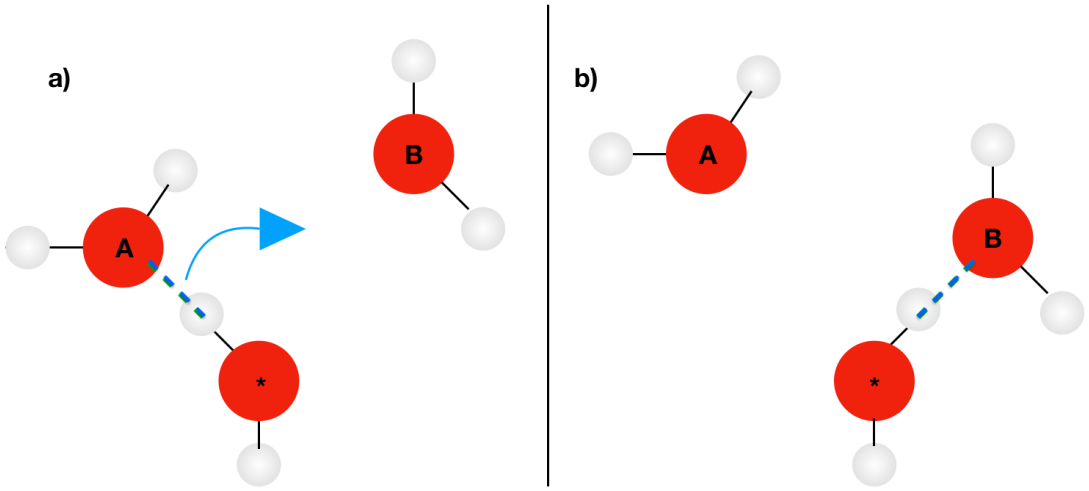

Figure 5.3: *Process of HB breaking by rotational jump, as described by Laage: a) A donor water molecule labelled ∗ is hydrogen-bonded to an acceptor molecule A. b) The HB rotates and the water molecule ∗ is now bonded with another molecule B. Green dashed lines stand for HBs. The phase where the two donor molecules are equidistant from the donor molecule ∗ is not displayed here.*

This mechanism is concerted: the reorientation occurs in parallel with the breaking and forming of HBs. Once the initial and final oxygen acceptors, respectively A and B on fig. 5.3, are equidistant from the rotating water oxygen, the O^*H bond from the rotating water molecule (denoted $*$) can suddenly execute a large-amplitude angular jump from one acceptor to another. The angular amplitude of this jump is about 60° [108], and other bonds remain unaffected. The rotational relaxation, and in particular the angular characteristics are presented in ref. [109].

5.2.2 Translational diffusion and caged model

Kikutsuji *et al.* [92] discuss another way of HB breaking, which is a nonstandard barrier crossing, not passing through the saddle point. This way is in total contrast with the picture suggested Laage. Kikutsuji indicates that "It has been clarified that HBs break due to translational rather

than rotational motions of the molecules" [86]. In particular, the MD simulations he and his coworkers performed [86] established a close link between the breaking of HBs and the self-diffusion of water molecules, as illustrated by fig. 5.5. Kikutsuji *et al.* [86] provide a view of a "caged model", as pictured on fig. 5.4.

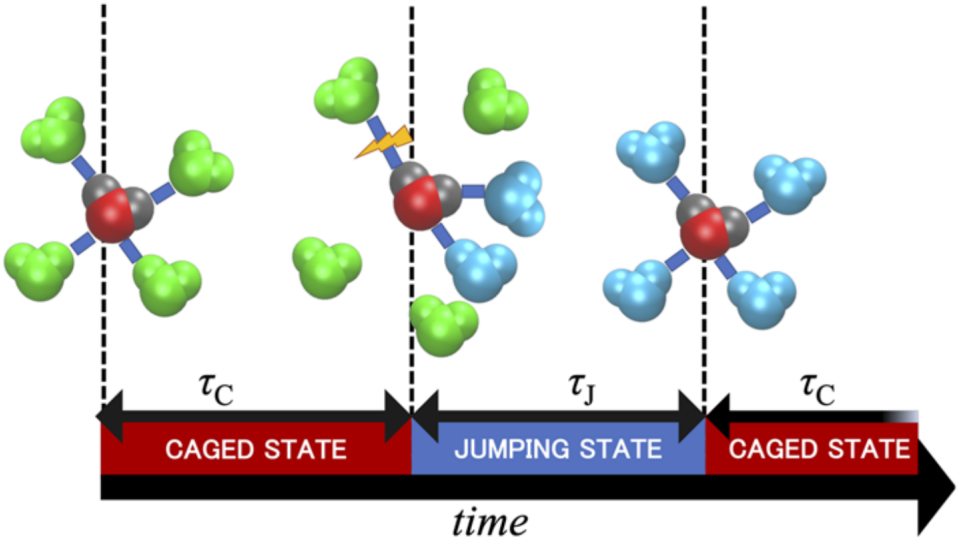

Figure 5.4: *Schematic view of a jump event of a water molecule, during which the four HBs are broken and new bonds are established with different oxygen neighbors. From ref. [86].*

The suggested translational HB breakage is thought to be associated with the cage-jump motion. This cage state is disrupted by a “jumping state” where the HBs are broken, before new bonds are formed with different neighbors. There are different characteristic times, describing the different steps of the caged state. The duration τ_C determines the lifetime of HBs and is given by the inverse jump rate. τ_J is the time to accomplish the jump from one cage state to another one.τ_J is shorter than τ_C, as described in the article, and τ_J displays a very weak variation with respect to temperature compared to τ_C [86], indeed τ_C shows the exponential temperature dependence of the inverse of the diffusion coefficient, as shown on fig. 5.5. In this picture, the HB lifetime τ_{HB} is dominated by the translational motion [92], and is given by τ_C.

This picture is opposed to the rotational diffusion presented earlier and encourages us to be quite careful if we want to take into account the way of HB formation / breaking for a model featuring HB dynamics. It appears that there is currently no scientific consensus that clearly explains a precise and unique mechanism of breaking for HBs in liquid water at ambient temperature. Nuclear spin relaxation gives clues about a relation between rotational and translational diffusion coefficients, as studied in ref. [119]. It seems to indicate that both mechanisms do exist, and that rotational jumps are correlated with translational jumps of adjacent molecules. Though, this study concludes that at ambient temperature, rotational jumps are four times more frequent than translational ones, which is consistent with what is suggested by Kikutsuji et al. Indeed, they found that when the temperature decreases, the population of the translational HB breaking (not through the saddle point) became comparable to that of the rotational breaking, passing this time through the saddle point.

As a result, we will have to be nuanced when taking into account the HB formation and breaking cycles. No proper consensus exists, and different provided images are in disagreement with each other. The different mechanisms will be considered for upcoming models.

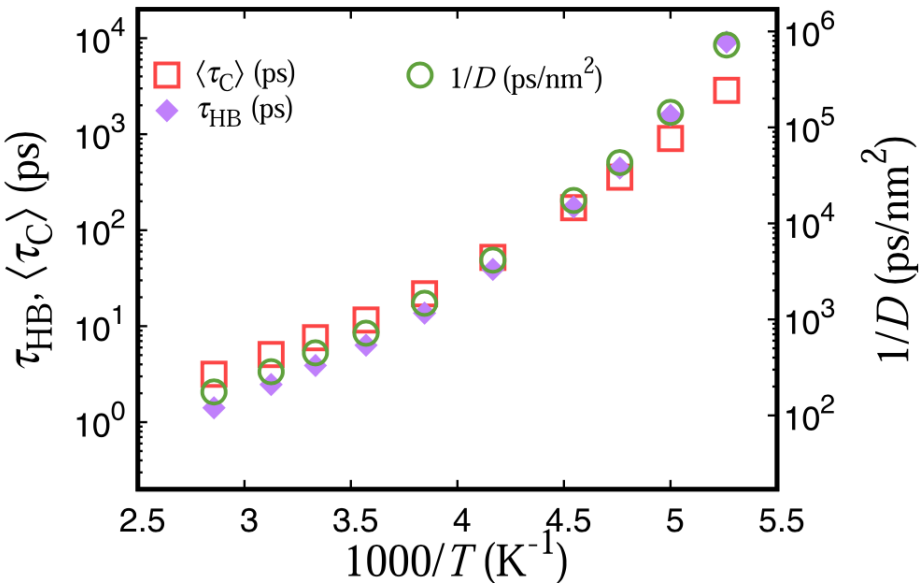

Figure 5.5: *Comparison of the temperature dependence of the duration of the duration of the "caged state" τ_C and the HB lifetime τ_{HB} with that of the inverse diffusion coefficient D. Note that only the first three points correspond to liquid water, the remaining ones to supercooled water. From ref. [86].*

5.3 Dynamical properties of water close to a surface

Since our study deals with the HB dynamics between water molecules and solute, we must evoke the impact of the presence of the interface solute/solvent on HB dynamics. Here we present what we know about the behavior of HBs close to a solute's surface. The essential point is that the dynamics of HBs are slowed down in the vicinity of surfaces.

5.3.1 Slowdown of water dynamics near a surface

As it is well known, water is a polar solvent, so water molecules are attracted by surfaces via van der Waals forces. Water molecules want to surround immersed polar compounds to minimize the energy involved in vdW interactions. This way vdW interaction is engaged for a maximum of water molecules. In the case of ionic solids for instance, water molecules end up to totally dismantle the solid to solvate it, then reorient themselves to screen the charge or to form HBs with the solute. Since ionic bonds are quite weak compared to vdW bonds, the system lowers its energy by exchanging ionic bonds between ions in solid phase with full vdW-bonded solvated ions in aqueous phase. However, concerning biological compounds, the covalent bonds are too strong to let water dismantle the solute. In any case, water creates a solvation shell (also called hydration shell) around the compound. This leads to modifications of water density close to those kind of compounds. Water density would be lower in this structure than in bulk water [120].

An interesting feature is the reorientational slowdown ow the HB network observed in the vicinity of hydrophobic groups [110, 121]. The ratio between the jump time $\tau_{jump}^{hydrophobic}$ for an OH bond in the hydration shell of an hydrophobic group and the jump time in the bulk τ_{jump}^{bulk} is indicated to be [121]:

$$\rho_v = \frac{\tau_{jump}^{hydrophobic}}{\tau_{jump}} = \frac{1}{1-f}. \tag{5.2}$$

f here is fraction of the ring representing the transition state location that overlaps with the hydrophobic solute excluded volume, that limits the spatial possibilities for the transition state. According to simulations [121], this ratio is comprised between 1.4 and 2.

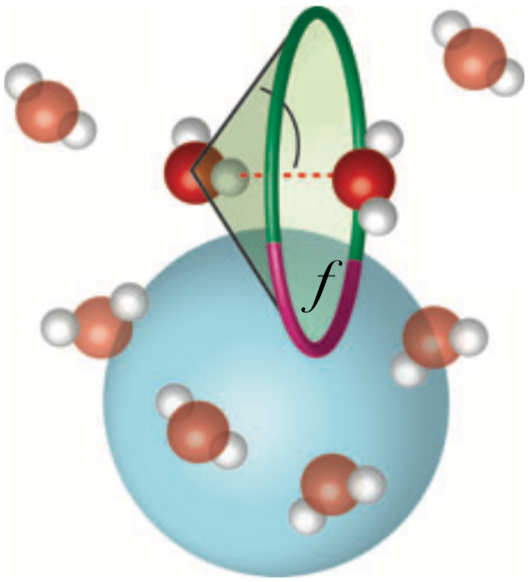

Figure 5.6: *Schematic illustration of the fraction f introduced by Laage. The ring stand for the available transition states position, and a fraction of this is not accessible because of hydrophobic group presence (in pink). Image adapted from ref. [110].*

However, this effect could be a consequence of the presence of nearby hydrophilic groups [110], and the effects of reorientational slowdown could be even more pronounced. Laage *et al.* [121] notably explain why hydrophobic groups slow water reorientation less than do some hydrophilic groups. The observed retardation of interfacial water seems to find its explanation resorting to the impact of the steric restrictions imposed by the corrugated surface of biomolecules on intermolecular motions [111]. Water reorientation is only moderately slowed in the hydration shell for dilute solutions, and the retardation factor with respect to the bulk is rarely 2 [110].

5.3.2 Observation of a greater retardation effect due to hydrophilic groups

NMR experiments on molecules featuring typical hydrophilic groups (amine, hydroxyl, carbonyl, and carboxylate groups) [122,123] indicate a retardation factor for hydration shell water reorientation compared to the bulk that could be inferior to 3. This retardation factor displays a diminution as temperature increases [123]. Concerning AAs, a smaller retardation has been also measured [110], donor amino-acids lead to a retardation factor of about 1.1 to 1.2. For acceptors the situation is different. Another factor ρ_{HB} is added to eq. 5.2. This factor is defined $\rho_{HB} = \mathrm{e}^{\frac{\Delta\Delta G^{\ddagger}}{k_B T}}$. $\Delta\Delta G^{\ddagger}$ is the difference in activation free energy between AA site and bulk water. The essential point is that AAs induce a slowdown in HB dynamics with respect

to the bulk, in particular jumping times [110].

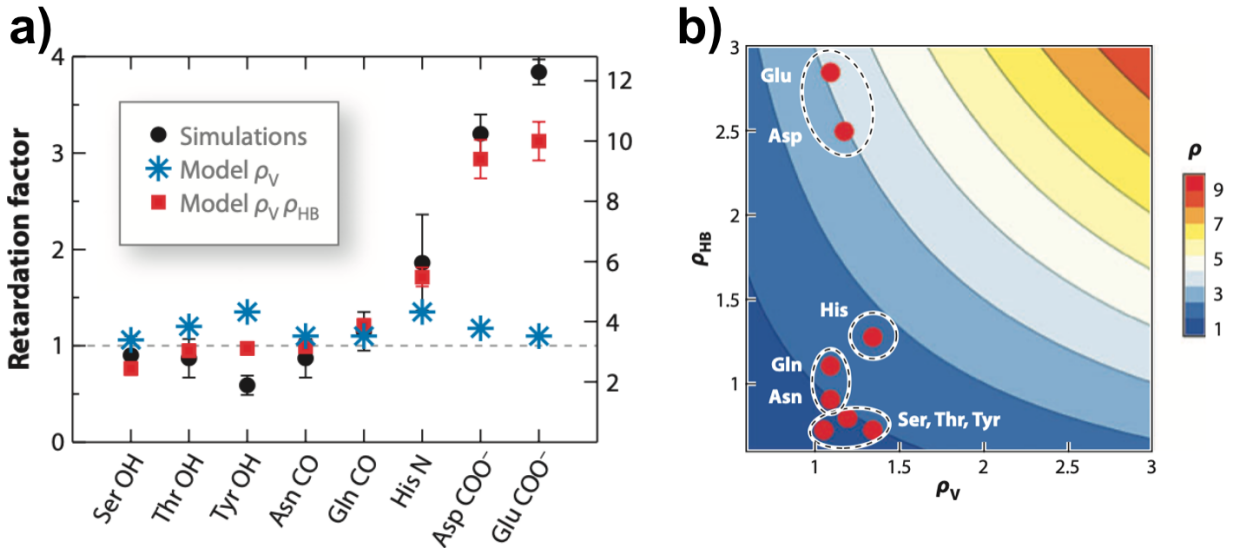

Figure 5.7: *a) Retardation factor with respect to the bulk of the HB exchange dynamics for AA HB-acceptor sites, with results from simulations (black circles), from the transition state excluded volume (TSEV) model (blue stars), and from the combined of the two corrections ρ_v and ρ_{HB} (red squares). b) Contour plot of the overall retardation factor $\rho_v \rho_{HB}$ as a function of its TSEV and TSHB components with the values of AA HB-acceptors [110]. Taken and adapted from ref. [110].*

It is worth noticing that the more hydrophilic AAs studied in the work of Laage *et al.* [110], that is to say Histidine, Aspartic Acid and Glutamic Acid, display the a large retardation factor compared to other amino acids. Those are among the most hydrophilic AAs and strong HB-acceptors because of their reversely nitrogen or carboxyl groups.

Studies [110, 111, 121, 124] suggest a marked slowdown of the water dynamics induce by the solvation of charged or polar solutes, where hydrophilic groups accept strong HBs from water. Ions influence the water structure of the first hydration layer, known as kosmotropic / chaotropic ions ordered in the Hofmeister series. The case of hydrated DNA, proteins, and phospholipids, and compared dynamics in the hydration shells to bulk water also received attention [111]. Duboué-Dijon *et al.* [124] interested themselves to the reorientation time of water molecules in the hydration shell. Thanks to MD, they investigated the reorientation of water molecules close to different sites of a ten-monomer DNA strand. They notably found that the reorientation times are larger in the hydration shell than in the bulk, and the largest time are those from with bonds made at inner sites of DNA, as illustrated on fig. 5.8.

The major part of the hydration shell appears to experience moderately retarded dynamics with respect to the bulk, notably next to the ribose groups, and phosphate backbone also induce a less pronounced retardation [124]. On the other hand, the slowest hydration dynamics are observed in the vicinity of adenine-thymine (A-T) base pairs in AATT center of DNA sample. An interesting feature is again the particularly higher factor of retardation for HB acceptor sites, which are a quite important fraction of the surface. Other studies worked on globular proteins (notably lysozyme) [125, 126] and confirmed this result, as shown by fig. 5.9.

Those effects have a short range, and only few layers of water molecules seem to be affected: a significant long-range modification of the structure and dynamics of water around biomolecules lack theoretical and experimental evidence [111]. Quantitatively, only the first layers displays

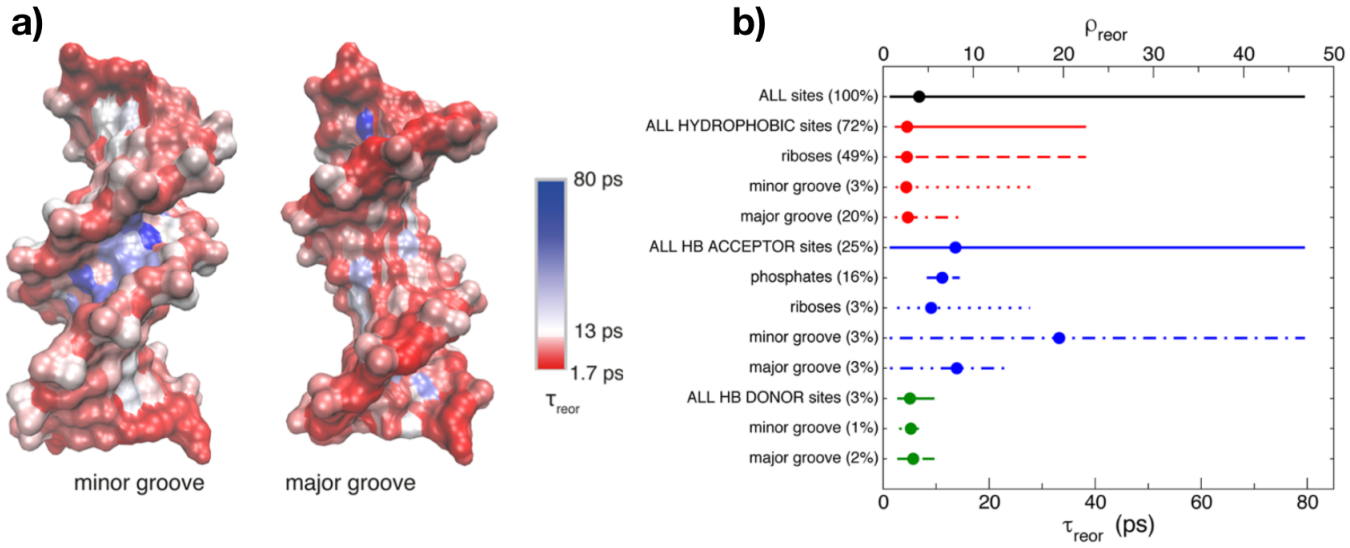

Figure 5.8: *a) Mapping of the reorientation time on DNA surface. b) Water reorientation time and slowdown for each type of DNA site, where each line shows the range of values, the dot gives the average value. Adapted from ref. [124].*

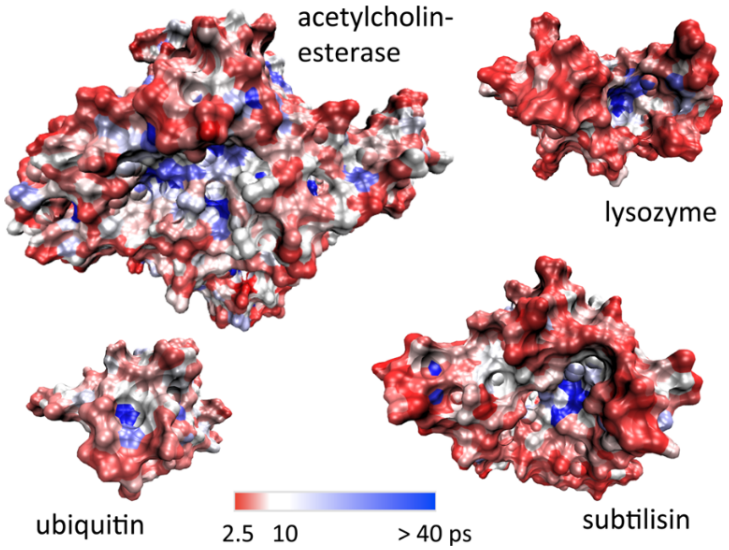

Figure 5.9: *Mapping of reorientation times onto the protein surface, for the four protein systems in aqueous solution. Figure taken from ref. [126].*

effects, typically less than five layers, starting from the interfacial water layer [111]. Beyond, water molecules have similar properties than bulk water. Duboué-Dijon *et al.* [124] indicate that for this retardation effects, hydrophobic and HB-donor groups, notably $-NH_2$ groups, behave in a similar manner. So the properties of HBs will be considered different to some extent at the protein surface with respect to the bulk, notably the energies of bonding. Appendix B presents elements of hydrophilicity of AAs.

In this chapter, we have seen that the dynamical properties of HBs are significantly modified by a surface, in particular hydrophilic sites. The rates of bonding of water molecules seem to follow an Arrhenius law. In the following, we will attempt to see if this phenomenon can result in a possible mechanism for negative thermodiffusion.

Chapter 6

A simple model involving jumps of water molecules on hydrophilic spots

Here we present a model that aims at explaining negative thermophoresis with thermo-osmosis induced by HBs. First we present the physical model, that exploits elements presented in the previous chapters. We display how we model the interactions between water molecules and the surface, then the dynamics. Then we detail how a temperature gradient results in a creep velocity. The following sections deal with the temperature dependence of the obtained velocity, and how it can match the experimental observation, and eventually we display the results concerning D_T and S_T. We show that this is in agreement both qualitatively and quantitatively with the result of Piazza *et al.*

6.1 Frame - Physical model

This section presents the physical model. We have seen in chapter 3 different treatments of the fluid surrounding the particle moving in the temperature gradient. Gases are described by the theory of gas kinetics, where molecules are described with a discrete approach, and liquids are modeled as continuous media. We try for this model a discrete approach for the treatment of water molecules that are bonding on hydrophilic spots to establish HBs. The idea is to make emerge a velocity based on a rates difference sparked by a temperature gradient, as evoked in chapter 5.

We start from the HB network in volume, which is then in contact with a solid surface. We present the dynamics of HB breaking / formation we consider, and finally explain how we can build a velocity.

6.1.1 HB essential properties

In this first part we present the essential properties of HBs that take place in our model. We notably present how we model HBs between water molecules and with a HS, then their dynamics and ways of breaking / formation. We precise which mechanism is envisaged for our model. Then we end with elements that suggest that a temperature gradient can induce a motion of the surface.

Here we set the frame of the HB network, exposed to a solid surface bearing HS. Since we suppose an invariance along y, we work in the (x, z) plan. We start from HB network in

volume, as illustrated by fig. 6.1.

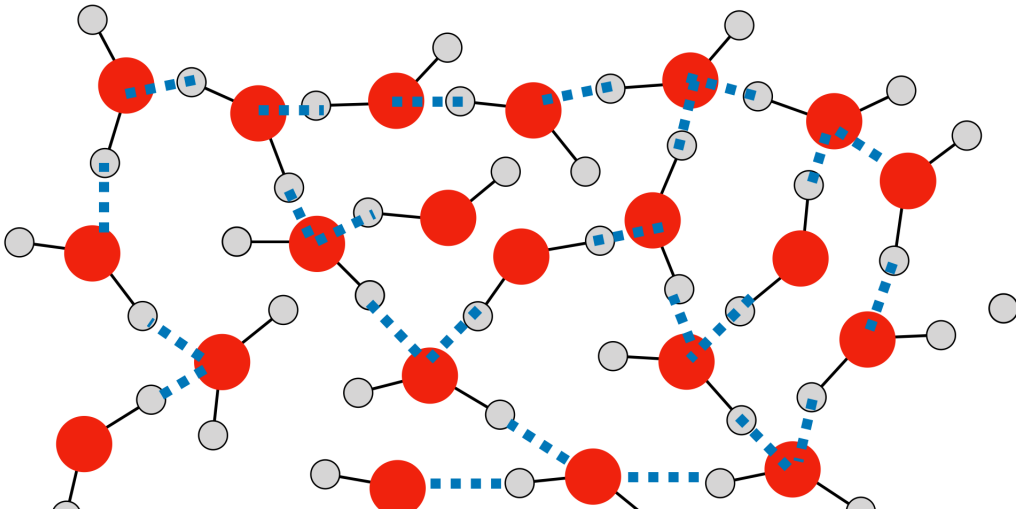

Figure 6.1: *HB network in volume. HB between water molecules are represented with blue dashed lines.*

Now we add a solid boundary featuring HS (oxygen or nitrogen groups), pictured by purple spheres as shown by fig. 6.2. HB between a water molecule and an HS are in green, to differentiate from HB between water molecules, as depicted by fig. 6.3. Some of their properties are supposed different from the bulk, such as energies, to match with the retardation effect observed presented in chapter 5.

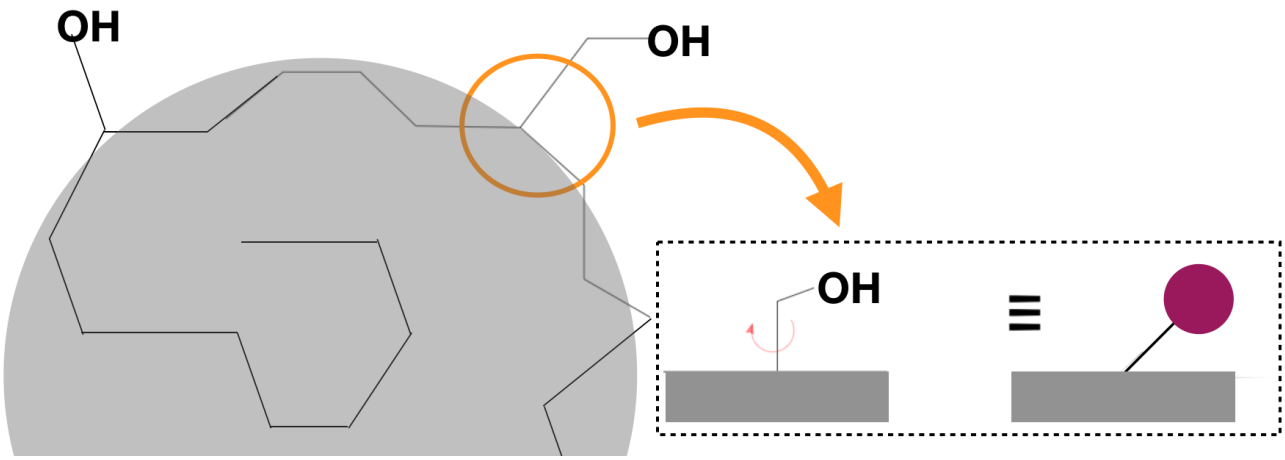

Figure 6.2: *Schematic approach of the surface of the particle around a hydrophilic spot, schematized by the hydroxyl group. The "surface" is not genuinely a flat area, but we assume for the sake of simplicity that in the vicinity of an HS on the carbon chain there is a place that can be supposed flat. We neglect the internal rotations of the chain. HS can have different inclinations with respect to the surface.*

Those HB dynamics are indeed determined by elementary jumps Γ and γ that depend on temperature. We have to discuss the ways of formation and breaking of HBs. We present the different options for those HB dynamics, with two possible scenarios: partner change, and formation/breaking of the HB. We present those in the cases the HS is HB acceptor, then HB donor.

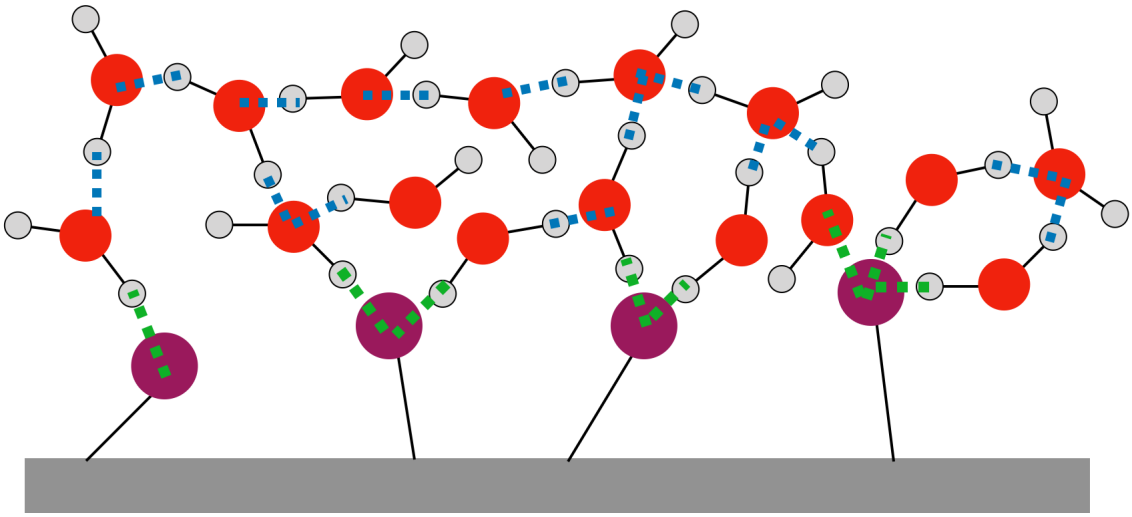

Figure 6.3: *Schematic view of the hydrogen bonds network at the surface of the particle. As seen in the previous section hydrophilic spots can establish in total four bonds, one being with the carbon chain of the particle. So it can be connected up to three water molecules.*

First scenario: as suggested by Laage [112], the HB ends because of brutal large amplitude reorientation of a water molecule and a partner change. The process is illustrated with fig. 6.4. The occupation n of the HS does not change during the HB cycle. This can be schematized by the equation N**...**HO $\rightarrow$ N**...**H*O*, where N is the an atom of the HS (here a nitrogen), the dashed line is an HB, the covalent bond is not explicitly represented, atoms are just attached.

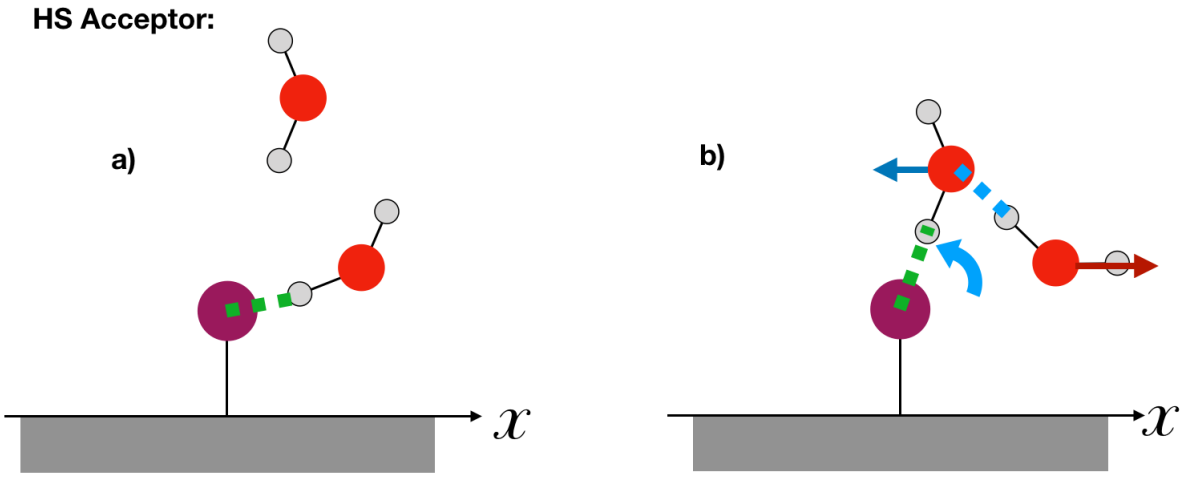

Figure 6.4: *Process of breaking via partner changing in the HS acceptor situation.*

A major hypothesis in this situation is that when the bond breaks, the water molecule escapes in a random direction. This way, the breaking of HB does not play a role in the motion of the surface, which is expected since there is no modification brought by the temperature gradient at this reference position.

Second scenario: a genuine forming / breaking cycle, where the HB really breaks without partner change, before the HS establishes another HB with a different molecule. This is illustrated on fig. 6.5. Concerning the creation of the HB, whether the water molecule first orientates, then approaches the HS or the contrary does not change the result. The molecule just approaches the HS, likely along a concerted motion of both diminishing distance and ori-

entating the HB, as presented by Kikutsuji *et al.* [100]. This corresponds to a situation N→ N**...**HO. When released, the water molecule, by counteraction, is likely to escape in the direction of the bond. In this scenario, on average, the molecule goes back to its original position, in particular if the HB network has kept some memory.

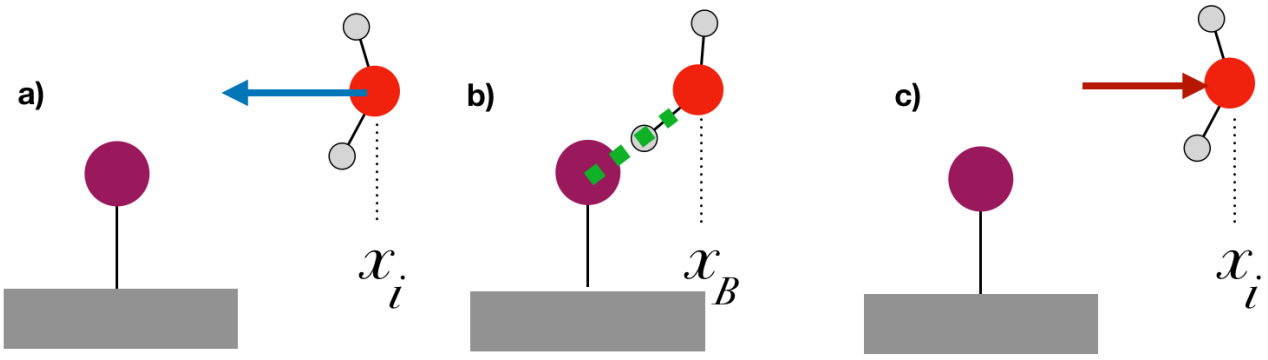

Figure 6.5: *Process of breaking via translational breaking. Here the HS is acceptor but the result is not changed when it is donor.*

Now we consider the case of an HS donor of HB, exploring once again the two options of breaking. Fig. 6.6 displays the situation of the partner change, and fig. 6.7 the genuine formation / breaking of HB without partner change.

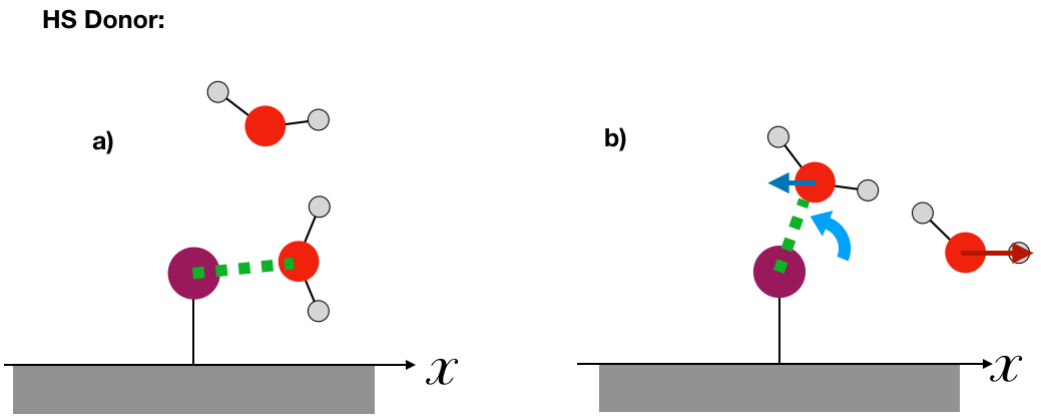

Figure 6.6: *Process of breaking via partner changing when the HS donor. In this case the population of HB of the HS does not change.*

Memory of the HB network is still discarded as evoked before. We always suppose that thermal agitation has reseted it during the HB lifetime.

As a result, in all cases water molecules are moving with respect to the surface, because getting closer to the HS when creating the bond. In the scenario of a partner change the factor of occupation n of the bond is not relevant. For our model, we consider in a first time the situation where the occupation number does not play a role. As suggested by [14, 110, 124], retardation effects are more significant when HS are HB acceptor. Therefore in the following we represent water molecules as HB donor.

In the following we discuss the case of a partner change.

When bounding, a water molecule is dragged, as suggested by Kikutsuji [100]. The mean distance of jump is ℓ. It corresponds to the diminution in the O-N distance. ℓ seems to depend

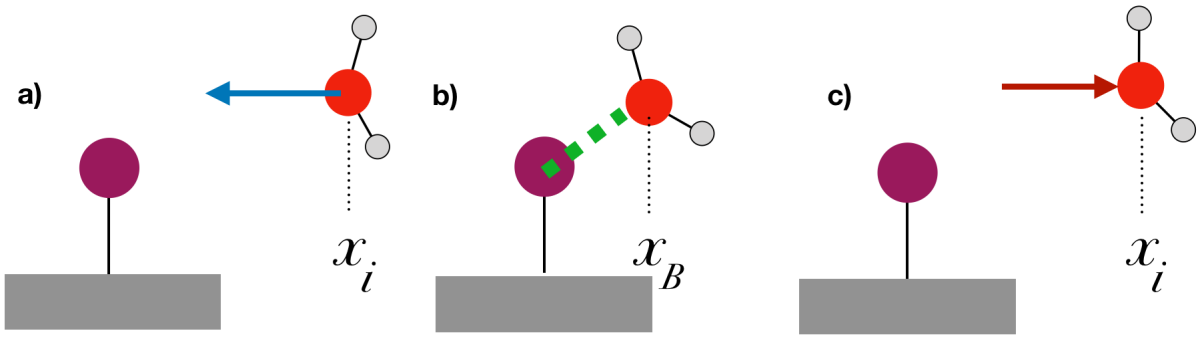

Figure 6.7: *Process of breaking via translational breaking. Here the HS is donor, the result is not changed from the acceptor situation.*

on T [129,130]. When the bond is created the HS (thus the surface) moves with respect to the bulk, see fig. 6.8.

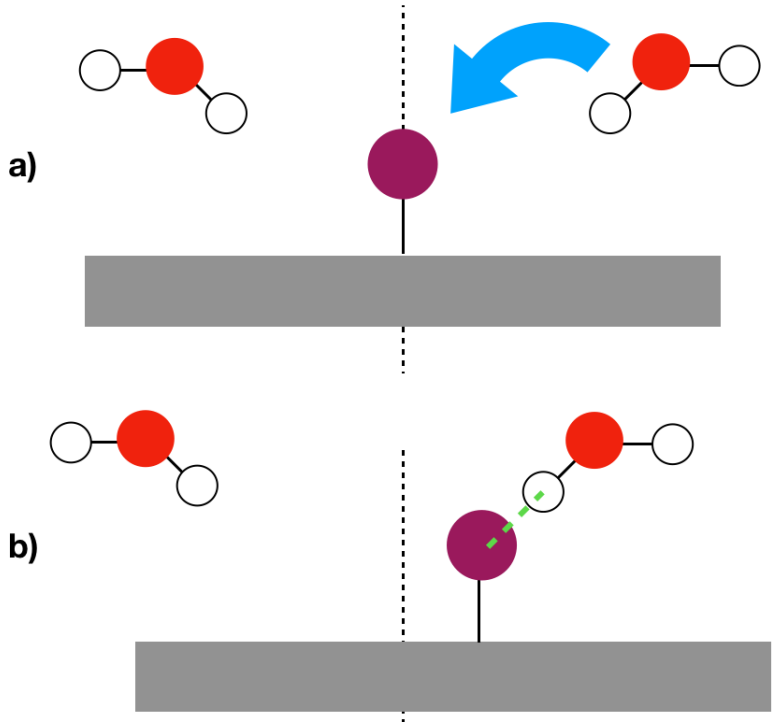

Figure 6.8: *a) a water molecule jumps on the HS b) The water molecule is H-bound, as schematized by the green dashed line, and has gotten closer to the HS, who has been dragged too, as the motion with respect to the black dashed lines indicates. In equilibrium, the rates are equiprobable whether the water molecule jumps from the left or the right of the HS, so on average there is no motion of the surface.*

So Γ and ℓ vary in the temperature gradient along the surface. This presented, we have the elements to build a velocity.

6.1.2 Elementary foundations of thermo-osmosis via HB

Here we exploit the temperature dependence of Γ and ℓ to build a velocity. We present the loss of memory and the non-specular emission of the HS which result in a net velocity of water molecules at the surface. In equilibrium, without any temperature gradient, jumps from both

sides of the HS are totally equiprobable. So on average, in equilibrium, no net displacement of the surface. Nonetheless, in a temperature gradient, the jump rates would be different and the symmetry broken because of the temperature gradient. That would lead to a creep flow that would propel the particle.

Consider a water molecule close to a HS in a temperature gradient, along x. This molecule can bond from the cold or the hot, as depicted on fig. 6.9. The temperature gradient would favor one side, since the rates of jumps depend on temperature.

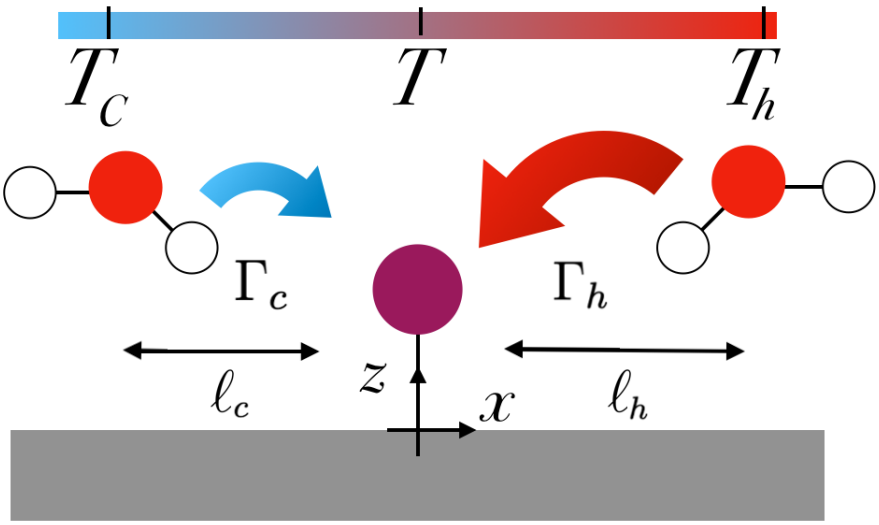

Figure 6.9: *Rectified jumping rates*

A net velocity can only emerge if the water molecules does not return to its initial position. The releasing of the water molecule after HB-breaking is supposed random, like a non-specular reemission, the molecule escapes in any direction. For instance we can notably suppose that after each jump, the molecular environment around the HS has been reseted because of thermal agitation. The considered oxygen atom has lost memory of its previous position, so the next jump is performed in a modified environment. We do not consider any correlation between the bonding and the breaking motion. This idea is inspired by the non-specular reemission of adsorbed gas molecules by the surface as presented in Maxwell's model in chapter 3.

Moreover, in the case of memory of the HB network, according to Onsager's principle of microscale reversibility, the particle is likely to return to its original position, since here everything is totally reversible. To sum up simply, this principle states that at the most elementary level (atomic, and even smaller) everything must be totally reversible, since time can be reversed in quantum mechanics. Onsager's theory is based on the principle of microscopic reversibility such that under equilibrium condition, any molecular process and reverse of that process will be taking place on the average at the same rate, though equilibrium was not maintained in molecular level. As a result the water molecule should go back precisely to its original position. However, doing so, the drag action between the particle and the surface would totally vanish. Indeed, it would be like a roam in water, that would give two opposed hits in a row. This does not make any move, neither would the particle. So this paradigm is totally incapable of explaining a creep flow a water molecules at the surface of the diffusion particle. Thus, we do not consider in the following any memory of the HB network. Anyway, we have presented in chapter 5, the dynamics of HB are slower at the surface than in the bulk,

so the HB network cannot evolve slower than the pair HS-water molecule. Thus, we dismiss any memory of the HB network.

The distance of jump accomplished by a water molecule when jumping on a HS will be named ℓ. ℓ is suspected to be activated [129,130]. In this model, the velocity emerges from the difference in the mean distance-rate product. Projected along the x axis, this gives:

$$\boxed{v_s =< \ell(T_c)\Gamma(T_c) > - < \ell(T_h)\Gamma(T_h) > .} \tag{6.1}$$

$\ell_c = \ell(T_c)$, $\ell_h = \ell(T_h)$, $\Gamma_c = \Gamma(T_c)$ and $\Gamma_h = \Gamma(T_h)$ as shown on fig. 6.9. Our water molecule experiences actions from the surface and from the liquid. This leads to the velocity from the surface v_s, and another contribution from the bulk v_b:

$$v_b = \langle \Gamma_c^* \ell_c^* \rangle - \langle \Gamma_h^* \ell_h^* \rangle . \tag{6.2}$$

Stared quantities refer to properties of bulk liquid. In the bulk there is no velocity sparked by a temperature gradient, so the overall velocity of the water molecule is given by:

$$v = v_s - v_b. \tag{6.3}$$

6.2 Model of temperature dependence of rates at the surface of a protein

This section is centered on hydrophilic spots (HS). We interest ourselves to the water molecules that bound and detach from the HS. We base our approach on a ratchet effect [128] observed recently for ionic conductors leading to huge Seebeck coefficients. This effect arises from activated jumps between neighbor sites, rectified by a temperature gradient, driving mobile ions towards the cold. We attempt to determine if a disparity in the rates of jump of water molecules at the surface of a molecule featuring HS that could quantitatively match the experimental observation.

6.2.1 Simplifying hypothesis for the protein surface

The particle experiencing thermodiffusion, such as a polypeptide, as presented in chapter 2, consists in a carbon chain with different ramified functional groups, those molecules in normal pH and temperature conditions tend to coil and form a globular object. We are well aware that proteins and more generally biopolymers have a folding behavior that depends on temperature [127]. But for the sake of simplicity, we do not take into account these differences in shape, and consider the protein is a rigid ball, whose radius remain constant during the thermophoretic motion.

HS are ramified chains with polar groups, that are in a perpetual agitation. For our work, we neglect their internal motions and model it as rigid sticks bearing a polar head. We also suppose that HS can be engaged in a maximum of three HB with other molecules, regardless the donor / acceptor nature of bonds. This idea comes from the tetrahedral structure of the HB network presented in chapter 4, taking into account that the HS is already connected to the rest of the particle with a covalent bond. To simplify even more the situation, we do not

consider the differences in inclination with respect to the surface, and consider the HS are systematically perpendicular to the surface. We suppose in the following that the temperature gradient is applied along the x axis.

The density of HS is suspected to have an impact on the magnitude of D_T and S_T. Indeed, HS density contributes to hydrophilicity, and we have already presented the link between S_T and P in chapter 4, which highlights a correlation between thermophilicity and hydrophilcity [16,17].

Effects of retardation are important only in the first layers [124], and for the sake of simplicity we assume that this concerns exclusively the first layer of water molecules. The bulk is assumed to begin at the second layer.

6.2.2 Rates of jumps on hydrophilic spots

Now we precise the expressions of the rates of jump and the probability of occupation of HS. As evoked in chapter 5, the HB lifetime τ_{HB} follows an Arrhenius law. The rate of formation Γ (and breaking $\gamma = 1/\tau_{HB}$), should have a similar form:

$$\Gamma(T) = \Gamma_0 \mathrm{e}^{-\frac{\Delta G_B}{k_B T}}. \tag{6.4}$$

So Γ is described by described by a temperature dependence and a free enthalpy ΔG_B:

$$\Delta G_B = B - TS_B, \tag{6.5}$$

where B is the gain in enthalpy and S_B the cost in entropy corresponding to the formation of an HB. B is suspected to be of the order of some $k_B T$, as evoked in chapter 5 for bulk water, but we do not discard larger values, since at our knowledge there is not experimental measure of this barrier. B must be a priori positive. Otherwise Γ does not grow with T, and we expect the jump form the hot side to occur more often than from the cold side to result in a velocity of the fluid towards the cold side. There are less constraints on S_B, though we set S_B in order to recover rates of the order of 10^{-12}/s to be consistent with observations presented in chapter 5.

Following [128], we set Γ_0 to be the ratio of the thermal energy and Planck's constant:

$$\Gamma_0 = \frac{k_B T}{h}. \tag{6.6}$$

Water molecules can be in two different states: free and bound. We describe this in terms of potential landscape, as suggested by Kikutsuji [100] and presented in chapter 4. Fig. 6.10 illustrates this 2-D potential landscape.

Fig. 6.10 provides:

$$\gamma = \mathrm{e}^{-\frac{\Delta G}{k_B T}} \Gamma. \tag{6.7}$$

ΔG the free enthalpy difference between the potential wells, as depicted on figure 6.10. This free enthalpy is once again associated to an enthalpy and an entropy: $\Delta G = \Delta H - T\Delta S$. ΔH must be positive. Indeed, we expect the population of bonds, that is to say n, to diminish with temperature, since HBs are weakened when temperature rises. This cannot be satisfied with ΔH negative, as presented in the next section.

Finally, since at high temperature the strength of HB diminishes, we expect the rates of

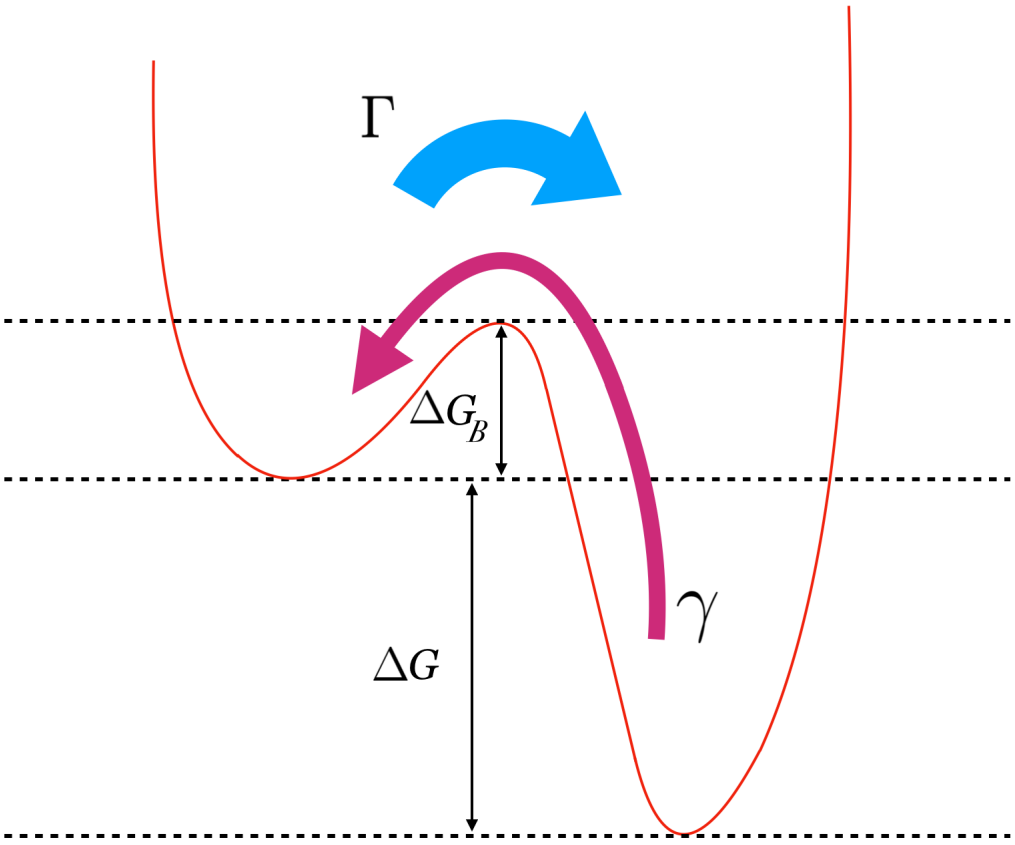

Figure 6.10: *Potential landscape for a water molecule in the vicinity of a HS. The molecule can be free, shallow well on the left, or bond, deep well on the right. To pass from free to bond, the water molecule has to overcome the barrier, that determines the rate of jump in eq. 6.4. The well of the bound state is deeper than the free state with an enthalpy ΔG. To return to the free state a water molecule must overcome the total barrier.*

jumping and breaking to be equal. This way, it is not that much energetically appealing for a water particle to bond as it was at low temperature, the two wells have the same depth and the rates are equal. This is fulfilled with $\Delta G = 0$. So a priori we expect $\Delta S \sim \frac{\Delta H}{T_b}$, with T_b a "high temperature", like the temperature at which the HB networks breaks down, supposed to be somewhere near 100 °C.

6.2.3 Populations of hydrogen bonds

We define a two-level system, the two levels being "the water molecule is not attached to the hydrophilic spot" and "the water molecule is bound to the hydrophilic spot", described by the value n the occupation of the bond. The limiting case $n = 1$ corresponds to a stable HB whereas $n = 0$ indicates the absence of HB. The occupation number n for the bound state is given by the master equation:

$$\dot{n} = -\gamma n + \Gamma(1 - n). \tag{6.8}$$

In the steady state, $\dot{n} = 0$, so the occupation number becomes:

$$n_{eq} = \frac{1}{1 + \frac{\gamma}{\Gamma}} = \frac{1}{1 + \mathrm{e}^{-\frac{\Delta G}{k_B T}}}. \tag{6.9}$$

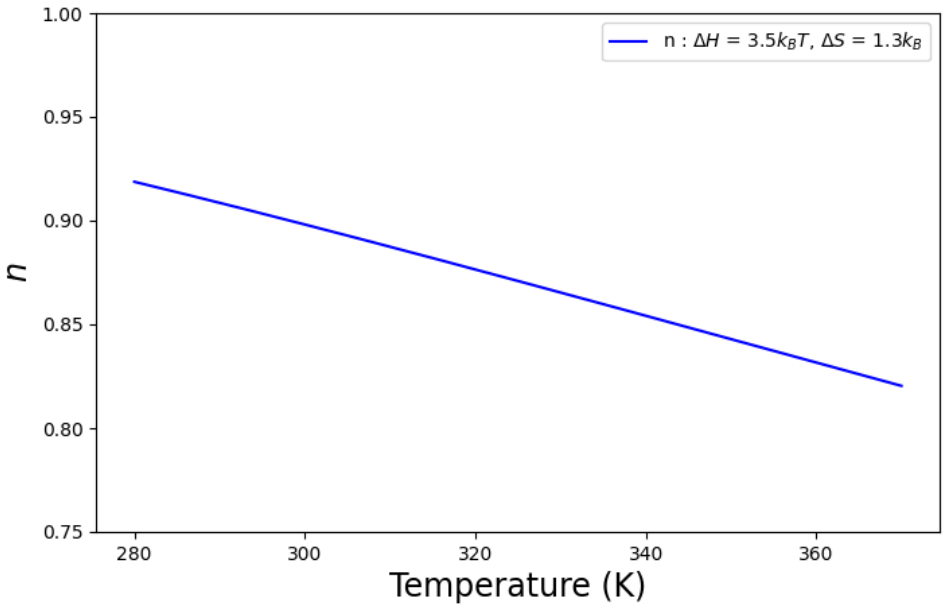

Figure 6.11: *Probability of formation of a HB between two nearby oxygen atoms as a function of temperature, according to eq. 6.9.*

Thermodynamic quantities such as the specific heat indicate that n decreases with temperature, as shown with fig. 6.11. Typical values in bulk water are $n = 0.90$ at $T = 25$ °C degrees and $n = 0.81$ at 100 °C. Then the number of donor HBs per oxygen is given by 2n, whereas each oxygen participates in 4n HBs.

To satisfy it with equation 6.9 this requires bulk values for the enthalpy to be $3.5k_BT_{amb}$ and for the entropy $1.3k_B$. We have no precise values for those parameters, especially when considering HB between a solute and a water molecule. For instance, the hydration entropy of alkanes changes sign from negative to positive by increasing their chain length [10]. Values for ΔH and ΔS for the surface will be a priori determining for our model to work, as long as B and S_B.

In this work though we assume that ℓ is the same on both sides of the HS for the sake of simplicity. Taking into account the activation of ℓ should however simply result in the addition of two new enthalpy and entropy parameters.

6.3 Computation of the velocity

Now we compute the rate difference resulting from the temperature gradient.

6.3.1 First try featuring the rate difference to obtain a negative velocity

As we have begun to evoke it, the jump rates depend on temperature, so we expect a breaking of symmetry because of the temperature gradient. We interest ourselves to a given HS, at the position $x = 0$. Our temperature of reference T is at this position $x = 0$. A molecule about to jump from the cold side of an hydrophilic site has a rate Γ_c different than the one from the hot site Γ_h. The breaking rate γ is not rectified by temperature since it depends on the bond position, still at the mean temperature T.

First we compute the rates Γ_c and Γ_h. We develop around the two positions of jumping considered, x_c and x_h, so that the water molecules are initially at a x-distance ℓ from the HS. The dimensionless quantity $\frac{\ell\nabla T}{T}$ is small before unity (about 10^{-8}), which justifies limited developments. We obtain:

$$\Gamma_c = \Gamma(T_c) = \Gamma(1 - \ell\frac{\nabla T}{T}(1 + \frac{B}{k_B T})), \tag{6.10a}$$

$$\Gamma_h = \Gamma(T_h) = \Gamma(1 + \ell\frac{\nabla T}{T}(1 + \frac{B}{k_B T})). \tag{6.10b}$$

The rate difference $\delta\Gamma = \Gamma_c - \Gamma_h$ is thus:

$$\delta\Gamma = -2\Gamma\ell\frac{\nabla T}{T}(1 + \frac{B}{k_B T}), \tag{6.11}$$

Γ being evaluated at the temperature T of the HS. This provide a first coarse evaluation for the creep flow velocity:

$$v_0 = \ell\delta\Gamma = -2\ell^2\nabla T\frac{d\Gamma}{dT}. \tag{6.12}$$

Since $\Delta\Gamma < 0$ (eq. 6.11), we expect a creep flow towards the cold, thus a motion of the particle towards the hotter area. And if $\nabla T = 0$, the velocity vanishes. Qualitatively, this is in good agreement with the experimental observation. We must now evaluate if this holds quantitatively. In the following we set $\nabla T = 10^6$ K/m, and $\ell = 0.2$ Å.

6.3.2 Temperature dependence of this first velocity

We want the thermodiffusion coefficient $D_T(T)$ to be compatible with Piazza's observation developed in chapter 2. We know $D_T \propto \frac{v}{\nabla T}$, as presented in chapter 3, so the behavior of D_T and v are the same. So we want the velocity to have the form $v(T) = aT - b$, with a and b two positive constants.

As displayed in eq. 6.12, v_0 only depends on one parameter, B, because S_B only sets an amplitude. We tried values in range -1 to 100 $k_B T$, which always result in a velocity that decreases with the temperature, as exemplified by fig. 6.12. The exponential dependence on $B/k_B T$ prevents to recover an increasing velocity. We must consider other options that could lead to a different behavior.

6.3.3 Action of the upper layer

Here we offer to take into account the action of the upper layer, independently from the occupation of water molecules developed previously. The water molecule in the first layer above the surface is also susceptible to be dragged by the second layer above, as displayed on fig. 6.13. We do not mention interactions of water molecules of the first layer between themselves, since it does not lead to a motion of the first layer.

A water molecule can be dragged by the upper layer, as illustrated by fig. 6.13. This happens when a molecule from the second layer bonds to the water molecule already attached to the HS. The first water molecule is pulled by the second water molecule, which brings another contribution to the velocity of the first layer. The contribution from the second layer, denoted

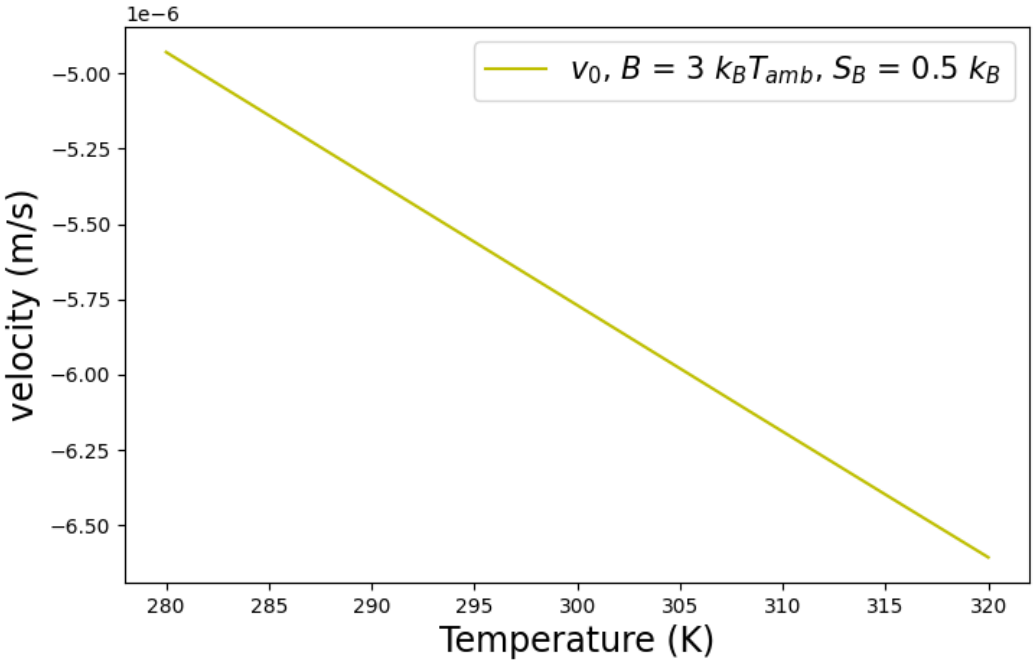

Figure 6.12: *Typical plot of v_0 vs T.*

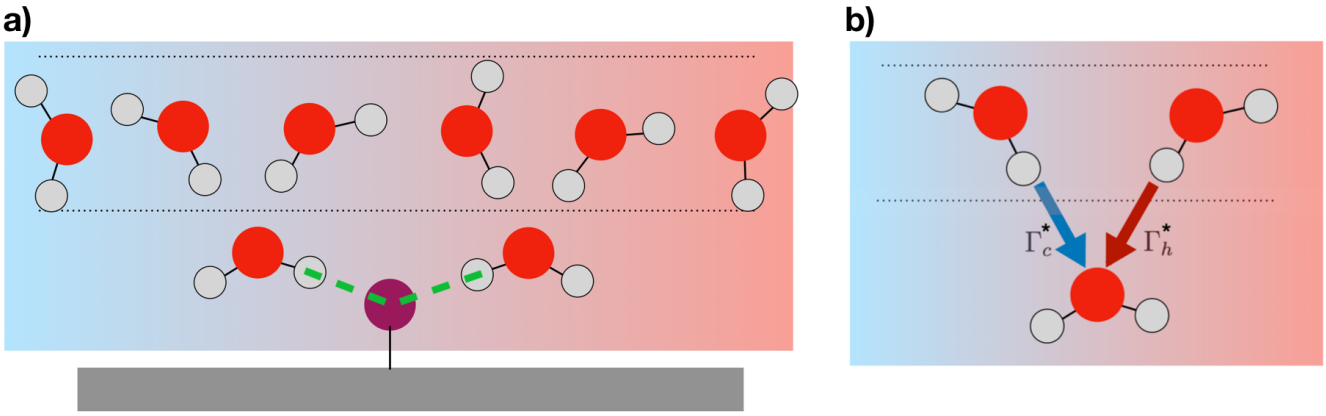

Figure 6.13: *a) Schematic view of the second layer of water molecules. We display the molecules of the first layer bound to the HS. Molecules from the second layer exert a motion on them when bonding b)Schematic view of the action of the adjacent layer on a first-layer water molecule.*

v_{bulk} arises from difference in temperature of the molecules bonding to the second layer molecule. So we can attempt to develop this contribution due to the second layer to compute the velocity of the first one, which would propel the particle to the hot side. We have to determine the velocity sparked by the temperature gradient in the bulk. the quantities relative to the bulk are denoted with stars: B^* and S_B^* are the enthalpy and entropy of jump in the bulk, that is to say for a water molecule to jump on another, at a rate Γ^*. The distance of displacement ℓ^* in the bulk is supposed different than the one at the surface v_0. We introduce the ratio $R = \frac{\ell^*}{\ell}$.

$$v_1 = v_0 + v_{bulk} \tag{6.13}$$

This time Γ_c^* pulls towards the cold, and Γ_h^* towards the hot, as illustrated on fig. 6.13.

Projecting on the x-axis we get:

$$v_{bulk} = -\ell^*(\Gamma_c^* - \Gamma_h^*) \tag{6.14}$$

This velocity also cancels when $\nabla T = 0$. But this bulk contribution is positive. We considered the different cases $R < 1$, $R = 1$ and $R > 1$.

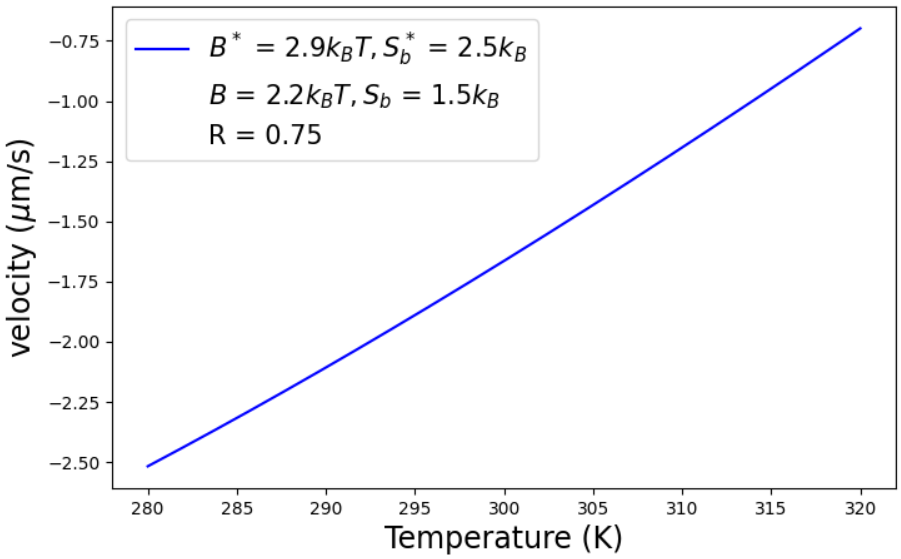

Figure 6.14: *Typical curve of v_1 with $R = 0.75$. The case $R < 1$ provided more flexibility on the different parameters so we displayed this case.*

In all cases, the situations that enabled to plot a linear velocity increasing with T are always $B < B^*$ and $S_B \leqslant S_B^*$. $B < B^*$ seems consistent, since this means that a water molecule jumps easier on a HS than on another water molecule, which seems reasonable for a hydrophilic spot. Concerning entropies, if we consider the entropy loss when bonding of on the one hand a pair of water molecules, and on the other a water molecule and an hydrophilic spot, the entropy loss seems larger in the first situation, since the hydrophilic spot is poorly mobile in both cases and does not lose that much entropy when bonding. But two water molecule pairing should lead to a greater entropy cost. Therefore, $S_B < S_B^*$ seems quite consistent.

6.3.4 Probabilities of occupation of hydrogen bonds

We try to add to our model weighing the jumps by the probability that the HS is able to accept a bond from a bonding water molecule, this probability is $1 - n_c$ for the molecule from the cold side, and $1 - n_h$ for the one coming from the hot side. The velocity becomes:

$$v_2 = v_1 + v_{bulk2}. \tag{6.15}$$

v_1 is the surface contribution weighed by probabilities of occupation:

$$v_1 = \ell\left((1 - n_c)\Gamma_c - (1 - n_h)\Gamma_h\right). \tag{6.16}$$

And v_{bulk2} the contribution of the bulk weighed by vacancy probabilities:

$$v_{bulk2} = \ell^*((1 - n_h^*)\Gamma_h^* - (1 - n_c^*)\Gamma_c^*) = \ell^*(\Gamma^*\delta n^* - (1 - n^*)\delta\Gamma^*). \tag{6.17}$$

We develop the populations n_c and n_h:

$$n_c = n + n^2\ell\frac{\nabla T}{T}\frac{\Delta H}{k_B T}\mathrm{e}^{-\frac{\Delta G}{k_B T}}, \tag{6.18a}$$

$$n_h = n - n^2\ell\frac{\nabla T}{T}\frac{\Delta H}{k_B T}\mathrm{e}^{-\frac{\Delta G}{k_B T}}, \tag{6.18b}$$

The difference in population δn is thus given by:

$$\delta n = n_c - n_h = 2\ell\frac{\nabla T}{T}n(1-n)\frac{\Delta H}{k_B T} \tag{6.19}$$

The same goes for the bulk with stared quantities. v_1 can thus be written:

$$v_1 = \ell((1-n)\delta\Gamma - \delta n\Gamma) = v_0 - \ell\left(n\delta\Gamma + \Gamma\delta n\right), \tag{6.20}$$

which can be seen as a added correction to v_0. If we compare the values of ΔH and ΔS to values of enthalpy and entropy for the hydration of alcohols that we find in the literature [123], those are of the same order of magnitude: some units of $k_B T$ for ΔH and some units of k_B for ΔS. Though our model requires a relatively high ΔS compared to the values found in ref. [123].

The order of the terms is different than in eq. 6.17 because the cold molecule of the second layer is pulling the molecule from the first layer towards the cold. $\delta\Gamma^*$ is a negative quantity, since we defined it as $\Gamma_c - \Gamma_h$, and the rate is larger at high temperature, so v_{bulk2} is a positive quantity. The velocity in this model is thus:

$$v_2 = \ell(\Gamma\delta n - \delta\Gamma(1-n)) + \ell^*(\delta\Gamma^*(1-n^*) - \Gamma^*\delta n^*). \tag{6.21}$$

Eq. 6.21 is totally ruled by parameters B, B^*, ΔH, ΔH^*, ΔS, ΔS^*, S_B, S_B^* and R. We must try combinations of those values that have physical meaning.

We set for the bulk $\Delta H^* = 3.5 k_B T_{amb}$, and $\Delta S = 1.3 k_B$, as evoked before. To enable the HB well depicted on fig. 6.10 to exist, we must have $\Delta H - T\Delta S > 0$. The same goes for stared quantities. To match with the observation of retardation dynamics of water near HS, we expect the relation:

$$\Delta H - T\Delta S > \Delta H^* - T\Delta S^*. \tag{6.22}$$

The well is supposed deeper when a HS is involved, which results in a longer lifetime at the surface than in the bulk. Fig. 6.15 shows a typical curve for a set of parameters that fulfills our hypothesis. It must be mentioned however that it was more difficult for us to obtain perfectly linear curves, depending on the parameters we obtained most of time some convexity, as displayed on fig. 6.15.

We must mention that taking negative values for B and B^* also provides velocities in good agreement with our expectations. However, we have defined B and B^* as enthalpic barriers, so considering them negative did not appeared physically meaningful to us, and even though it enabled to recover the experimental observation, we only considered positive values in the following.

As a result, we developed different approaches that permitted to show that a temperature gradient rectifying the rates of jumps can lead to creep flow of the first layer of molecules in contact with the surface of a particle featuring hydrophilic spots. In this paradigm, the

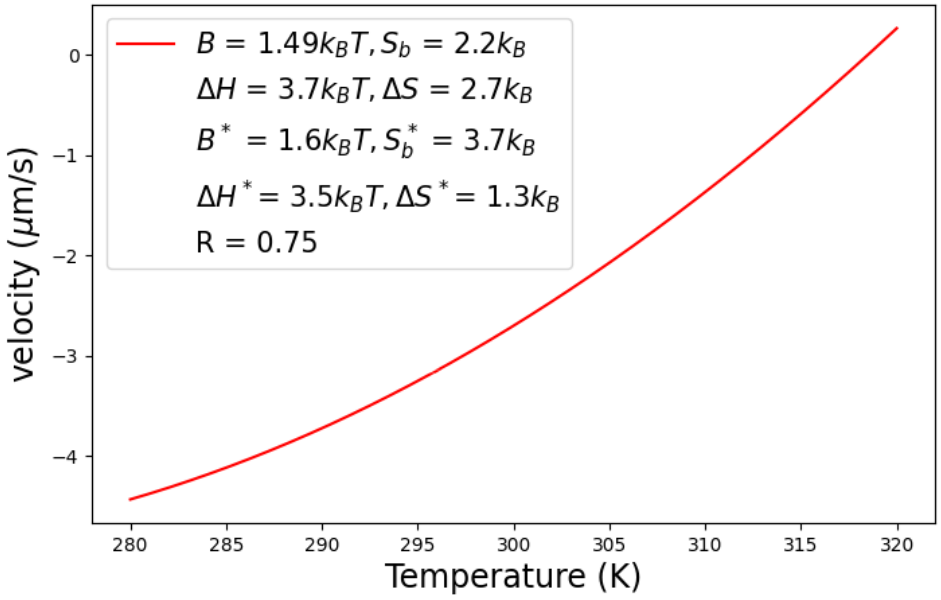

Figure 6.15: *Typical curve of v_2, with $R = 0.75$.*

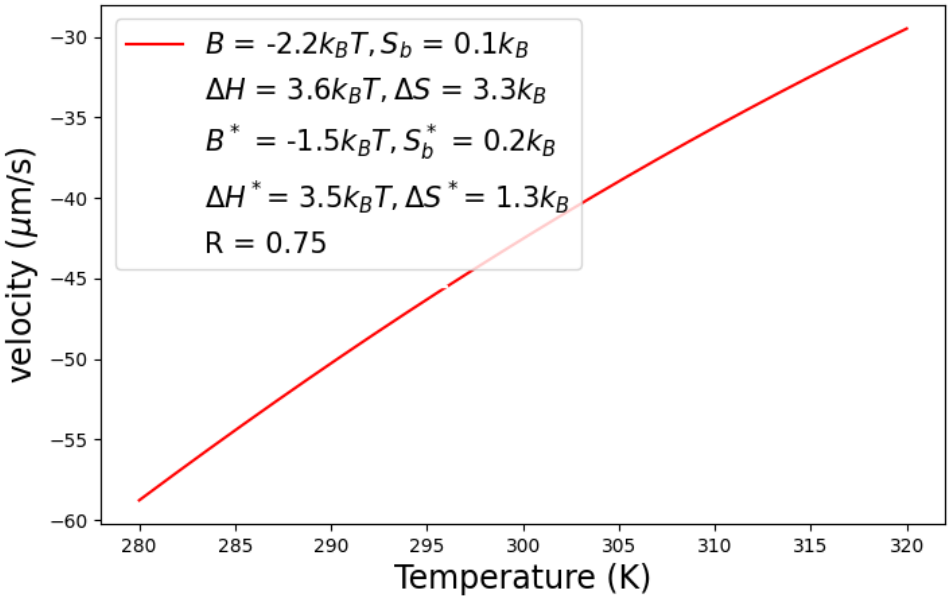

Figure 6.16: *Typical curves of v_2 with negative values for B and B^*.*

hydrophilic spot act as a ratchet that attract more often water molecules from the hot side, resulting in a motion of the particle towards the hotter area. We have thought about weighing the velocity by the fraction of hydrophilic areas of the surface over the total surface, but since this quantity is about one half it was not modifying the order of magnitude of the velocity, and would have only result in a adaptation of the entropy of jump S_B. So we did not implemented this parameter in our model.

6.4 Resulting thermodiffusion and Soret coefficients

In this section we attempt to plot the thermodiffusion coefficient, and then the Soret coefficient, resulting from the velocity we computed. In the following we use the velocity v_2 which is the most sophisticated we developed. We show that our expression is compatible with the

observation for $D_T(T)$ presented in chapter 2.

6.4.1 Thermodiffusion coefficient

To recover the thermodiffusion coefficient emerging from the HB interaction D_T^{HB}, we simply use the relation $D_T \propto \frac{v}{\nabla T}$. So we use $D_T^{HB} = \frac{v_2}{\nabla T}$. One must now add the thermo-osmotic contribution D_T^{OS}, from ES and vdW interactions, as developed in chapter 3. For the ES interaction, D_T has the form:

$$D_T^{ES} \sim \frac{\epsilon \zeta^2}{3\eta T}, \tag{6.23}$$

where ϵ is the dielectric permittivity of water, ζ the surface potential of the particle, and η the viscosity of water, which depends on temperature, as evoked in chapter 4. For the van der Waals interaction, the thermodiffusion contribution can be expressed:

$$D_T^{vdw} \propto -\frac{A}{\eta T d_0}, \tag{6.24}$$

with A an Hamaker constant and d_0 a cut-off distance. Following suggestions found in ref. [76], we set $\zeta = 40$ mV, $A_{vdW} = 6.\,10^{-22}$ J, and $d_0 = 1$ nm. Using this, we can obtain typical curves presented with fig. 6.17:

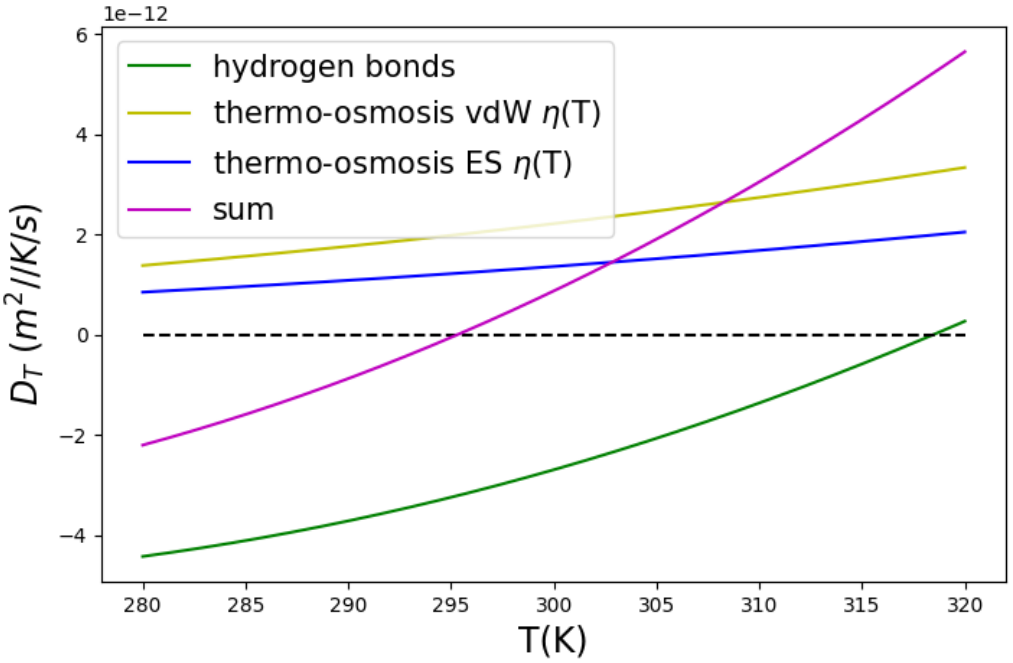

Figure 6.17: *Typical example of plot of the thermophoretic coefficients. For this one the model with v_2 has been used, with the parameters expressed in units of $293k_B$ for enthalpies and k_B for entropies: $B = 1.49$, $B^* = 1.6$, $\Delta H = 3.7$, $\Delta H^* = 3.5$, $S_B = 3$, $S_B^* = 4$, $\Delta S = 2.7$, $\Delta S^* = 1.3$ $R = 0.75$, $\nabla T = 10^6$ K/m, and $\ell = 0.2$ Å.*

So the curves obtained for the velocity are consistent with the observation for D_T: a negative curve, linear with temperature, and increasing. This is compatible with the experimental observation. For instance, the temperature dependence of D_T is relatively similar to the one of BLGA and lysozyme displayed in chapter 2, with the amplitude twice larger. Adding the

surface fraction factor of about one half enable to retrieve quantitatively the curve presented by Piazza and coworkers [7].

6.4.2 Soret coefficient

Now we can attempt to retrieve the Soret coefficient's dependence with temperature displayed in chapter 2. We use the relation $S_T = D_T/D$. Using Stokes-Einstein relation, we only need to set the hydrodynamic radius of the particle. We keep the same temperature dependence of the viscosity. The radius of a protein, and other colloids used by Piazza and coworkers are typically about some nanometers. For instance, the radius of BLGA can be estimated to ~ 1.5 nm, and lysozyme to 1 nm. We use a mean radius of about 1.2 nm, and plot the temperature evolution of the Soret coefficient on fig. 6.18.

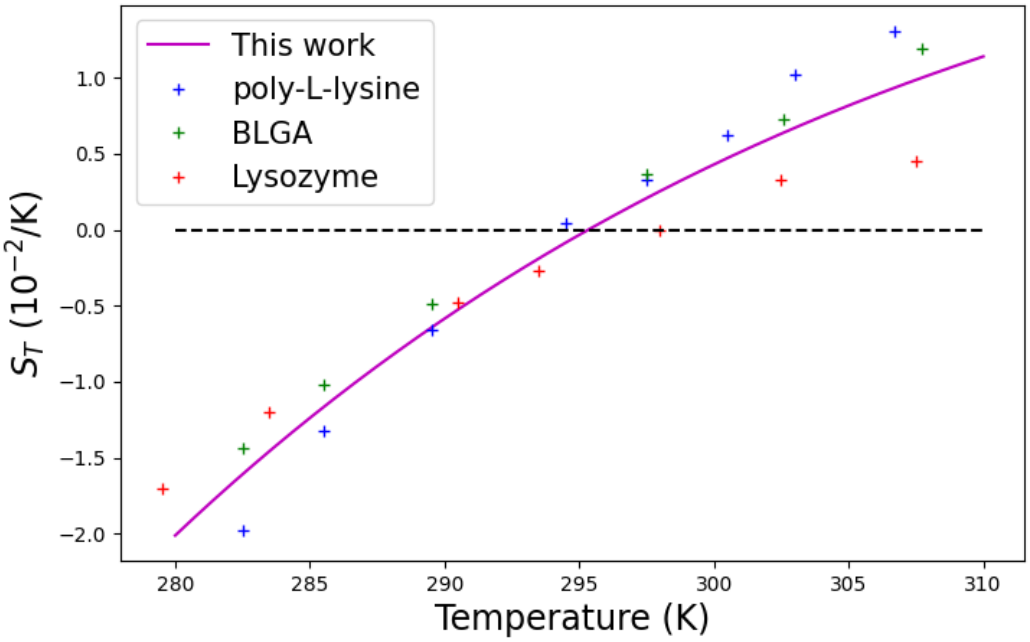

Figure 6.18: *Plot of S_T vs T according to our model compared with experimental data from ref. [7]. For our plot we used the same parameters than for fig. 6.17, and took a radius of the colloid of* 1.2 nm.

We can see that our model fits relatively well the experimental data for the thermophoresis of polypeptides reported by Piazza *et al.* [7]. As a conclusion, the temperature dependence of the rates of jumps, combined with a temperature gradient, can lead to a creep flow of the first layer of water at the surface of a particle featuring hydrophilic spots. Qualitatively, we have shown that the velocity is negative, and quantitatively, by taking into account the probabilities of occupation of the hydrogen bonds and the action of the upper layer, that the thermodiffusion coefficient and the Soret coefficient are in a relatively good agreement with the data available. However, this approach is relatively simple, and supposed that all the statistics of the jump are systematically constant and do not have a variance.

As a conclusion, hydrogen bonds between solute and solvent are a relevant actor to explain thermophilic motion of proteins and other biomolecules at low temperature. The decreasing strength of the hydrogen bond network when temperature rises is in good agreement with the experimental observation, and enables to understand the sign-switch of the Soret coefficient that has been reported.

Conclusion

We have seen through this work that thermophoresis is the emergence of a concentration gradient induced by a temperature gradient, observed in the stationary state. We have presented the most relevant quantities used to describe quantitively the phenomenon, that is to say the Soret coefficient S_T and the thermodiffusion coefficient D_T. The sign of those quantities dictates the direction of accumulation of the species.

We have seen that in the case of biomolecules in the dilute regime, these quantities feature intriguing temperature dependences. Indeed, for proteins, DNA, sugars, the Soret coefficient is concave and seems to follow an exponential law proposed by Piazza, and the thermodiffusion coefficient is linear with temperature. A sign change is reported, which is observed at the same temperature for polypeptides. Those shared elements are even more surprising given the fact that the systems studied have very different structures and size, but feature the same behavior.

The theories developed so far explain successfully the thermophoretic motion towards the cold in several cases, but are unable to explain the drift towards the hot and even less the sign change.

The experimental observation has discarded any major contribution from electrostatic or van der Waals interaction, as well as hydrophobicity. Some clues, such as the increased sensibility to temperature with increased hydrophilicity, the glucose-ring contribution, and the effect from donor/acceptor site seem to indicate that hydrophilicity, and more precisely hydrogen bonds could play a major role in the thermophoresis of biomolecules.

Molecular dynamics simulations seem to suggest a retardation effect of hydrogen-bond dynamics in the vicinity of hydrophilic spots. Quasi-Elastic Neutron Scattering experiments suggest an Arrhenius law for the HB lifetime, which would be thus extended in the vicinity of hydrophilic spots.

We used this last element to build a model relying on activated jumps. We used the Arrhenius law suggested previously to model the different jump rates. This leads to a situation of a two-level system, and to the computation of occupation probabilities of hydrogen bonds. All those quantities have shown a dependence on thermodynamical parameters, notably enthalpic and entropic barriers. Those parameters dictate the whole behavior of the evolution of the rates with the temperature. We tried different situations, taking into account the role of the second water layer and the hydrogen bond occupation. The results give encouraging trends: a compatible order of magnitude can be found for the thermodiffusion coefficient and the Soret coefficient. The behavior obtained are compatible with experiments, displaying the same linearity for the thermodiffusion coefficient and a convexe curve for the Soret coefficient.

However, the model we built used up to nine parameters, which gives excessive flexibility to fit the experimental data. Moreover, those parameters have to account for the behaviors of systems of notably different sizes and surfaces. So one has to remain quite cautious with those

results. The obtention of the expected behavior with the good order of magnitude suggests a positive answer to a major impact of hydrogen bonds on biomolecules thermophoresis. However, further investigations on the different ranges for the thermodynamical parameters enabling to match he experimental observation, and the use of more specific values for different systems would enable to go in the model in depth, to take into account the diversity of systems studied in this work.

Appendix A

Thermo-osmosis in gases: elements of understanding of Maxwell's work

Here we provide the method followed by Maxwell in his work to compute the coefficients required to obtain the creep velocity at the interface.

We remind that all means of velocity-component functions are calculated thanks to the probability density function $p = (1+F)p_0$, with $(1+F)$ the linearization containing all corrections due to the temperature gradient, here occurring along y, and p_0 the pdf in equilibrium, as presented in chapter 3. p is a probability density function, so:

$$\iiint d\xi d\eta d\zeta \, p = 1. \tag{A.1}$$

This gives:

$$C_{200} + C_{020} + C_{002} = 0. \tag{A.2}$$

Since $\langle\xi\rangle$, $\langle\eta\rangle$ and $\langle\zeta\rangle$ are all zero in the frame of the center of mass, this provides notably:

$$C_{010} + \frac{1}{2}\left(C_{030} + C_{210} + C_{012}\right) = 0. \tag{A.3}$$

This enables to link order 1 and order 3 coefficients. The mean values $\langle\eta^2\rangle$, $\langle\xi\eta\rangle$, $\langle\xi^3\rangle$, $\langle\xi^2\eta\rangle$ and other powers of velocity components, calculated with equation 3.5 are:

$$\left\langle\eta^2\right\rangle = v_T^2(1 + C_{020}), \tag{A.4a}$$

$$\langle\xi\eta\rangle = v_T^2 C_{110}, \tag{A.4b}$$

$$\left\langle\eta^3\right\rangle = v_T^3 C_{030}, \tag{A.4c}$$

$$\left\langle\xi\eta^2\right\rangle = v_T^3 C_{120}, \tag{A.4d}$$

$$\langle\xi\eta\zeta\rangle = v_T^3 C_{111}, \tag{A.4e}$$

$$\left\langle\eta^4\right\rangle = 3v_T^4(1 + 2C_{020}), \tag{A.4f}$$

$$\left\langle\eta^3\xi\right\rangle = 3v_T^4 C_{110}, \tag{A.4g}$$

$$\left\langle \eta^2\zeta^2 \right\rangle = v_T^4(1 + C_{020} + C_{002}), \tag{A.4h}$$

$$\left\langle \xi\eta^2\zeta \right\rangle = v_T^4 C_{101}, \tag{A.4i}$$

where $v_T^2 = \frac{k_B T}{m}$ is the thermal mean value of each component.

We display the coefficients that are useful for our work, that is to say in the case of a stationary regime, with a temperature gradient applied along y in table A.1. They are expressed with the mean free path $\ell = v_T\tau$, $\tau = \frac{\mu}{P}$ the relaxation time of elastic collisions between molecules, independent from temperature [4].

$C_{010} = \frac{15}{4}\frac{\ell}{T}\frac{\partial T}{\partial y}$	$C_{210} = -\frac{3}{2}\frac{\ell}{T}\frac{\partial T}{\partial y}$
$C_{012} = -\frac{3}{2}\frac{\ell}{T}\frac{\partial T}{\partial y}$	$C_{030} = -\frac{9}{2}\frac{\ell}{T}\frac{\partial T}{\partial y}$

Table A.1: *Approximated values for the coefficients for the correction F.*

$\langle\eta\rangle$ in the bulk is still zero. A temperature difference does not lead to a drift velocity of the gas, a surface is required. In the following we precise the way to obtain those coefficients.

To compute the values of the coefficients featured in F, Maxwell used what he called "equation of continuity" at the surface, for $x = 0$. He started by tracing the variation of $\langle Q\rangle$, Q being a function of the velocity-components, in an element of volume, moving in the laboratory frame with the velocity-components U, V, W. The center of mass has velocity components (u, v, w) in the laboratory frame. So, in the element of volume frame, the velocity of molecule $\vec{S}$ is: $u + \xi - U$,$v + \eta - V$ and $w + \zeta - W$. In the stationary regime, the variation of the quantity $\langle Q\rangle$ can be expressed by an "equation of continuity" [4], as proceeded in fluid mechanics:

$$0 = \operatorname{div}\left\langle Q\vec{S}\right\rangle + \frac{\partial}{\partial x}\left\langle Q\vec{n}.\vec{S}\right\rangle\Big|_{x=0}, \tag{A.5}$$

where the action of the solid boundary lies in the second term. In the vicinity of the surface, the boundary conditions are altered because of the non-specular reemission fraction f. Maxwell the first derived from the Maxwell-Boltzmann equation, which acts as a source term in this equation of continuity, arising from collisions between gas particles and the surface. Maxwell seemed to suggest that collisions with the surface generate a modification of $\langle Q\rangle$, even in the stationary state. Setting $U = u$, $V = v$ and $W = w$, Maxwell obtained [4]:

$$\frac{\partial}{\partial x}\langle Q\xi\rangle\Big|_{x=0} = \frac{\partial}{\partial x}\langle Q\xi\rangle + \frac{\partial}{\partial y}\langle Q\eta\rangle + \frac{\partial}{\partial z}\langle Q\zeta\rangle. \tag{A.6}$$

First, we compute the term on the left of the equation. From Maxwell-Boltzmann equation, Maxwell as shown [4] that the variation due to collisions for some polynomial functions P_1 of velocity components, conjugated with functions P_2, is:

$$\frac{\partial}{\partial x}\langle P_1\xi\rangle\Big|_{x=0} = \frac{1}{3\tau}\iiint d\xi d\eta d\zeta\, P_2\,(1 + F)p_0. \tag{A.7}$$

Integrations are systematically between $-\infty$ and $+\infty$. The conjugation relations between functions P_1 and P_2 arise from variation before-after collisions, the relations used for this work are gathered in tab. A.2.

We perform in the equation of continuity $Q = v + \eta$, which is requisite for upcoming

P_1	P_2
η	0
η^3	$-\frac{3}{2}\left(2\eta^3 - \eta\xi^2 - \eta\zeta^2\right)$
$\xi^2\eta$	$-\frac{1}{2}\left(8\xi^2\eta - \eta^3 - \eta\zeta^2\right)$
$\eta\zeta^2$	$-\frac{1}{2}\left(8\eta\zeta^2 - \eta^3 - \xi^2\eta\right)$

Table A.2: *Conjugated functions P_1 and P_2 used to compute the variations due to collisions in the source term of the equation of continuity [4].*

calculations. From tab. A.2 and eq. A.7, we deduce $\frac{\partial}{\partial x}\langle\eta\xi\rangle\Big|_{x=0} = 0$. The equation of continuity gives:

$$\begin{aligned}\frac{\partial}{\partial x}\langle\xi v\rangle\Big|_{x=0} &= \langle\xi\rangle\frac{\partial v}{\partial x} + \langle\eta\rangle\frac{\partial v}{\partial y} + \langle\zeta\rangle\frac{\partial v}{\partial z} \\ &+ \frac{\partial\langle\xi\eta\rangle}{\partial x} + \frac{\partial\langle\eta^2\rangle}{\partial y} + \frac{\partial\langle\eta\zeta\rangle}{\partial z} + v\left(\frac{\partial\langle\xi\rangle}{\partial x} + \frac{\partial\langle\eta\rangle}{\partial y} + \frac{\partial\langle\zeta\rangle}{\partial z}\right).\end{aligned} \tag{A.8}$$

We have seen that $\langle\xi\rangle = \langle\eta\rangle = \langle\zeta\rangle = 0$. So:

$$\frac{\partial}{\partial x}\langle\xi v\rangle\Big|_{x=0} = \frac{\partial\langle\xi\eta\rangle}{\partial x} + \frac{\partial\langle\eta^2\rangle}{\partial y} + \frac{\partial\langle\eta\zeta\rangle}{\partial z}. \tag{A.9}$$

With equations A.4a and A.4b:

$$\frac{\partial}{\partial x}\langle\xi v\rangle\Big|_{x=0} = \frac{k_B}{m}\frac{\partial T}{\partial y} + \frac{k_B}{m}\left(\frac{\partial TC_{110}}{\partial x} + \frac{\partial TC_{020}}{\partial y} + \frac{\partial TC_{011}}{\partial z}\right). \tag{A.10}$$

This is Euler's equation for a gas in presence of a temperature gradient in the stationary regime. We now calculate the coefficients C_{030}, C_{210} and C_{012}, for this we have to compute $Q = (v+\eta)^3$. The same way, using equation A.7 with $P_1 = \eta^3$, we obtain:

$$\frac{\partial}{\partial x}\left\langle\xi(v+\eta)^3\right\rangle\Big|_{x=0} = -\frac{1}{\tau}v_T^3\left(C_{030} - \frac{C_{210}+C_{012}}{2}\right) + 3\frac{v_T^4}{T}\frac{\partial T}{\partial y}. \tag{A.11}$$

Now we are ready to resort to the continuity equation to compute the expressions for the coefficients C. Starting from the equation of continuity, we have:

$$\frac{\partial}{\partial x}\left\langle\xi(v+\eta)^3\right\rangle\Big|_{x=0} = \frac{\partial}{\partial x}\left\langle(v+\eta)^3)\xi\right\rangle + \frac{\partial}{\partial y}\left\langle(v+\eta)^3\eta\right\rangle + \frac{\partial}{\partial z}\left\langle(v+\eta)^3\zeta\right\rangle. \tag{A.12}$$

After differentiation, we set $v = 0$. The calculation led here has for objective to determine relations between coefficients C (here C_{030}, C_{210}, and C_{012}), the relation must hold whatever v, u, w. So setting $v = 0$ simplifies equations. This also cancels all derivatives of powers of v. We get:

$$\begin{aligned}-\frac{1}{\tau}v_T^3\left(C_{030} - \frac{C_{210}+C_{012}}{2}\right) + 3\frac{v_T^4}{T}\frac{\partial T}{\partial y} &= 3\left\langle\eta^2\xi\right\rangle\frac{\partial v}{\partial x} + \frac{\partial}{\partial x}\left\langle\eta^3\xi\right\rangle + 3\left\langle\eta^3\right\rangle\frac{\partial v}{\partial y} \\ &+ \frac{\partial}{\partial y}\left\langle\eta^4\right\rangle + 3\left\langle\eta^2\zeta\right\rangle\frac{\partial v}{\partial z} + \frac{\partial}{\partial z}\left\langle\eta^3\zeta\right\rangle.\end{aligned} \tag{A.13}$$

Coefficients C all are supposed small before unity. Indeed, if we take $\frac{dT}{dy} \sim 10^4$ K/m, which is compatible with Reynolds' experiment [3], $C_{030} \sim 10^{-3}$. Thus, on the right of equation A.13, the only significant contribution is from $\langle \eta^4 \rangle = 3v_T^4(1 + 2C_{020})$, with the 1 in the parenthesis. The only remaining term on this side is $3\frac{d}{dy}\left(\frac{k_B T}{m}\right)^2$, which is about $\sim 10^{13}$ m^3/s^4. All other terms are neglected because they all bear coefficients C. On the other side the first term $\frac{1}{\tau}v_T^3\left(C_{030} - \frac{C_{210}+C_{012}}{2}\right)$ remains, the factor P/η enables it to be of the order of $\sim 10^{12}$ m^3/s^4. The other quantity is subtracted on both sides, and finally obtain:

$$C_{030} - \frac{C_{210} + C_{012}}{2} \simeq -3\frac{\ell}{T}\frac{dT}{dy}. \tag{A.14}$$

Proceeding the same way, with $Q = (\eta + v)(\xi + u)^2$ and $Q = (\eta + v)(\zeta + w)^2$, we obtain:

$$C_{030} - 8C_{210} + C_{012} \simeq 6\frac{\ell}{T}\frac{dT}{dy}, \tag{A.15a}$$

$$C_{030} + C_{210} - 8C_{012} \simeq 6\frac{\ell}{T}\frac{dT}{dy}. \tag{A.15b}$$

We have used equation A.7 with $P_1 = \xi^2\eta$ and $P_1 = \eta\zeta^2$, to obtain $\frac{\partial}{\partial x}\langle \xi(\xi^2\eta)\rangle\Big|_{x=0}$ and $\frac{\partial}{\partial x}\langle \xi\eta\zeta^2\rangle\Big|_{x=0}$, needed for this last step. The corresponding functions P_2 are given in table A.2. Combining equations A.14, A.15a and A.15b, we obtain:

$$C_{210} = C_{012} = \frac{1}{3}C_{030} = -\frac{3}{2}\frac{\ell}{T}\frac{dT}{dy}. \tag{A.16}$$

Thanks to equation A.3 we can determine $C_{010} = \frac{15}{4}\frac{\ell}{T}\frac{dT}{dy}$. This way, we obtain all the coefficients presented in tab. A.1. We can totally determine the probability density function at the position considered, and perform the calculation led by Maxwell to compute the creep flow at the solid surface.

Appendix B

Amino-Acids and hydrophilicity

Here we give some supplementary elements about the hydrophilic character of amino-acids.

The different amino-acids (AA) bear different groups that condition their hydrophilicity. There are different scales [53, 131–133] to determine whether an AA is rather hydrophilic or hydrophobic. Different criterions are used, for instance the needed energy to pass from the organic phase to the aqueous phase [132]. Anyway, some patterns seem to emerge.

The AA that feature apolar carbon groups (aliphatic), such as Phenylalanine, Valine, Leucine and Isoleucine (the notorious BCAA (Branched Chains Amino-Acids)) are systematically classified as hydrophobic AA, and are very likely to be located in the core of a globular protein to limit the contact with water molecules. On the other hand, AA that feature polar chains, charged or not, are systematically very hydrophilic AAs, such as Arginine, Leucine, Aspartic Acid, Asparagine, Glutamic Acid, Glutamine and Histidine. One can notice that those feature specific groups such as carboxyl, N-H, carbonyl, which are HB acceptors. Lysine is very hydrophilic but only bears HB donor sites. The other AAs have less pronounced hydrophilicity, and feature groups that are mainly hydroxyl groups (-OH), that seems to lead to a less hydrophilic behavior.

Note that hydroxyl groups (-OH) are more acceptors than donor HB sites, which is consistent with the thermophilic behavior observed with DM and other sugar molecules.

We remind that PLL (Poly-L-Lysine) is an homo-polymer only constituted of the AA Lysine (K), which feature a -NH2 HB-donor site (and of course a carboxyl group on the backbone). PLL displays thermophilic behavior very similar of the one of BLGA as presented in chapter 2. Now if we compare the amino-grams of BLGA and lysozyme, we can notice that BLGA carries all hydrophilic AA in larger quantities than lysozyme, excepted Arginine (R), which is the most hydrophilic AA, present only twice in BLGA and thirteen times in lysozyme. We have seen that for lysozyme the temperature of sign switch T^*, and the asymptotic value S_T^∞, are respectively higher and lower compared to other polypeptides.

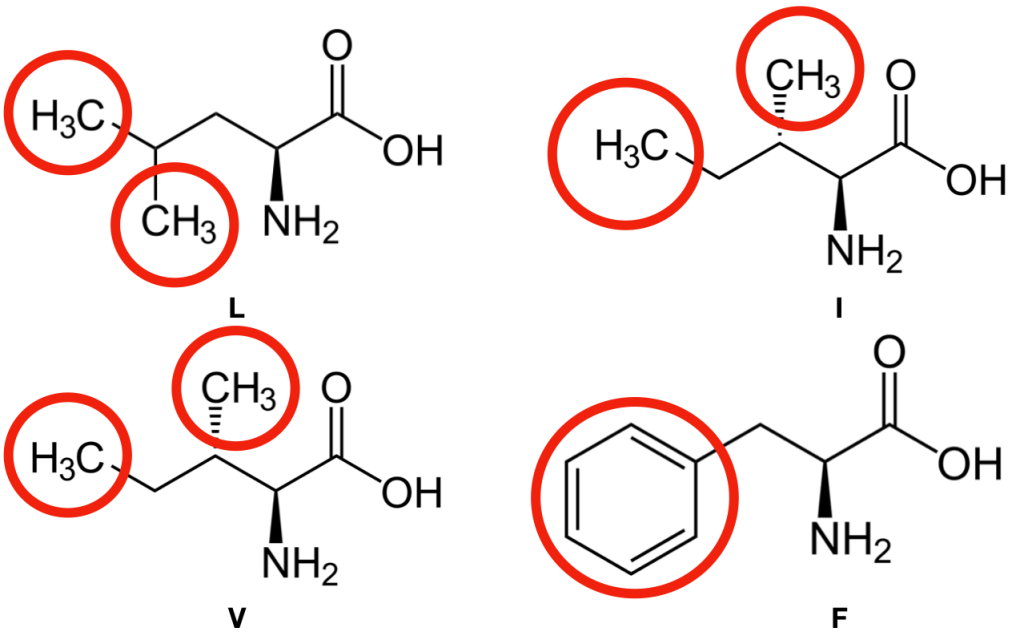

Figure B.1: *Structures of the most hydrophobic amino-acids: L Leucine, I Isoleucine, V Valine and F Phenylalanine. The red circles indicate carbon hydrophobic groups on the radical.*

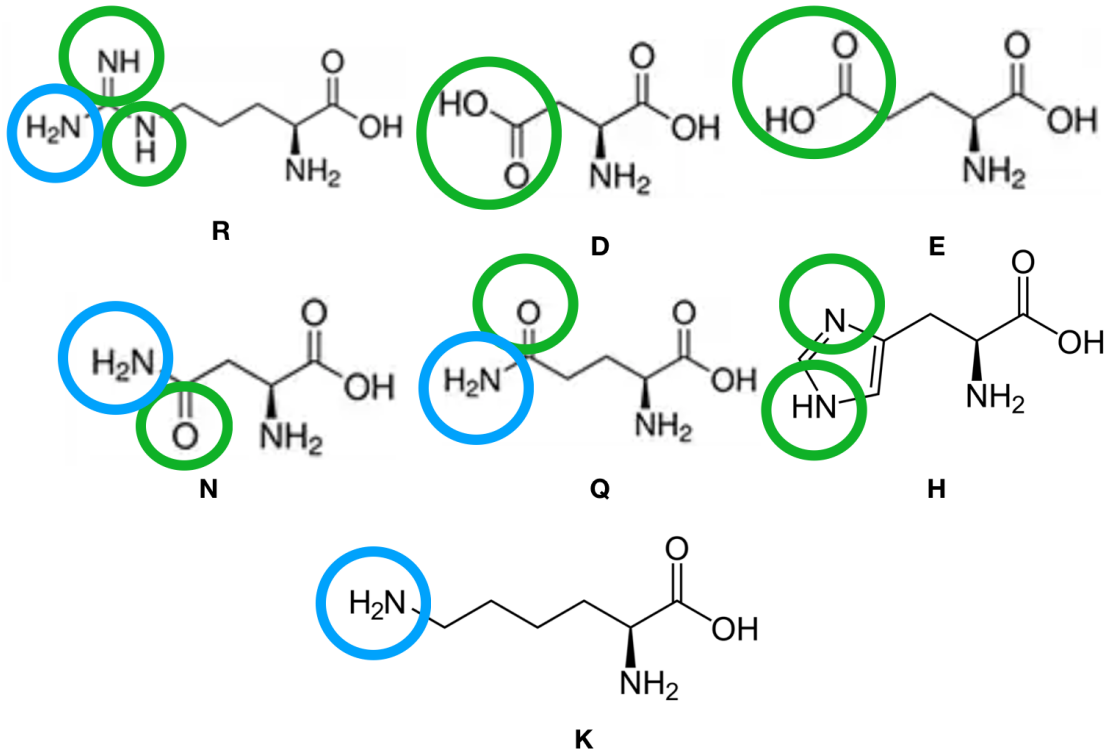

Figure B.2: *Structures of the most hydrophilic amino-acids: R Arginine, D Aspartic Acid, E Glutamic Acid, N Asparagine, Q Glutamine, H Histidine and K Lysine. The green circles indicate sites that are at least as acceptor than donor (eg the NH group in Histidine can accept one HB via the electron pair and give one HB via the H atom), and blue circles sites that are more donor than acceptor (2 HB donor via H atoms, and 1 HB accepted via the electron pair carried by the N atom) on the radical.*

Bibliography

[1] C. Soret. Sur l'état d'équilibre que prend au point de vue de sa concentration une dissolution saline primitivement homogène dont deux parties sont portées à des températures différentes. *Arch. Sci. Phys. Genève*, 2:1, 1879.

[2] J. Tyndall. On dust and disease. *Proc. R. Inst. GB*, 6:1, 1870.

[3] O. Reynolds. On certain dimensional properties of matter in the gaseous state. *Phil. Trans. Roy. Soc.*, 170:727, 1879.

[4] J.C. Maxwell. On stresses in rarified gases arising from inequalities of temperature. *Phil. Trans. Roy. Soc.*, 170:231, 1879.

[5] B. Derjaguin and G. Sidorenkov. Thermo-osmosis at ordinary temperatures and its analogy with the thermomechanical effect in helium 2. *Dokl. Acad. Nauk SSSR*, 32:622, 1941.

[6] R. Rusconi, L. Isa, and R. Piazza. Thermal-lensing measurement of particle thermophoresis in aqueous dispersions. *J. Opt. Soc. Am. B*, 21:605, 2004.

[7] S. Iacopini, R. Rusconi, and R. Piazza. The "macromolecular tourist": universal temperature dependence of thermal diffusion in aqueous colloidal suspensions. *Eur. Phys. J.E*, 19:59, 2006.

[8] S. Iacopini and R. Piazza. Thermophoresis in protein solutions. *Europhys. Lett.*, 63:247, 2003.

[9] R. Piazza and A. Guarino. Soret effect in interacting micellar solutions. *PRL*, 88:1, 2002.

[10] R. Piazza, S. Iacopini, and B. Triulzi. Thermophoresis as a probe of particle-solvent interactions: the case of protein solutions. *Phys. Chem. Chem. Phys.*, 6:1616, 2004.

[11] S. Wongsuwarn, D. Vigolo, R. Cerbino, A.M. Howe, A. Vailati, R. Piazza, and P. Cicuta. Giant thermophoresis of poly(N-isopropylacrylamide) microgel particles. *Soft Matter*, 8:5857, 2012.

[12] S. Wiegand. Thermal diffusion in liquid mixtures and polymer solutions. *J. Phys.: Condens. Matter*, 16:357, 2004.

[13] K. Maeda, N. Shinyashiki, S. Yagihara, S. Wiegand, and R. Kita. How does thermodiffusion of aqueous solutions depend on concentration and hydrophobicity? *Eur. Phys. J.E*, 37:1, 2014.

[14] K. Maeda, N. Shinyashiki, Shin Yagihara, S. Wiegand, and R. Kita. Ludwig-Soret effect of aqueous solutions of ethylene glycol oligomers, crown ethers, and glycerol: Temperature, molecular weight, and hydrogen bond effect. *J. Chem. Phys.*, 143:1, 2015.

[15] D. Niether, T. Kawaguchi, J. Hovancová, K. Eguchi, and J.K.G Dhont. Role of hydrogen bonding of cyclodextrin-drug complexes probed by thermodiffusion. *Langmuir*, 33:8483, 2017.

[16] D. Niether, H. Kriegs, J.K.G Dhont, and S. Wiegand. Peptide model systems: correlation between thermophilicity and hydrophilicity. *J. Chem. Phys.*, 149:1, 2018.

[17] D. Niether and S. Wiegand. Thermophoresis of biological and biocompatible compounds in aqueous solution. *J. Phys.: Condens. Matter*, 31:1, 2019.

[18] H. Jiang, H. Wada, N. Yoshinaga, and M. Sano. Manipulation of colloids by a nonequilibrium depletion force in a temperature gradient. *PRL*, 102:208301, 2009.

[19] C.B. Mast and D. Braun. Thermal trap for DNA replication. *PRL*, 104:1, 2010.

[20] Y. Kishikawa, H. Shinohara, K. Maeda, Y. Nakamura, S. Wiegand, and R. Kita. Temperature dependence of thermal diffusion for aqueous solutions of monosaccharides, oligosaccharides and polysaccharides. *Phys. Chem. Chem. Phys.*, 14:10147, 2012.

[21] P. Reineck, C. Wienken, and D. Braun. Thermophoresis of single stranded DNA. *Electrophoresis*, 31:279, 2010.

[22] H. Shinohara, R. Kita, and N. Shinyashiki. Temperature dependent study of thermal diffusion for aqueous solutions of alpha, beta and gamma cyclodextrin. *AIP Conf. Proc.*, 1518:710, 2013.

[23] M. Braun, A. Bregulla, K. Günther, M. Mertig, and F. Cichos. Single molecules trapped by dynamic inhomogeneous temperature fields. *Nano Lett.*, 15:5499, 2015.

[24] J.C. Giddings, V. Kumar, P.S. Williams, and M.N. Myers. Polymer separation by thermal field-flow fractionnation. high-speed power programming. *Adv. Chem. Ser.*, 227:3, 1990.

[25] M. Hartung, J. Rauch, and W. Köhler. Thermal diffusion of dilute polymer solutions: the role of solvent viscosity. *J. Chem. Phys.*, 125:214904, 2006.

[26] M.E. Schimpf and J.C. Giddings. Characterization of thermal diffusion in polymer solutions by thermal field-flow fractionation: dependence on polymer and solvent parameters. *J. Polym. Sci.*, 27:1317, 1989.

[27] M.E. Schimpf and J.C. Giddings. Characterization of thermal diffusion in polymer solutions by thermal field-flow fractionation: effects of molecular weight and branching. *Macromolecules*, 20:1561, 1987.

[28] P.M. Shiundu, P.S. Williams, and J.C. Giddings. Magnitude and direction of thermal diffusion of colloidal particles measured by thermal field-flow fractionation. *J. Colloid Interface Sci.*, 266:366, 2003.

[29] R.M. Sisson and J.C. Giddings. Effects of solvent composition on polymer retention in the thermal field-flow fractionnation: rentention enhancement in binary solvent mixtures. *Anal. Chem.*, 66:4043, 1994.

[30] K.A. Eslahian, A. Majee, M. Maskos, and A. Würger. Specific salt effects on thermophoresis of charged colloids. *Soft Matter*, 10:1931, 2014.

[31] P. Debye. Zur Theorie des Clusiusschen Trennungsverfahrens. *Annalen der Physik*, 428:284, 1939.

[32] B.C. Reed. Liquid thermal diffusion during the Manhattan project. *Phys. Perspect.*, 13:161, 2011.

[33] W. Köhler and K. Morozov. The Soret effect in liquid mixtures - A review. *J. Non-Equil. Thermodyn.*, 41:151, 2016.

[34] M. Kreysing, L. Keil, S. Lanzmich, and D. Braun. Heat flux across an open pore enables the continuous replication and selection of oligonucleotides towards increasing length. *Nature Chem.*, 7:203, 2015.

[35] D. Braun and A. Libchaber. Thermal force approach to molecular evolution. *Phys. Biol.*, 1:1, 2004.

[36] S. Duhr, S. Arduini, and D. Braun. Thermophoresis of DNA determined by microfluidic fluorescence. *Eur. Phys. J.E*, 15:277, 2004.

[37] L. Aboubraky and A. Würger. Hydrodynamic interactions in DNA thermophoresis. *Soft Matter*, 14:848, 2018.

[38] S. Duhr and D. Braun. Optothermal molecule trapping by opposing fluid flow with thermophoretic drift. *PRL*, 97:038103, 2006.

[39] M. Jerabek-Willemsen, T. André, R. Wanner, H.M. Roth, S. Duhr, P. Baaske, and D. Breitsprecher. Microscale thermophoresis: interaction analysis and beyond. *J. Mol. Struct.*, 1077:101, 2014.

[40] M.F. Riley and A. Firoozabadi. Compositional variation in hydrocarbon reservoirs with natural convection and diffusion. *AIChE J.*, 44:452, 1998.

[41] D.E. Rosner, R.S. Israel, and B. La Mantia. "Heavy" species Ludwig-Soret transport effects in air-breathing combustion. *Combust. Flame*, 123:547, 2000.

[42] G. Vasaru. Thermal diffusion in isotopic gaseous mixtures. *Fortschritte der Physik*, 15:1, 1967.

[43] J. Leng, G. Zhengrong, Z. Hongwei, C. Tienchong, G. Xingming, and G. Huajian. Negative thermophoresis in concentric carbon nanotube nanodevices. *Nano Lett.*, 16:6396, 2016.

[44] S.R. de Groot. L'effet Soret : diffusion thermique dans les phases condensées. *N. v. Noord-hollandsche uitgevers maatschappi*, 1945.

[45] K.J. Zhang, M.E. Briggs, and R.W. Gammon. Optical measurement of the Soret coefficient and the diffusion coefficient of liquid mixtures. *J. Chem. Phys.*, 104:6881, 1996.

[46] S.R. de Groot and P. Mazur. *Non-Equilibrium Thermodynamics*. Dover, 1962.

[47] W. Crookes. On attraction and repulsion resulting from radiation. Part 2. *Proc. R. Soc. A*, 23:373, 1875.

[48] S.P. Bakanov and B. Derjaguin. Thermophoresis of aerosol particles. *Nature*, 198:669, 1962.

[49] D. Baker. A surprising simplicity to protein folding. *Nature*, 405:39, 2000.

[50] D. Eisenberg, R. M. Weiss, T. C. Terwilliger, and W. Wilcox. Hydrophobic moments and protein structure. *Faraday Symp. Chem. Soc.*, 17:109, 1982.

[51] R.A. Curtis, C. Steinbrecher, M. Heinemann, H.W. Blanch, and J.M. Prausnitz. Hydrophobic forces between protein molecules in aqueous solutions of concentrated electrolyte. *Biophys. Chem.*, 98:249, 2002.

[52] D.P. Kharakoz. Volumetric properties of proteins and their analogs in diluted water solutions. *Biophys. Chem.*, 34:115, 1989.

[53] J. Kyte and R. F. Doolittle. A simple method for displaying th hydropathic character of a protein. *J. Mol. Biol.*, 157:105, 1982.

[54] S. Matysiak, P.G. Debenedetti, and P. Rossky. Dissecting the energetics of hydrophobic hydration of polypeptides. *J. Phys. Chem. B*, 115:14859, 2011.

[55] S. Matysiak, P.G. Debenedetti, and P. Rossky. Role of hydrophobic hydration in protein stability: a 3D water explicit protein model exhibiting cold and heat denaturation. *J. Phys. Chem. B*, 116:8095, 2012.

[56] R. Sweet and D. Eisenberg. Correlation of sequence hydrophobicities measures similarity in three-dimensional protein structure. *J. Mol. Biol.*, 171:479, 1983.

[57] A.W. Senior, R. Evans, J. Jumper, J. Kirkpatrick, L. Sifre, T. Green, C. Qin, A. Zidek, A.W.R. Nelson, A. Bridgland, H. Penedones, S. Petersen, K. Simonyan, S. Crossan, P. Kohli, D.T. Jones, D. Silver, K. Kavukcuoglu, and D. Hassabis. Improved protein structure prediction using potentials from deep learning. *Nature*, 577:706, 2020.

[58] J. Giddings, K.D. Caldwell, and M. Myers. Thermal diffusion of polystyrene in eight solvents by an improved thermal field-flow fractionation methodology. *Macromolecules*, 9:106, 1976.

[59] D.R. Caldwell. Measurement of negative thermal diffusion coefficients by observing the onset of thermohaline convection. *J. Phys. Chem.*, 77:2004, 1973.

[60] M. Giglio and A. Vendramini. Soret-type motion of macromolecules in solution. *PRL*, 38:26, 1977.

[61] B.J de Gans, R. Kita, B. Müller, and S. Wiegand. Negative thermodiffusion of polymers and colloids in solvent mixtures. *J. Chem. Phys.*, 118:8073, 2003.

[62] R. Piazza. "Thermal forces": colloids in temperature gradient. *J. Phys.: Condens. Matter*, 16:4195, 2004.

[63] H. Ning, J. Buitenhuis, J.K.G Dhont, and S. Wiegand. Thermal diffusion behavior of hard-sphere suspensions. *J. Chem. Phys.*, 125:204911, 2006.

[64] K.J. Zhang, M.E. Briggs, R.W. Gammon, J.V. Sengers, and J.F. Douglas. Thermal and mass diffusion in a semidilute good solvent-polymer solution. *J. Chem. Phys.*, 111:2270, 1999.

[65] A. Würger. Molecular-weight dependent thermal diffusion in dilute polymer solutions. *PRL*, 102:1, 2009.

[66] J. Chan, J. Popov, S. Kolisnek-Kehl, and D.G. Leaist. Soret coefficients for aqueous polyethylene glycol solutions and some tests of the segmental model of polymer thermal diffusion. *J. Solut. Chem.*, 32:197, 2003.

[67] D. Stadelmaier and W. Köhler. From small molecules to high polymers: investigation of the crossover of thermal diffusion in dilute polystyrene solutions. *Macromolecules*, 41:6205, 2008.

[68] J. Rauch and W. Köhler. On the molar mass dependence of the thermal diffusion coefficient of polymer solutions. *Macromolecules*, 28:3571, 2005.

[69] S. Semenov and M.E. Schimpf. Thermophoresis of dissolved molecules and polymers: consideration of the temperature-induced macroscopic pressure gradient. *PRE*, 69:011201, 2004.

[70] S.A. Putnam and D.G. Cahill. Transport of nanoscale latex spheres in a temperature gradient. *Langmuir*, 21:5317, 2005.

[71] S.A. Putnam, D.G. Cahill, and G.C.L. Wong. Temperature dependence of thermodiffusion in aqueous suspensions of charged nanoparticules. *Langmuir*, 23:9221, 2007.

[72] J.C. Maxwell. On the dynamical theory of gases. *Phil. Trans. Roy. Soc.*, 157:49, 1867.

[73] E.H. Kennard. *Kinetic Theory of Gases*. New York: McGraw-Hill, 1938.

[74] R. Piazza and A. Parola. Thermophoresis in colloidal suspensions. *J. Phys.: Condens. Matter*, 20:153102, 2008.

[75] J. Anderson. Colloid transport by interfacial forces. *Ann. Rev. Fluid Mech.*, 21:61, 1989.

[76] A. Würger. Thermal non-equilibrium transport in colloids. *Rep. Prog. Phys.*, 73:1, 2010.

[77] B. Derjaguin, N. V. Churaev, and V. M. Muller. *Surface Forces*. Plenum, New York, 1987.

[78] A.P. Bregulla, A. Würger, K. Günther, M. Mertig, and F. Cichos. Thermo-osmotic flow in thin films. *PRL*, 116:1, 2016.

[79] A. Würger. Transport in charged colloids driven by thermoelectricity. *PRL*, 101:108302, 2008.

[80] E. Ruckenstein. Can phoretic motions be treated as interfacial tension gradient driven phenomena? *J. Colloid Interface Sci.*, 83:77, 1981.

[81] J. N. Israelachvili. *Intermolecular and surface forces*. Elsevier, 2011.

[82] D. Eisenberg and A.D. McLachlan. Solvatation energy in protein folding and binding. *Nature*, 319:199, 1986.

[83] C. Lipinski, F. Lombardo, B. Dominy, and P. Feeney. Experimental and computational approaches to estimate solubility and permeability in drug discovery and development settings. *Adv. Drug Deliv. Rev.*, 64:1, 2012.

[84] R. Kita, G. Kircher, and S. Wiegand. Thermally induced sign change of soret coefficient for dilute and semidilute solutions of poly(n-isopropylacrylamide) in ethanol. *J. Chem. Phys.*, 121:9140, 2004.

[85] A.Königer, N. Plack, W. Köhler, M. Siebenbürger, and M. Ballauf. Thermophoresis of thermoresponsive polystyrene-poly(N-isopropylacrylamide) core-shell particles. *Soft Matter*, 9:1418, 2013.

[86] T. Kikutsuji, K. Kim, and N. Matubayasi. Diffusion dynamics of supercooled water modeled with the cage-jump motion and hydrogen-bond rearrangement. *J. Chem. Phys.*, 150:1, 2019.

[87] B.E. Poling, J.M. Prausnitz, and J.P. O'Connel. *The properties of gases and liquids*. New York: McGraw-Hill, 2001.

[88] R. Kumar, J.R. Schmidt, and J.L. Skinner. Hydrogen bonding definitions and dynamics in liquid water. *J. Chem. Phys.*, 126:204107, 2007.

[89] M.C. Bellissent-Funel and J.C. Dore. Hydrogen bond networks. *NATO ASI Series*, 435:23, 1994.

[90] P. Ball. Water as an active constituent in cell biology. *Biophys. Chem.*, 108:74, 2008.

[91] A. Coccia, P.L. Indovina, F. Podo, and V. Viti. PMR studies on the structures of water-ethyl alcohol mixtures. *Chem. Phys.*, 7:30, 1975.

[92] T. Kikutsuji, K. Kim, and N. Matubayasi. How do hydrogen bonds break in supercooled water? Detecting pathways not going through saddle point of two-dimensional potential of mean force. *J. Chem. Phys.*, 148:1, 2018.

[93] K. Modig, B.G. Pfrommer, and B. Halle. Temperature-dependent hydrogen-bond geometry in liquid water. *PRL*, 90:075502, 2003.

[94] J.D. Smith, C.D. Cappa, K.R. Wilson, B.M. Messer, R.C. Cohen, and R.J. Saykally. Energetics of hydrogen bond network rearrangements in liquid water. *Science*, 306:851, 2004.

[95] I. Ohmine and H. Tanaka. Fluctuation, relaxations and hydration in liquid water. Hydrogen-bond rearrangement dynamics. *Chem. Rev.*, 93:2545, 1993.

[96] N. Galamba. On the hydrogen-bond network and the non-Arrhenius transport properties of water. *J. Phys.: Condens. Matter*, 29:015101, 2017.

[97] F.N. Keutsch and R.J. Saykally. Water clusters: untangling the mysteries of the liquid, one molecule at a time. *PNAS*, 98:10533, 2001.

[98] F.W. Starr, J.K. Nielsen, and H.E. Stanley. Fast and slow dynamics of hydrogen bonds in liquid water. *PRL*, 82:2294, 99.

[99] A. Geiger, F.H. Stillinger, and A. Rahman. Aspects of the percolation process for hydrogen-bond networks in water. *J. Chem. Phys.*, 70:4185, 1979.

[100] T. Kikutsuji, K. Kim, and N.Matubayasi. Consistency of geometrical definitions of hydrogen bonds based on the two-dimensional potential of mean force with respect to the time correlation in liquid water over a wide range of temperatures. *J. Mol. Liq.*, 294:1, 2019.

[101] A. Faraone, L. Liu, and S.H. Chen. Model for the translation-rotation coupling of molecular motion in water. *J. Chem. Phys.*, 119:6302, 2003.

[102] N. Galamba. On the effects of temperature, pressure and dissolved salts on the hydrogen-bond network of water. *J. Phys. Chem. B*, 117:589, 2013.

[103] A. Luzar. Resolving the hydrogen bon dynamics conundrum. *J. Chem. Phys.*, 113:10663, 2000.

[104] H.F.M.C. Martiniano and N. Galamba. Insights on hydrogen-bond lifetimes in liquids and supercooled water. *J. Phys. Chem. B*, 117:16188, 2013.

[105] R. Schulz, Y. von Hansen, J.O. Daldrop, J. Kappler, F. Noé, and RR. Netz. Collective hydrogen-bond rearrangement dynamics in liquid water. *J. Chem. Phys.*, 149:244504, 2018.

[106] J.T. Titantah and M. Karttunen. Water dynamics: relation between hydrogen bond bifurcations, molecular jumps, local density and hydrophobicity. *Sci. Rep.*, 3:1, 2013.

[107] T. Kikutsuji, K. Kim, and N. Matubayasi. Transition pathway of hydrogen bond switching in supercooled water analyzed by the Markov state model. *J. Chem. Phys.*, 154:1, 2021.

[108] D. Laage and J.T. Hynes. A molecular jump mechanism of water reorientation. *Science*, 311:1, 2006.

[109] D. Laage and J.T. Hynes. On the mechanism of water reorientation. *J. Phys. Chem. B*, 112:14230, 2008.

[110] D. Laage, G. Stirnemann, F. Sterpone, R. Rey, and J.T. Hynes. Reorientation and allied dynamics in water and aqueous solutions. *Annu. Rev. Phys. Chem.*, 62:395, 2011.

[111] D. Laage, T. Elsaesser, and J.T. Hynes. Water dynamics in the hydration shells of biomolecules. *Chem. Rev.*, 117:10694, 2017.

[112] D.M. Wilkins, D.E. Manolopoulos, S. Pipolo, D. Laage, and J.T. Hynes. Nuclear quantum effects in water reorientation and hydrogen-bond dynamics. *J. Phys. Chem. B*, 8:2602, 2017.

[113] J. Teixeira. Dynamics of hydrogen bonds: how to probe their role in the unusual properties of liquid water. *J. Phys.: Condens. Matter*, 18:2353, 2006.

[114] O. Conde and J. Teixera. Hydrogen bond dynamics in water studied by depolarized Rayleigh scattering. *J. Phys. France*, 44:525, 1983.

[115] J. Teixeira, M.C. Bellissent-Funel, S.H. Chen, and A.J. Dianoux. Experimental determination of the nature of diffusive motions of water molecules at low temperatures. *PRA*, 31:1, 1985.

[116] S.H. Chen, J. Teixeira, and R. Nicklow. Incoherent quasielastic neutron scattering from water in supercooled regime. *PRA*, 26:1, 1982.

[117] R. Laenen, K. Simeonidis, and A. Laubereau. Subpicosecond spectroscopy of liquid water in the infrared: effect of deuteration on the structural and vibrational dynamics. *J. Phys. Chem. B*, 106:408, 2002.

[118] F.H. Stillinger. Water revisited. *Science*, 209:451, 1980.

[119] J. Qvist, C. Mattea, and E.P. Sunde. Rotational dynamics in supercooled water from nuclear spin relaxation and molecular simulations. *J. Chem. Phys.*, 136:1, 2012.

[120] D.D. Doshi, E.B. Watkins, J.N. Israelachvili, and J. Majewski. Reduced water density at hydrophobic surfaces: effect of dissolved gases. *PNAS*, 102:9458, 2005.

[121] D. Laage, G. Stirnemann, and J.T. Hynes. Why water reorientation slows without iceberg formation around hydrophobic solutes. *J. Phys. Chem. B*, 113:2428, 2009.

[122] S. Okouchi, T. Moto, Y. Ishihara, H. Numajiri, and H. Uedaira. Hydration of amines, diamines, polyamines and amides studied by NMR. *J. Chem. Soc., Faraday Trans.*, 92:1853, 1996.

[123] Y. Ishihara, S. Okouchi, and H. Uedaira. Dynamics of hydration of alcohols and diols in aqueous solutions. *J. Chem. Soc., Faraday Trans.*, 93:3337, 1997.

[124] E. Duboué-Dijon, A. C. Fogarty, J. T. Hynes, and D. Laage. Dynamical disorder in the DNA hydration shell. *J. Am. Chem. Soc.*, 138:7610, 2016.

[125] F. Sterpone, G. Stirnemann, and D. Laage. Magnitude and molecular origin of water slowdown next to a protein. *J. Am. Chem. Soc.*, 134:4116, 2012.

[126] A.C. Fogarty and D. Laage. Water dynamics in protein hydration shells: the molecular origins of the dynamical perturbation. *J. Phys. Chem. B*, 118:7715, 2014.

[127] M.L. Scalley and D. Baker. Protein folding kinetic exhibit an Arrhenius temperature dependence when corrected for the temperature dependence of protein stability. *Proc. Natl. Acad. Sci. USA*, 94:10636, 1997.

[128] A. Würger. Thermoelectric ratchet effect for charge carriers with hopping dynamics. *PRL*, 126:1, 2021.

[129] A. Gomez, Z. Piskulich, W. Thompson, and D. Laage. Water diffusion proceeds via a hydrogen-bond jump exchange mechanism. *J. Phys. Chem. Lett.*, 13:4660, 2022.

[130] D.M. Wilkins, D. Manolopoulos, S. Pipolo, D. Laage, and J.T. Hynes Hynes. Nuclear quantum effects in water reorientation and hydrogen-bond dynamics. *J. Phys. Chem. Lett.*, 8:2602, 2017.

[131] R.M. Sweet and D. Eisenberg. Correlation of sequence hydrophobicities measures similarity in three-dimensional protein structure. *J. Mol. Biol.*, 171:479, 1983.

[132] D. Eisenberg, R. Weiss, T.C. Terwilliger, and W. Wilcox. Hydrophobic moments and protein structure. *Faraday Symp. Chem. Soc.*, 17:109, 1982.

[133] D.M. Engelman, T.A. Steitz, and A. Goldman. Identifying nonpolar transbilayer helices in amino-acid sequences of membrane proteins. *Annu. Rev. Biophys. Biophys. Chem.*, 15:321, 1986.